Spring 1994

# On the Low-Frequency Current and Temperature Fluctuations Along the Shelf Break in the South Atlantic Bight

Sunny Yu Wu
*Old Dominion University*

# ON THE LOW-FREQUENCY CURRENT AND TEMPERATURE FLUCTUATIONS ALONG THE SHELF BREAK IN THE SOUTH ATLANTIC BIGHT

by

Sunny Yu Wu
B.S. July 1984, Shandong College of Oceanology, Qingdao, China

A dissertation submitted to
the Faculty of Old Dominion University
In partial fulfillment of the Degree of

DOCTOR OF PHILOSOPHY

Oceanography

Old Dominion University

May, 1994

Approved by:

Larry P. Atkinson (Director)

Shenn-Yu Chao

Gabriel T. Csanady

Chester Grosch

John M. Klinck

## ABSTRACT

ON THE LOW FREQUENCY
CURRENT AND TEMPERATURE FLUCTUATIONS
ALONG THE SHELF BREAK
IN THE SOUTH ATLANTIC BIGHT

Sunny Y. Wu
Old Dominion University
Director : Dr. Larry P. Atkinson

Current and temperature data collected along the shelf edge in the South Atlantic Bight were analyzed using a spectral analysis technique. The power spectra of both alongshore currents and temperatures (upon removal of seasonal trends) in the mid- to lower water column suggest a significant energy peak at 28 days. The spatial characteristics of the fluctuations around this period band were determined using the frequency domain empirical orthogonal function (EOF) analysis applied to the concurrent current and temperature records. Consistent results were obtained from the upstream side of the Charleston Bump. Around the 28-day period, temperature seems to have little correlation with currents, suggesting distinct controlling mechanisms over the two variables. Temperature fluctuations in the mid- to lower water column appear to be advected downstream by the mean current. The first and second current EOF modes each represent a southward propagating signal with a wavelength *ca.* 5000 km and a northward propagating signal with a wavelength *ca.* 360 km. This modes account for 64.5% and 18.2% of the total normalized variance, respectively. The first mode is probably related to

the interaction between topographically induced wave signals and the Gulf Stream current. The wave characteristics of the second mode fit the dispersion relationship sought by Brooks (1978) for similar bottom topographic profile and mean flow conditions. The nature of the second alongshore current mode is therefore likely to be a barotropic shelf wave.

Although the limitation of the current data in the cross-shore direction prohibited calculating the cross-shore shear of the mean flow, the signs of the transfer of energy between the fluctuations and the mean flow were determined. The results were consistent with earlier findings (*e.g.*, Schmitz and Niiler, 1969; Csanady, 1989; Lee, Yoder and Atkinson, 1991) in that the transfer is a two-way process: the fluctuations draw energy from the mean flow and at times also feed back to the mean flow. It seems, though, there are preferable areas where the transfer is a predominantly one-way process.

To my parents

## Acknowledgements

I express my deepest gratitude to Dr. Larry Atkinson, who gave me the opportunity to come to Old Dominion University and has served as my advisor ever since. I thank Larry for his guidance and support, both academically and financially, through my study at ODU. My family will always treasure the help and friendship Larry and his wife Ann have given us all these years.

I am extremely fortunate to have a great committee supervising my dissertation work. Dr. Chet Grosch has been most patient and supportive from the very beginning of this work. His encouragement has always been a source of my motivation. With in-depth physical insight, Dr. Gabe Csanady has been most helpful in guiding me to stay on the right track. Through course work and personal communication, I have come to know Dr. John Klinck as a great teacher and an enthusiastic researcher, whose lectures I had thoroughly enjoyed. As my current supervisor, Dr. Shenn-Yu Chao has been very supportive. I greatly appreciate the opportunity to work for him, which has been an enjoyable learning experience. In short, I am most grateful to each and every member of my committee, for their time, comments, and suggestions.

I am obliged to the faculty at Oceanography Department, especially, Drs. Eileen Hofmann, George T.F.Wong, Ron Johnson, Denny Kirwan, and Gregory Carter for their help at various stages of my study. I am also indebted to Dr. Wayne Schroll for his generous help with the computer system, to Carole Blett, Karal Gregory, Beverly Mitchell, and Dana Oblak for their administrative assistance,

to Elizabeth Williams at Rosenstiel School of Marine and Atmospheric Science, University of Miami, for providing me the current meter data used in this study, and to Dr. Jerry Miller for the helpful discussions on this work.

I am thankful to my fellow students at CCPO for their friendship and help, among them in particular, Eiichi Oka, Cheolsoo Kim, Peter Becker, Sangki Lee, Ana Martins, Ajoy Kumar, and G.V.R.K.Vittal.

Finally, I take this opportunity to thank my parents for their everlasting love and support. My older brother Charles has always been my inspiration and best friend from as early as I can remember. I thank him for always being there for me when needed. I thank my husband, Xiutian Zhao, for his unconditional love and understanding, for always sharing the joy as well as enduring the difficulties with me, and my little boy Leon for bringing so much fun and joy into my life. I thank my parents, parents- and sister-in-law for taking such a great care of Leon in the past year and a half while Leon was away from his parents.

Financial support for this research was provided by the Department of Energy (under contract DE-FG05-85ER60351), National Science Foundation (Grant OCE-8519203), Slover Endowment, and the Center for Coastal Physical Oceanography at Old Dominion University.

TABLE OF CONTENTS

Page

# LIST OF TABLES

# LIST OF FIGURES

Figure Page

Figure Page

Figure Page

# 1. Introduction

The continental shelf and slope area between West Palm Beach, Florida, and Cape Hatteras, North Carolina is commonly referred to as the South Atlantic Bight (SAB) (Figure 1.1). It is geomorphologically characterized by a broad shallow continental shelf (less than 75 m) and a relatively steep continental slope (on the order of $5 \times 10^{-3}$). South of 32°N the western edge of the Gulf Stream generally lies within 15 km of the shelf break (Bane and Brooks, 1979). Between 32° and 33°N a topographic anomaly known as the "Charleston Bump" protrudes into the Gulf Stream. By virtue of the conservation law of potential vorticity, the Stream deflects eastward. Downstream of the Charleston Bump, the wavelike Gulf Stream meanders are observed amplified in magnitude. The enlarged meanders can displace the Gulf Stream front up to 100 km east from the shelf break (Legeckis, 1979; Bane and Brooks, 1979).

The shallow shelf water is readily affected by heating, cooling and wind induced turbulent mixing. Consequently strong thermal and density contrasts (fronts), which separate the cool, fresh, usually nutrient-depleted shelf water from the warm, saline and nutrient-bearing Gulf Stream water, are persistent features along the shelf break in the SAB area. During the summer, these shelf break fronts are submerged under a warm, highly stratified surface layer (Figure 1.2(a), from Atkinson, 1977). During the winter, convective mixing due to cooling on the surface and mechanical mixing due to high winds result in vertically homogenized water on the

shelf. The shelf break front becomes narrower in the cross-shelf direction, reaching the sea surface (Figure 1.2(b), from Atkinson *et al.*, 1989). Besides the persistent shelf break front, a transient thermal front can also be formed on the mid- to outer shelf during a severe cold air outbreak in the winter season (Figure 1.3(a), from Chandler *et al.*, 1987). The formation of the front is due to the following processes: 1) the breakdown of the shelf break front by Gulf Stream meanders or strong southward winds or both; 2) shoreward intrusion of upper Gulf Stream warm water by persistent southward winds; and 3) mixing of this warm water with continental shelf water cooled by cycles of cold air outbreaks (Oey, 1986). This front, in the absence of the above mentioned forcings, is subject to enhanced diffusion due to the large gradient and quickly dissipates within a few days (Figure 1.3(b), from Chandler *et al.*, 1987). The cross-shelf density gradient during the winter season in this area is mainly controlled by the temperature distribution. The density is therefore decreasing seaward on the outer shelf, causing the shelf break front to intersect the bottom on the continental slope. The orientation of the front is unlike most of shelf break fronts in other coastal region, such as those in the Middle Atlantic Bight (See, for instance, Figure 1 in Huthnance, 1981).

The shelf break is, as we have demonstrated in the foregoing discussion, a site where fronts are formed. Frontal zones are of great interest in physical oceanography since they are regions where vertical advection and the exchange of momentum and other properties are locally intense. Physical activities taking place at fronts have a profound impact on the biogeochemical cycle in the ocean margins. In order to refine the conceptual and dynamical diagnostic and prognostic models of fronts, it is very important to characterize the frontal zone variabilities.

The objective of this study is two-fold: 1) to quantify the low-frequency current and temperature variability along the shelf break in the SAB area during winter;

Chapter 2 briefly reviews the studies carried out in the past three decades or so on the low-frequency current variabilities near the shelf break in the South Atlantic Bight area. Chapter 3 describes our data sources and statistical methods adopted in this study, namely, the basic statistical calculations, power spectral analysis and frequency-domain empirical orthogonal function (EOF) analysis. Chapter 4 presents and interprets the results of the various methods outlined in Chapter 3. The power spectra of both alongshore currents and temperatures presented in this chapter strongly suggest that there are energetic fluctuations at around a 28-day period. In an attempt to capture their characteristics and further determine the nature(s) of these fluctuations, the frequency-domain EOF analysis was performed for the frequency band centered around 0.036 cpd (corresponding to the 28-day period). Chapter 5 discusses three physical mechanisms: 1)the long-period tides, in particular, the lunar monthly tide which has a period of 27.6 days; 2)various types of shelf waves; and 3)Gulf Stream associated low-frequency fluctuations, all of which may be a contributing factor to the 28-day fluctuations. Chapter 6 summarizes and concludes this study.

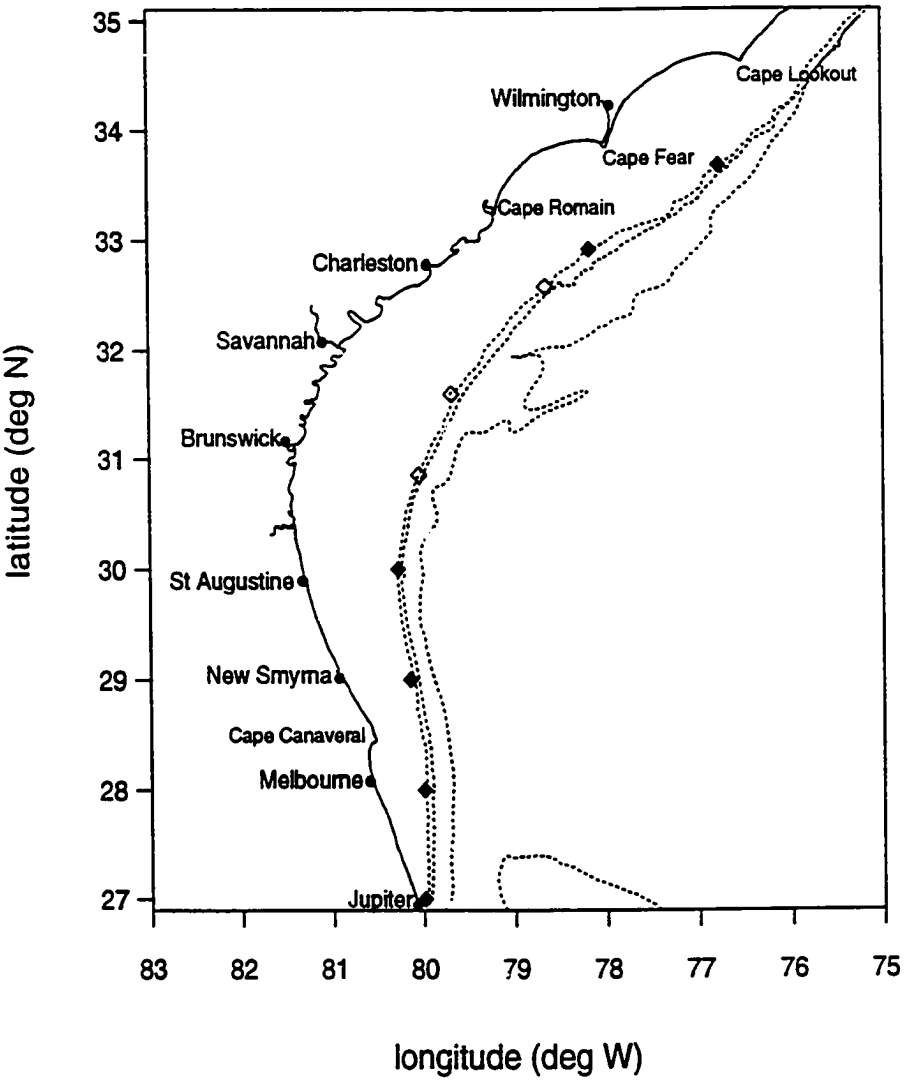


Figure 1.1. Bathymetry in the South Atlantic Bight. Dotted lines indicate 40-, 100- and 500-fathom isobaths. The open and solid diamonds indicate the locations of current meter moorings where data analyzed in this study were obtained.

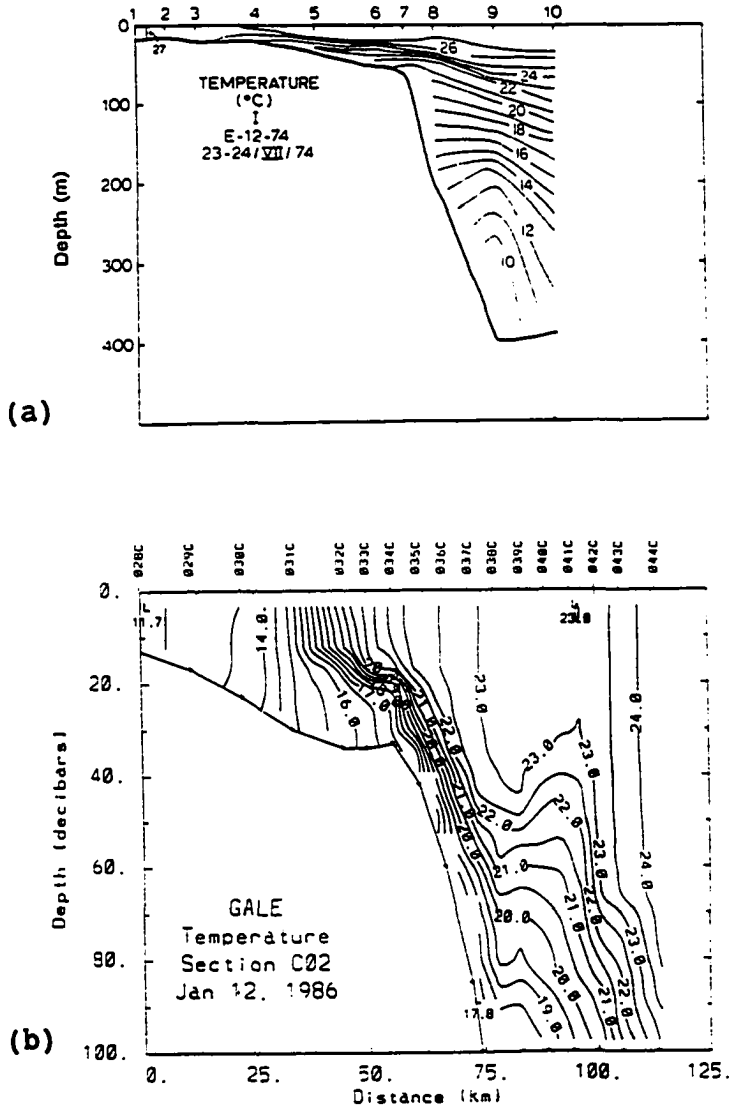


Figure 1.2. (a). Temperature section in summer, from Atkinson, 1977. (b). Temperature section in winter, from Chandler *et al.*, 1987.

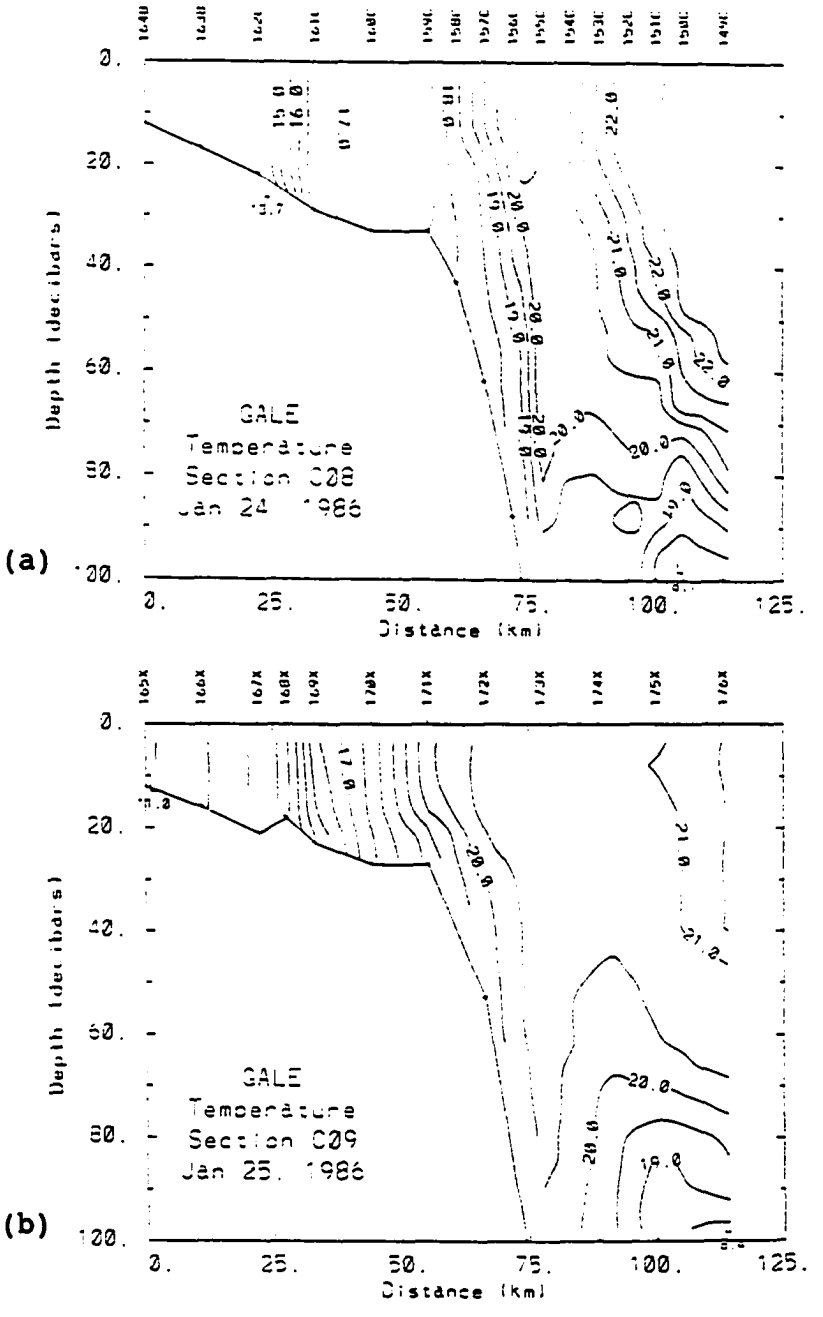


Figure 1.3. (a). Temperature section in winter, showing a "transient" thermal front at mid-shelf; (b). Temperature section in winter, one day after the section shown in (a) was taken, showing a much diffused thermal front at mid-shelf.

# 2. Low-frequency Flow and Thermal Variability along the Shelf Break

In this chapter, we review earlier studies relevant to low-frequency current variability along the shelf break in the SAB area. This is a prelude to the examination of even lower frequency variability that is the topic of this thesis. We first examine the fluctuations and the principal mechanisms governing them. To better understand the dynamics involved, we also look into the energy source of the fluctuations. This is followed by a discussion on energy budget. We end this chapter by summarizing some of the profound impacts these fluctuations may exert on the biogeochemical cycle in the SAB.

## 2.1 Controlling Mechanisms

*Gulf Stream Frontal Disturbances*

Low-frequency* current and temperature records often indicate a substantial amount of energy being concentrated in a 2-day to 2-week period band (see, for example, Düing, Mooers and Lee, 1977; Lee and Brooks, 1979; Brooks and Bane, 1981; Lee and Atkinson, 1983). Low-frequency flow variability and water exchange along the shelf break have been shown to be greatly influenced by Gulf Stream frontal disturbances which occur on the time scale of 2 days to 2 weeks. South of 32°N, the frontal eddies have been shown to propagate along the shelf break, causing an exchange of water and momentum and a net flux of nutrients to the shelf

*"Low-frequency variability" in oceanography is almost always synonymous to "subtidal variability". Here it refers to fluctuations with a time scale longer than the periods of the diurnal and semi-diurnal tides, as well as inertial oscillations.

(Lee, Yoder and Atkinson, 1991). Between 32° and 33°N the Charleston Bump appears to force an offshore meander of the Gulf Stream. Downstream of the Bump, the wavelike Gulf Stream meanders are amplified significantly (Legeckis, 1979; Bane and Brooks, 1979). These enlarged meanders have similar kinematic properties as those observed in the smaller frontal disturbances upstream and suggest a dynamic connection between the two (Brooks and Bane, 1981; Bane, Brooks and Lorenson, 1981).

Webster (1961a) first documented the characteristics of flow under the influence of the Gulf Stream meanders. He described the meander as "... a sort of skewed wave motion". Figure 2.1(a) (from Pietrafesa, Janowitz and Wittman, 1985) shows the characteristics of current and temperature records while a series of frontal waves (or meanders) moving past a current meter moored in the vicinity of the shelf break. The meander typically consists of an intense shoreward flow (lasting for 1–2 days), followed by a broad, confused flow offshore (lasting for 2–3 days). Figure 2.1(b) illustrates schematically the streamline pattern on a level plane at one instant during the event. As shown in Figure 2.1, at the meander trough (the offshore excursion of the Gulf Stream front), the water parcels experience a cyclonic rotation, accompanied by the upwelling in the center of the trough which causes a few degrees temperature drop at the meter site.

One interesting and intriguing phenomenon associated with the wavelike Gulf Stream meanders is that they frequently evolve into a series of "backward breaking" waves at the inshore edge of the Stream, a feature sometimes referred to as a "shingle" structure following von Arx *et al.* (1955). Figure 2.2 is a satellite VHRR (very high resolution radiometer) imagery of the sea surface temperature (from Lee and Atkinson, 1983). A series of "shingles" are seen to develop at 28° to 29°N and again at 32.5° to 34.5°N at the inshore edge of the Gulf Stream. The

first area is where the Gulf Stream emerges from the Straits of Florida. The second is downstream of the Charleston Bump. The "shingle" pattern indicates an "engulfment" of relatively cool coastal water and the "backward" (in contrast to "forward", the direction the lateral wave propagates to) breaking of the warmer Gulf Stream water (being referred to as the "warm filament"), as the latter wraps around the engulfed water (being referred to as the "cold-core frontal eddy"). Figure 2.3 shows the near surface temperature distributions of two such "shingle" structures, as they were mapped extensively by an AXBT (air-deployed expendable bathythermograph) survey, while they propagated from Charleston to Cape Hatteras (from Luther and Bane, 1985). A schematic representation of a fully developed Gulf Stream frontal eddy-meander field, identifying the various features, is shown in Figure 2.4 (from Lee *et al.*, 1991).

Stern (1985) used a so-called "equivalent" barotropic model to explain the development of the "shingles". The model consists of a heavy and dynamically passive layer lying beneath the shear flow in the upper layer, simulating the vertical density variation in the Gulf Stream system. The shear flow, in turn, consists of two piecewise uniform potential vorticity regions separated by a vorticity front across which the velocity is continuous. Under the long-wave approximation, an equation governing the evolution of the frontal disturbance is then obtained and solved. The solution implies that a trough ($L < 0$) propagates faster than a crest and that the continually steepening part of the front rotates in the same (cyclonic) sense as the shear of the mean flow. The model results demonstrate how a frontal disturbance eventually evolves into a "shingle" structure from the initial symmetric wave form. Stern (1985) shows that *sufficiently large* amplitude disturbances on the front separating fluid of low relative vorticity (*e.g.*, coastal water) from one with large shear (*e.g.*, the cyclonic side of the Gulf Stream) will lead to backward

wavebreaking and the entrainment of the low vorticity fluid into the shear flow. However, a vorticity front is not a necessary condition for the "shingle" structure to be developed. As a matter of fact, the real Gulf Stream front more closely resembles a density front accompanied by a strong shear flow. Given sufficiently large perturbation, a density front or a shear flow alone can harbor the "shingle" structure (Csanady, private communication).

*Atmospheric Forcing*

Atmospheric forcings enter the governing equations of water movement in two forms: atmospheric pressure fluctuation affects the vertical pressure balance, while wind stresses influence the horizontal momentum balances as the upper boundary condition. Atmospheric-pressure forcing is, in general, an insufficient process in driving currents compared to the winds (*e.g.*, Mysak, 1980; Wunsch, 1980).

Near the coast, the alongshore wind stress and subsequent sea level set-up (or set-down) dominate the circulation pattern in the SAB (*e.g.*, Lee *et al.*, 1985). Although its effect tends to decrease rapidly seaward and is usually overshadowed by the Gulf Stream disturbances at shelf edge, wind stress can at times play an important role in determining flow patterns near the shelf break. One such example is the upwelling along upper continental slope which is frequently induced by southerly winds during summer (Green, 1944; Taylor and Steward, 1959; Stone and Azarovitz, 1968; Stefánsson, Atkinson and Bumpus, 1971). Wind stress can also reinforce the onshore intrusion of the Gulf Stream water. For instance, Atkinson *et al.* (1987) found subsurface water of Gulf Stream character extended far beyond shelf break during the passage of Gulf Stream frontal eddies with the help of upwelling-favorable winds.

In analyzing a set of daily mean sea level records from Sydney to Coff's Harbor (situated 500 km to the north of Sydney), Hamon (1962) detected a northward

propagating signal of several days period. The nature of this propagating signal was unclear at the time. The question was answered shortly afterward by Robinson (1964). He developed a simple theory of coastally trapped, subinertial, nondispersive vorticity waves based on the linearized shallow water equations which included the Coriolis force and varying depth. The essence of Robinson's model is that the strongly sloping seafloor of the shelf-slope region acts as a wave guide, in the sense that motions further offshore are negligible. Robinson named these low-frequency, highly rotational wave motions "continental shelf waves". Following this early work, the subject of shelf waves has been extensively explored from both theoretical and observational aspects. Based on either sea level data or current meter data, shelf waves have been observed at many continental margins, *e.g.*, the east coast of Australia (Hamon, 1962), the west coast (Mooers and Smith, 1968; Kundu and Allen, 1976; Wang and Mooers, 1977) and east coast (Mysak and Hamon, 1969; Schott and Düing, 1976; Brooks and Mooers, 1977) of the United States. On the theoretical side, a question of particular interest is the generation mechanism of shelf waves. It was originally proposed (Robinson, 1964; Mysak, 1967a,b) that shelf waves are generated when the sea surface near the coast responds resonantly to the atmospheric fluctuations. Later, Adams and Buchwald (1969) demonstrated that the alongshore component of the wind stress is the dominant driving force. A more thorough account of this generation mechanism was given by Gill and Schumann (1974). Their formulation of the generation problem was then used by Hamon (1976) to show that along the east Australian coast, shelf waves are more likely generated by the alongshore component of the wind stress.

It seems possible that given the right condition wind forcing can excite shelf waves along the SAB, though there has been no convincing report on this account except that Düing *et al.* (1977) attributed a southward propagating signal in the

Florida Straits (situated at the southern end of the SAB) to the wind forcing. In fact, Lee and Atkinson (1983) show that the energy peaks in the power spectrum of the alongshore current along the outer shelf offset that of the alongshore wind in the frequency dimension, suggesting a weak, if at all significant, correlation between the two variables.

## 2.2 Energy Budget

Because of the proximity of the Gulf Stream front, one cannot obtain a clear picture of the energetics along the shelf break without first considering those of the Stream. Wavelike meanders along its path have been observed to be the dominant mode of oscillations in the Stream from the Straits of Florida to Cape Hatteras. They do not appear to be responses to any apparent forcing (*e.g.*, Kielmann and Düing, 1974; Brooks and Bane, 1981; Lee and Atkinson, 1983). These meanders propagate northward along the Stream with a period on the order of one week, downstream wavelengths of a few hundred kilometers, and cross-stream amplitudes of a few tens of kilometers. They have been found to play an important role in the mass and energy exchanges between deep ocean and continental shelf waters.

What is the mechanism of these wavelike meanders? Where do they draw energy from? Before the 1960's, it had been proposed by some (*e.g.*, Rossby, 1936, p.6; von Arx, 1954; Stommel, 1958) that the meanders draw their energy from the kinetic energy of the mean flow through a mechanism of frictional dissipation of the mean flow. The rate of kinetic energy transfer from mean flow to fluctuations equals the eddy momentum flux (Reynolds stress). Should the Reynolds stresses be "viscosity-like", the kinetic energy transfer is down the mean flow gradient, from mean flow to fluctuations (or perturbations, eddies). If maintained by this mechanism, the meanders could be attributed to so-called "barotropic" instability

(or ordinary shear flow instability).

Webster (1961b) was the first one to challenge this conventional concept of energy transfer in oceanography. Based on the GEK (geomagnetic electrokinetograph) current data, he calculated the lateral transfer of kinetic energy by the meanders in the surface layer for two cross-shelf transects in the SAB, one in the Florida Straits, the other in Onslow Bay. Figure 2.5 shows the results of Webster's calculations, where Figures 2.5(a) and (b) are for regions in Onslow Bay and in Florida Straits, respectively. A positive value for the transfer of energy indicates the energy is from the meanders to the mean flow, while a negative value indicates the opposite is true. As can be seen from Figure 2.5, for both regions, the energy transfer is from the meanders to the mean flow for most part of the cyclonic side of the Stream, and the maximum energy transfer occurs in the region of maximum shear. Furthermore, it was found that the cross-stream integral of energy transfer is positive in Onslow Bay, indicating a net transfer of kinetic energy from the meanders to the mean flow. Webster concluded from his results that the mean flow was enhanced by the kinetic energy of the meanders, and that the meanders should derive their kinetic energy from sources other than the kinetic energy of the mean flow. The source of the energy maintaining the meanders remained to be found.

Webster (1961b) noticed the similarity between the profiles of velocity and kinetic energy transfer in the Gulf Stream system and in an atmospheric jet system (Starr, 1954). He further suggested an analogy between the two systems by stating:

> "It is possible that necessary frictional dissipation is carried out by perturbations of a scale smaller than the meanders. If so, then the energy balance is analogous to that in the atmosphere, where the mean zonal flow is sustained by large-scale eddies, but dissipated by small-scale eddies and molecular viscosity."

Schmitz and Niiler (1969) carried out the same calculations as Webster (1961b) using data from their free-fall instrument measurements. Their results confirm

Webster's in that there is a narrow zone in the region of lateral cyclonic shear where intense kinetic energy transfer occurs. The net cross-stream integral of energy transfer is, however, not significantly different from zero. Schmitz and Niiler thus questioned the necessity of an external energy source. According to their arguments, the kinetic energy is *redistributed* between fluctuations and mean flow: it is transferred intensely to the mean flow in a narrow zone of cyclonic side of the Stream, while an equal amount is transferred from the mean flow less intensely over a wider zone covering most of the rest of the Stream. Overall, the energy transfer merely carries out an internal adjustment requiring no external energy source.

The conclusion drawn from the energetics calculations of Webster (1961b) and Schmitz and Niiler (1969) have provoked extensive discussion in the literature on the driving mechanism of the meanders (*e.g.*, Orlanski and Cox, 1973; Killworth, Paldor and Stern, 1984; Luther and Bane, 1985; Oey, 1988). The general approach is an instability analysis based on the assumption that the dominant meanders are natural mode oscillations of the Gulf Stream. Much insight about the dynamics of the meanders has been gained as a result. Luther and Bane (1985) analyzed linear wave motion superimposed on steady alongshore flow over sloping bottom topography. The background velocity field resembles the Gulf Stream, and is in geostrophic balance with the mean density field. The momentum equations governing the perturbations are ageostrophic. The fluid is assumed to be inviscid, incompressible, nondiffusive, and continuously stratified. The study sought small-amplitude alongshore propagating perturbations with real frequency and complex alongshore wavenumber. Of the four eigenmodes identified, one particular eigenmode with a period of eight days (referred to as the eight-day wave hereafter) exhibited a perturbation velocity and buoyancy field similar to Gulf Stream mean-

ders. The instability mechanism of this eight-day wave was the mixed barotropic-baroclinic type, with the majority (about 80%) of the perturbation energy derived from the potential energy of the background flow. The potential energy conversion occurs in the center of the background current, the region of maximum isopycnal slope. The kinetic energy conversion occurs in the cyclonic frontal zone, where the maximum horizontal current shear is found. The energy conversion associated with the wave motions extracts the potential energy from the background by eroding the horizontal temperature gradient, while returning energy to the background by increasing the horizontal shear.

The eight-day eigenmode found in Luther and Bane's numerical investigation reproduces many observed features within the limits of linear theory. One, in particular, is the skewed vertical velocity pattern near the surface, resembling the observed meander and warm filament structure. This skewness means that $u$ (cross-shore velocity) and $w$ (vertical velocity) are not in phase so that there is no contribution from $w$, and that $u$ and $b$ (buoyancy anomaly) are not in quadrature signifying the release of potential energy from the background flow to the perturbation. However, the linear model does not reproduce the observed skewed wave form, as small-amplitude linear instability theory is inherently incapable of simulating finite wavelike motions. It is not certain, therefore, to what extent these linear results can be applied to the Gulf Stream system. Also, the numerical solutions depend on the background flow. While the flow profile used by Luther and Bane agrees reasonably well with observation on the cyclonic side of the Stream, it is unrealistic on the anticyclonic side of the Stream.

Oey (1988) took a step forward in analyzing the same problem. He used a simplified model of the Gulf Stream front near a vertical wall (simulating the continental slope) over an ocean basin of a constant depth. The dynamics governing

frontal instabilities, meanders and eddies in his case depends primarily on two well-defined ratios: $L_0/R_0$ and $h_0/H_0$, the former being the ratio of the cross-stream distance of the stream axis from the slope ($L_0$) to the baroclinic Rossby radius of deformation ($R_0$), the latter being the ratio of the upper layer depth ($h_0$) to the ocean basin depth ($H_0$). Oey used a nonlinear, time-dependent, three-dimensional model to study this interdependency. The computed flow displays realistically skewed waves (meanders), with gradually varying offshore currents at troughs followed by sudden shoreward turning upstream of the following crest. The model results show strong dependence on the available potential energy of the system, which is proportional to $(h_0/H_0)(L_0/R_0)$. At the initial instant, the perturbed field contains a finite amount of potential energy due to the small-scale wave introduced. Within a time span of a few inertial periods, the flow undergoes inertial oscillations, while energy is being transferred from the perturbation field to the mean field as short waves decay and rotational-dominated long waves evolve on a smoothed-out front. This result agrees with laboratory frontal experiments of Griffiths and Linden (1982) in which short waves were observed at the frontal region in the first one or two rotational periods before longer waves evolved. The duration time of decay of the short waves varies inversely with APE. After initial adjustments perturbation energy grows exponentially until the process of frictional "spin-down" sets in.

A typical pathway of energy conversion is given in Figure 2.6 (from Oey, 1988). Thus, PEP is provided by initial APE due to the initial perturbation*, and sub-

*In Oey's (1988) numerical investigations, the initial perturbation is produced by explicitly introducing short ($2\Delta y$) waves. While in laboratory experiments (such as those of Griffiths and Linden, 1982) and conceivably in nature, the initial perturbations can be produced by turbulent mixing in the form of Kelvin-Helmholtz billows (Gill, 1982, p.325).

sequently loses its energy through viscous dissipation and also to kinetic energy of the perturbation field (KEP). The kinetic energy conversion between perturbation field and mean field takes place through:

$$KEC = \int (-uv\bar{v}_x - vw\bar{v}_z)dy \tag{2.1}$$

where a positive value indicates the energy transfer is from mean field. The perturbation field not only gains its kinetic energy from PEP, but also from the mean vertical shear through the second term in equation (2.1). Nonetheless, the energy conversion through equation (2.1) is generally from perturbation field to mean field, because the first term is negative and has an absolute value larger than the second term. The net result is a depletion of potential energy of the mean field *via* the perturbation and a feedback of kinetic energy to the mean field. The energy conversion has a characteristic of baroclinic instability. The model results also show that perturbation kinetic energy is transferred to the mean stream on the cyclonic side while the mean field feeds the perturbation field on the anti-cyclonic side, which agree with the observations (*e.g.*, Webster, 1961b).

Based on the evidence obtained from field and laboratory experiments, Csanady (1989) summarized the characteristics of energy balance in a western boundary current or other intense oceanic jet as the following:

1. Potential energy is converted into kinetic energy as primary eddies (meanders and eddies) grow on a baroclinic current;
2. Eddy-mean flow kinetic energy transfer proceeds both ways, but contributes little to eddy energy balance over the cross section of a boundary current;
3. The primary eddies transfer their energy to the surrounding fluid by an essentially inviscid mechanism and are themselves unaffected by energy dissipation, much as the "energy containing eddies" of laboratory turbulence;

4. Secondary eddies* and topographic waves spreading out over the region surrounding the boundary current eventually dissipate their energy in bottom boundary layers.

## 2.3 Implication for the Biogeochemical Cycle

The upper thermocline of the Gulf Stream contains a rich load of nutrients, such as nitrate, phosphate and silicate, and is sometimes referred to as the "nutrient stream". The transport of new nutrients from the "nutrient stream" provides a major food source for a succession of biological responses (see, for instance, Yoder *et al.*, 1983; 1985; Paffenhöfer, Sherman and Lee, 1987). It is found that along-isopycnal inflow of new nutrients from the subtropical gyre can triple the nutrient transport between the Florida Straits and the Mid-Atlantic Bight (Pelegri and Csanady, 1991). Geostrophic uplifting of the thermocline on the western side of the gyre in the Gulf Stream brings the 10- and 20-$\mu M$ nitrate concentrations to within 100 and 200 m below the surface, respectively. Unlike in the MAB, where the Gulf Stream is separated from the shelf by the slope sea (Csanady, 1990), the Gulf Stream interacts directly with the shelf waters in the SAB through the mechanism of baroclinic instability that leads to the growth of meanders and frontal eddies. Atkinson *et al.* (1983) found evidence from climatological hydrography that active exchange of water properties occurs across the shelf break: an estimated 80% of the shelf water (by volume) is replaced by Gulf Stream water per month.

A shelf edge exchange model for the SAB is shown in Figure 2.4, where waters with nitrate concentration exceeding 10 $\mu M$ is shaded. The Gulf Stream flows

*"Secondary eddies" are presumably eddies of smaller spatial scales. The energy transfer between them and the surrounding fluid is hypothesized as viscousity-like, in that they lose energy through viscous dissipation. Very little is actually known about them to date.

along the shelf edge over almost entire stretch of the SAB, except in the area of Long Bay (immediately downstream of the Charleston Bump) where the Stream can be displaced offshore for periods of 1 to 3 months (Bane and Dewar, 1988; Lee *et al.*, 1989). Frontal eddies extend across the outer shelf, causing direct interaction of the Stream with shelf water. Upwelling and onshore transport in the cold core of frontal eddies "pumps" new nutrients from the "nutrient bearing strata" (NBS) directly onto the outer shelf and into the euphotic zone for biological uptake. For instance, Yoder *et al.* (1983) found phytoplankton (diatom) blooms in the frontal eddies upwelled waters that match the physical dimensions of eddy features; Ishizaka (1990) analyzed CZCS (coastal zone color scanner) images from the 30° to 32°N region together with optimally interpolated flow and temperature fields from the GABEX (Georgia Bight Experiment) I data set to show that the outer shelf chlorophyll distributions were produced by the passage of the frontal eddies.

Since long time series of biological measurements are not available for southeastern shelf waters, seasonal, annual and interannual effects of Gulf Stream-induced upwelling on productivity of this region has to rely on models, satellite imagery and extrapolation of limited field data. Long time series of current and temperature data are extremely useful in estimating nutrient fluxes. For example, O'Malley *et al.* (1978) found a linear correlation between temperature and new nitrate from the NBS for temperature less than 20°C as:

$$[NO_3] = 53.0 - 2.6T$$

Lee and Atkinson (1983) used this empirical relationship to calculate nitrate flux profiles at the shelf break from moored current and temperature time series. This calculation led to an estimate of nitrogen input from the NBS to the outer shelf area. Using Redfield's carbon:nitrogen ratio of phytoplankton biomass, Lee *et al.*

(1991) were able to further estimate the annually-averaged potential new carbon production rate. These papers all indicate that instabilities on the Gulf Stream front are an important controlling mechanism for nutrient supplies to the shelf and thus are a key factor in the response of biological systems.

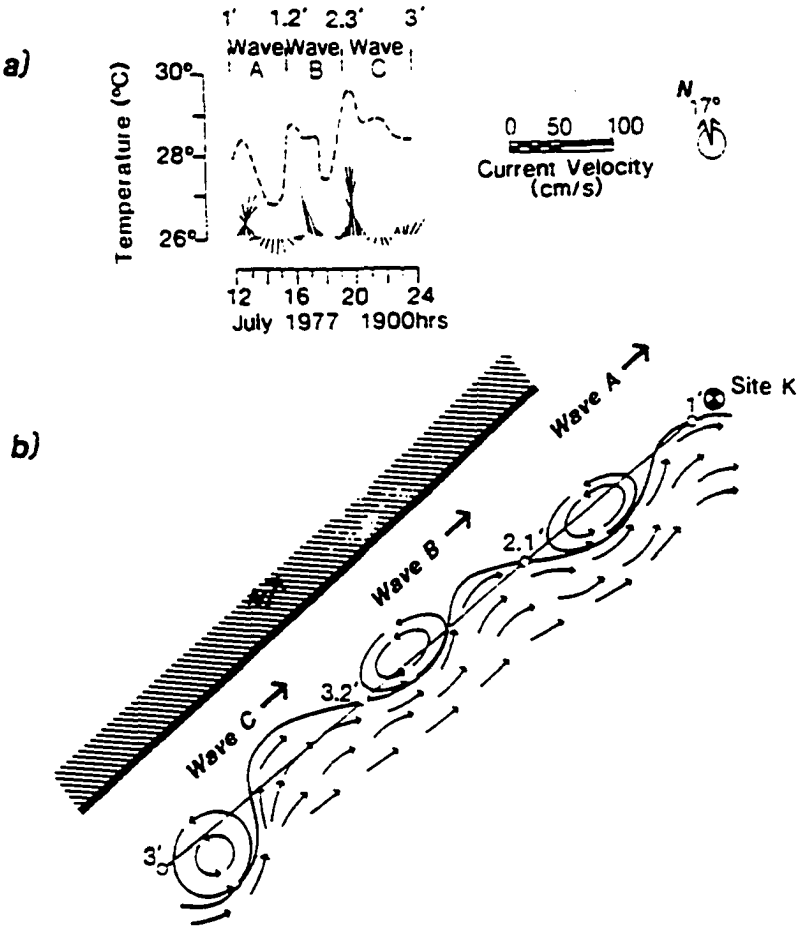


Figure 2.1. (a). Time series of current and temperature from Site K-top during passage of Gulf Stream frontal waves. (b). Schematic streamline pattern of three consective Gulf Stream frontal meanders moving past Site K. Both (a) and (b) are from Pietrafesa *et al.*, 1985.

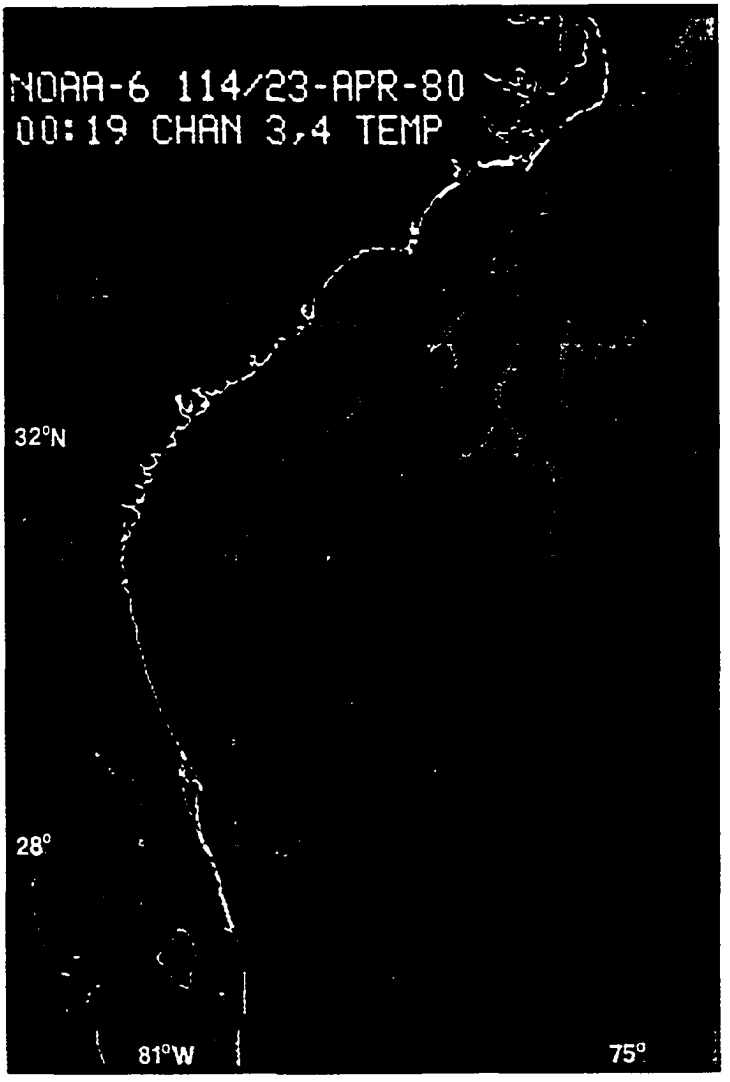


Figure 2.2. Satellite VHRR thermal image of the Gulf Stream on April 22, 1980, from Lee, Yoder and Atkinson, 1991.

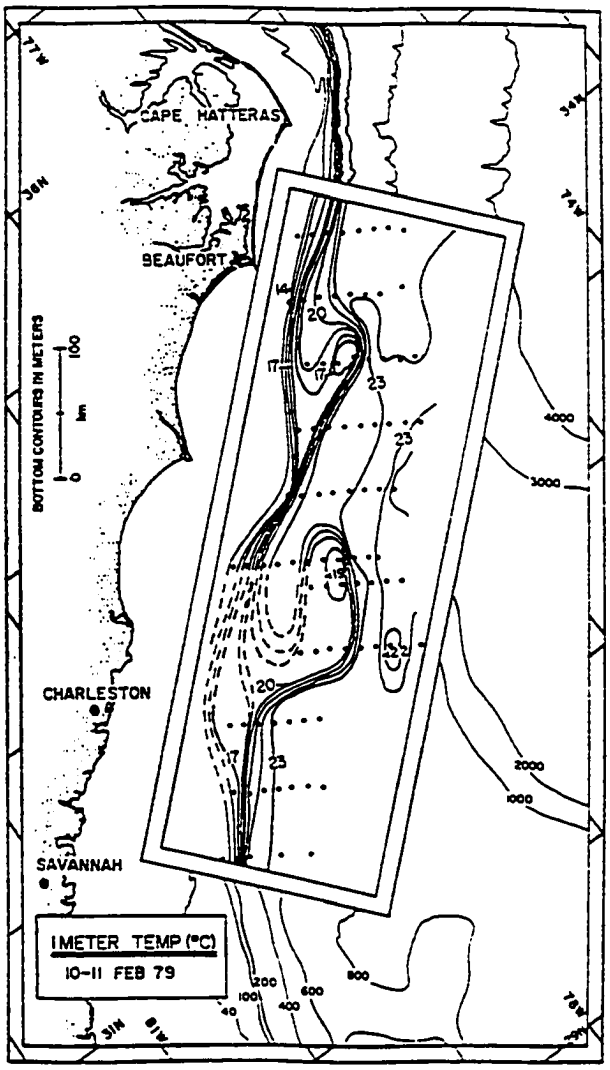


Figure 2.3. Near surface temperature distribution of two "shingle" structures, as mapped by an AXBT survey, from Luther and Bane, 1985.

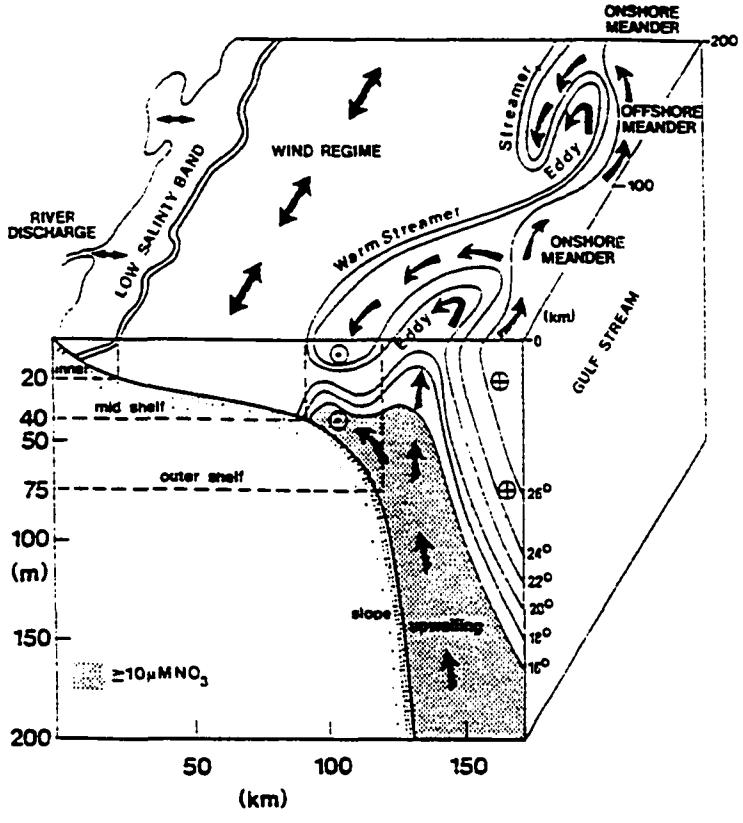


Figure 2.4. A schematic representation of a fully developed Gulf Stream frontal eddy-meander field, various features are identified, from Lee, Yoder and Atkinson, 1991.

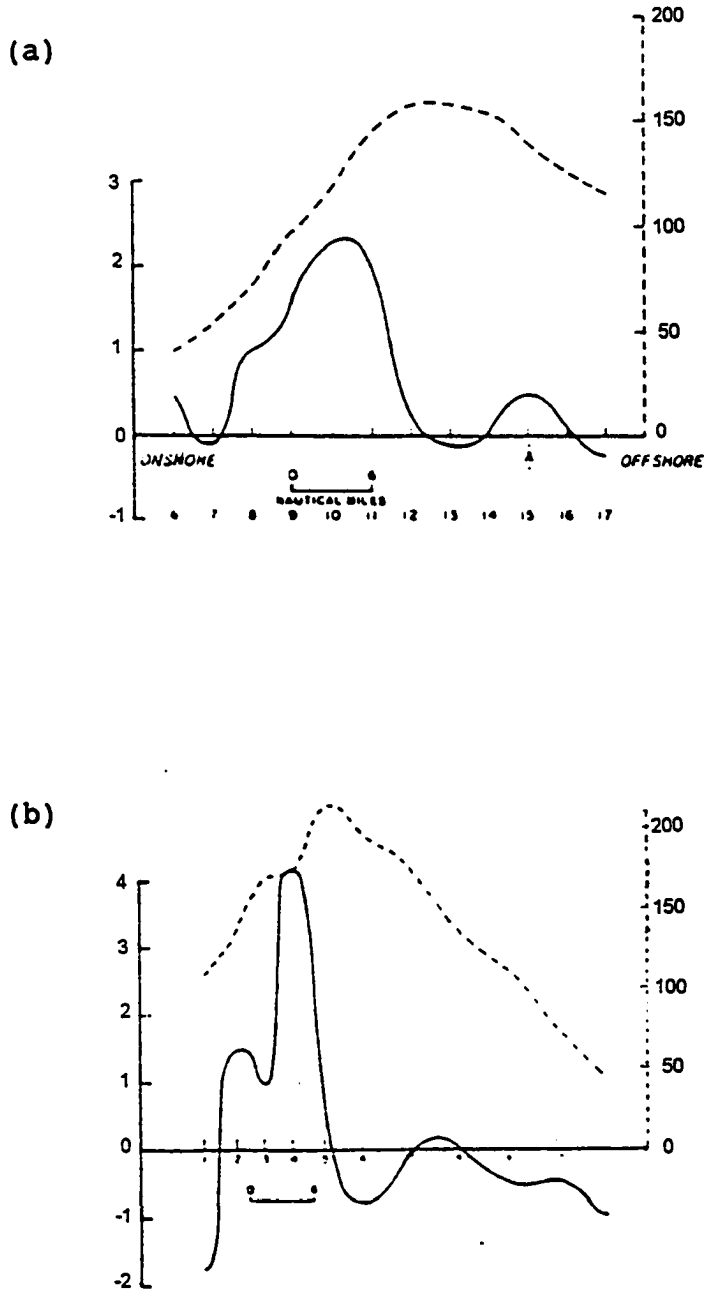


Figure 2.5. (a). A cross-shelf transect in Onslow Bay, solid line indicates eddy kinetic energy transfer rate in $10^{-2}$ ergs/cm$^3$/sec (a positive value means energy is from the meander to the mean flow), dash line indicates the alongshore velocity in cm/sec. (b). a cross-shelf transect in Florida Straits, others same as in (a), both (a) and (b) are from Webster, 1961b.

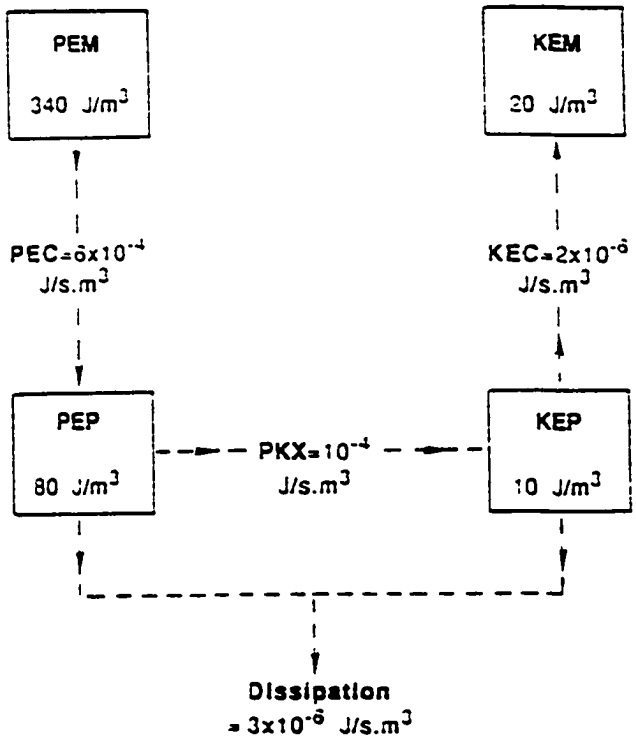


Figure 2.6. A sample energy conversion pathway from a numerical calculation, by Oey, 1988.

# 3. Data Sources and Statistical Methods

## 3.1 Data Sources

The current meter data analyzed in this study were from a number of field experiments: the second leg of Florida Atlantic Coast Transport Study (FACTS-II); Winter 76/77; SAI Long Term Measurement and Blake Plateau Array. The locations of current meter moorings are shown in Figure 3.1. Further details about the data are given in Table 3.1. The data sets share one common feature in that they were all collected in the vicinity of the shelf break during winter season. Current meter data from FACTS-II have been previously analyzed by Lee *et al.* (1986). Some were analyzed in Lee, Yoder and Atkinson (1991).

As can be seen in Figure 3.1, the selected current meter array covers the SAB from Jupiter, Florida (27°N) to Wilmington, North Carolina (33.4°N). The distances between adjacent moorings ranges from 59 km to 146 km. The temporal spans of individual time series ranges from 47 days to 223 days. Niskin Winged Current Meters (NWCM) were used at all stations except at BTOP, ETOP and EBOT, where Aanderaas Current Meters (AACM) were used.

During data preprocessing, hourly temperature and eastward and northward current components data were filtered with a forty-hour low-pass (40-HLP) Lanczos filter and subsampled at six-hour interval. Signals of diurnal and semi-diurnal tides, inertial oscillations and other high-frequency motions were removed this way. Current components were then rotated to align with the local bathymetry, with $u$ being perpendicular and $v$ parallel to the isobaths. The angles of rotation for all

moorings are given in Table 3.1. Since the temperature data exhibit predominant seasonal variations, the seasonal trends were first fitted, assuming they have a sinosoidal form with a period of 365 solar days, by the least-square method and subsequently removed from the records before any spectral analysis was applied. The time spans of the current meter data did not all coincide with each other. The best concurrent records were from the transects at 27°N, 28°N, 29°N, 30°N, 32.5°N and 33.4°N (solid diamonds shown in Figure 3.1), from early October, 1984 to early March, 1985. Data from other locations (open diamonds in Figure 3.1) are good for time domain calculations and individual power spectrum calculations only.

## 3.2 Basic Statistical Methods

There are two basic types of approach to the time series analysis: "time domain" (or "correlation") approach and "frequency domain" (or "spectral") approach. The time domain approach concerns the mean, variance or standard deviation, autocorrelation function and cross-correlation function. The frequency domain approach, on the other hand, transforms the information obtained in the time domain into the frequency domain by calculating the power-spectral density function (or power spectrum) and cross-spectral density function (or cross-spectrum). The time domain approach is often used to capture the "mean" and "variability" of an observed variable, while the frequency domain approach is often used to analyze the periodicity of a time series. In this section we will describe the basic statistical methods used in this study.

### 3.2.1 Statistics in Time Domain

Two of the most frequently calculated quantities in the time domain approach are the *sample mean* and *sample standard deviation.* For a time series $\{x_t\}$ with

the number of observation being $N$, the sample mean (or ensemble average) is defined as

$$\bar{x} = \frac{1}{N}\sum_{t=1}^{N} x_t. \tag{3.1}$$

The sample standard deviation $\sigma$ is defined as

$$\sigma = \sqrt{\frac{1}{N}\sum_{t=1}^{N}(x_t - \bar{x})^2}. \tag{3.2}$$

To obtain information about the correlation structure *within* each process, one needs to estimate the auto-covariance function $R(\tau)$. For each time lag $\tau$ ($\tau = m\Delta t, m = 0, \pm 1, \pm 2, \cdots, \pm(N-1)$), $R(\tau)$ measures the covariance between pairs of values in the process separated by an interval of length $\tau$ if defined as

$$R(\tau) = \mathrm{E}[\{x_t - \mu\}\{x_{t+\tau} - \mu\}],$$

where E[ ] is the expectation operand, $\mu$ is the "true" mean (not the *sample mean*) of the process $\{x_t\}$. To estimate this quantity, we used the "biased estimate", following Priestley's terminology (Priestley, 1981, p323), as

$$\hat{R}(\tau) = \frac{1}{N}\sum_{t=1}^{N-|\tau|}(x_t - \bar{x})(x_{t+\tau} - \bar{x}). \tag{3.3}$$

Similar to the autocovariance function, the cross-covariance function describes the correlation structure *between* processes, and is defined by

$$R_{jk}(\tau) = \mathrm{E}[\{x_{j,t} - \mu_j\}\{x_{k,t+\tau} - \mu_k\}],$$

provided that $\{x_{j,t}\}$ and $\{x_{k,t}\}$* are jointly stationary.

We used a natural extension of Eq.3.3 to estimate $R_{jk}(\tau)$

$$\hat{R}_{jk}(\tau) = \frac{1}{N}\sum_{t}(x_{k,t} - \bar{x})(x_{j,t+\tau} - \bar{x}), \quad \tau = 0, \pm 1, \cdots, \pm(N-1), \tag{3.4}$$

where the summation goes from $t = 1$ to $N - \tau$ when $\tau \geq 0$, and from $t = (1 - \tau)$ to $N$ when $\tau < 0$.

*All processes considered here are real-valued.

### 3.2.2 Statistics in Frequency Domain

The frequency domain approach studies the behavior of the time series in frequency domain by calculating various spectra. To justify this approach, one has to assume that the process is *stationary*, meaning that the statistical properties of the process do not change over time. In practical applications, though, the best we can hope for is that the process, over the observed time span, would not depart "too far" from the stationarity for the results of the subsequent analysis to be invalid. In this approximate sense, we consider the (forty-hour low-pass filtered) velocity components over the course of several months to be *stationary*, while temperature, apparently exhibiting seasonal trend, to be *non-stationary*. It was for this reason the temperature data were first transformed into stationary forms by subtracting the seasonal trends (detrending).

**Power Spectrum**

Power spectrum displays the distribution of energy density (or "power") in the frequency dimension. It shows the relative contribution of various components each having their own characteristic frequencies. In this study the individual power spectra were calculated using Fourier cosine transform of the autocovariance function. Each time series was first demeaned (in the case of temperature, the time series was first detrended and then demeaned), and then Fourier transformed using the Parzen window (Priestley, 1981, p443). This window has two superior properties: 1) it produces non-negative estimates of the spectral density function; and 2) it provides the maximum equivalent degrees of freedom for a given $N/M$ ratio (Priestley, 1981, P467, Table 6.2), where $N$ denotes the number of observations in a time series, $M$ ($< N-1$) is called the "window parameter" and, ideally, is chosen to match the rate of decay of the autocovariance function.

Let $\hat{R}(s)$ be the estimate of the autocovariance function $R(s)$ of a demeaned

time series $\{x_i\}$, in mathematical terms, the discrete Fourier cosine transform is carried out as

$$\hat{h}(\omega) = \frac{1}{2\pi} \sum_{s=-(N-1)}^{(N-1)} \lambda(s)\hat{R}(s)\cos(\omega s), \tag{3.5}$$

where $\hat{h}(\omega)$ is the estimated power spectrum, $\omega$ is the frequency at which power density is estimated, $\lambda(s)$ is called the "lag window". For the reason mentioned in the last paragraph, the Parzen window was chosen for the calculation. This window has the following form (Priestley, 1981, p443),

$$\lambda(s) = \begin{cases} 1 - 6(s/M)^2 + 6(|s|/M)^3, & |s| \leq M/2, \\ 2(1 - |s|/M)^3, & M/2 \leq |s| \leq M, \\ 0, & |s| > M. \end{cases} \tag{3.6}$$

**Cross-spectrum**

Cross-spectrum reveals the relation between two time series at a certain frequency. It is generally-complex valued, and may be written in the form

$$h_{jk}(\omega) = c_{jk}(\omega) - iq_{jk}(\omega),$$

where $c_{jk}(\omega)$ and $\{-q_{jk}(\omega)\}$ denote the real and imaginary parts of $h_{jk}(\omega)$, respectively. The function $c_{jk}(\omega)$ is called the co-spectrum, and $q_{jk}(\omega)$ is called the quadrature spectrum, of time series $\{x_{j,t}\}$ and $\{x_{k,t}\}$. Alternatively, $h_{jk}(\omega)$ can be written in the "polar" form

$$h_{jk}(\omega) = \alpha_{jk}(\omega)\exp\{i\phi_{jk}(\omega)\},$$

where

$$\alpha_{jk}(\omega) = |h_{jk}(\omega)| = \sqrt{c_{jk}{}^2(\omega) + q_{jk}{}^2(\omega)}$$

and

$$\phi_{jk}(\omega) = \arctan\{-q_{jk}(\omega)/c_{jk}(\omega)\}.$$

The function $\alpha_{jk}(\omega)$ is called the cross-amplitude spectrum, and $\phi_{jk}(\omega)$ is called the phase spectrum. When $\alpha_{jk}(\omega)$ is scaled by the root of the product $h_{jj}(\omega) \cdot h_{kk}(\omega)$, we obtain the coherency spectrum

$$|w_{jk}(\omega)| = \sqrt{\frac{c_{jk}{}^2(\omega) + q_{jk}{}^2(\omega)}{h_{jj}(\omega)h_{kk}(\omega)}}.$$

The coherency spectrum $w_{jk}(\omega)$ may be interpreted as a correlation coefficient between two components $\{x_{j,t}\}$ and $\{x_{k,t}\}$ at frequency $\omega$, with the maximum being unity and the minimum being zero; while the phase spectrum $\phi_{jk}(\omega)$ represents the "average value" of the phase shift between two components $\{x_{j,t}\}$ and $\{x_{k,t}\}$ at frequency $\omega$.

As an analogy to Eq.3.5, we estimated the cross-spectrum as

$$\hat{h}_{jk}(\omega) = \frac{1}{2\pi} \sum_{s=-(N-1)}^{(N-1)} \lambda_N(s)\hat{R}_{jk}(s)\exp(-i\omega s), \tag{3.7}$$

or, in terms of co- and quadrature spectrum,

$$\hat{c}_{jk}(\omega) = \frac{1}{2\pi} \sum_{s=-(N-1)}^{(N-1)} \lambda_N(s)\hat{R}_{jk}(s)\cos(\omega s) \tag{3.8}$$

$$\hat{q}_{jk}(\omega) = \frac{1}{2\pi} \sum_{s=-(N-1)}^{(N-1)} \lambda_N(s)\hat{R}_{jk}(s)\sin(\omega s) \tag{3.9}$$

where $\lambda_N(s)$ is the Hanning lag window for this study, $\hat{R}_{jk}(s)$ is the estimate of cross-covariance function.

## 3.3 Empirical Orthogonal Function Analysis

In analyzing multiple time series concurrently collected at a spatial array, we need to find a quantative and objective means to extract as much statistical information as possible. Often wave-like oscillations are present in the time series we obtain. It is highly desirable to define the number of significant wave disturbances present in certain frequency intervals and to separate the total disturbance

field into individual wave components. A "wave" is defined observationally by the presence of statistically significant spatial and inter-parameter correlations which can be interpreted in terms of a diagnostic physical model. The method we have adopted to achieve such a goal is the empirical orthogonal function (EOF) analysis (also referred as the principal component analysis). As in basic statistical methods we outlined in the last section, there are two approaches in this technique as well: the time-domain and the frequency-domain EOF analysis. Since we are primarily interested in looking for the propagating wave signals in this study, the frequency-domain approach (also referred to as the complex eigenvector analysis) is more suitable in this case. In this section we will summarize the fundamental idea and the general procedure of the EOF analysis. This is followed by a discussion on the mode-selection rules. Finally we will give a brief account of the adventages and shortcomings inherit in this technique.

### 3.3.1 Basic Idea of the EOF Analysis

Assuming the time series under consideration are well-correlated in a specified frequency band, the basic idea of the frequency-domain EOF analysis is that each time series may be expressed as a linear combination of a same set of base functions (or modes) which are mutually orthogonal to each other, in a manner similar to the Fourier series expansion. In the case of the frequency-domain EOF expansion, each base function (mode) happens to be a time series representing the "typical" temporal behavior associated with this mode, while the complex-valued coefficients, which constitute the spatial part of the mode, give the relative amplitudes and phase differences of the coherent signals across the array.

To summarize the kind of data available, we typically have data at $L$ different levels for $M$ different stations and $N$ different variables for a total of $p = L \times$

$M \times N$ records. They define a $p$-dimensional vector-valued time series which can be subjected to the cross-spectral analysis. For any given frequency band, the cross-spectra between all possible pairs of variables can be displayed in a $p \times p$ matrix, the cross-spectrum matrix. The diagonal elements of this matrix are the power spectral estimates obtained by crossing each time series with itself. The off-diagonal elements are complex, the real part being the co-spectrum and the imaginary part being the quadrature spectrum.

To better understand the development of the frequency-domain empirical orthogonal function analysis technique, we first review the procedure of the time-domain EOF analysis. Let us suppose the time series has components $u_j(t)$. Then a covariance matrix $U_{jl}$* can be generated by

$$U_{jl} =< u_j(t)u_l(t) > \tag{3.10}$$

where the angular brackets denote an ensemble average. In the method of empirical orthogonal functions we introduce new variable $z_i(t)$, which is statistically uncorrelated. This is done by finding eigenvectors of the symmetric matrix $U_{jl}$. The $j$th element of the $i$th eigenvector $e_{ij}$ gives the desired transformation

$$z_i(t) = \sum_{j=1}^{p} e_{ij}u_j(t). \tag{3.11}$$

The covariance matrix of the $z_i(t)$ is diagonal, *i.e.*, all off-diagonal elements are identically zero, or, if we use the notation

$$\delta_{ik} = \begin{cases} 1 & \text{if} \quad i = k \\ 0 & \text{if} \quad i \neq k, \end{cases}$$

then,

$$z_{ik} =< z_i(t)z_k(t) >= \delta_{ik}\lambda, \tag{3.12}$$

*Throughout this thesis, $i$ and $k$ are designated to the $i$th and $k$th eigenvectors, while $j$ and $l$ are designated to the $j$th and $l$th elements of parameter space.

where $\lambda_i$ are the eigenvalues of $U_{jl}$, which are real because $U_{jl}$ is symmetric.

For proper normalizations of the $u_j(t)$ as we will discuss later, we can measure the relative importance of the $i$th component of the new time series $z_i(t)$ by its contribution to the trace of the covariance matrix,

$$T = \sum_{j=1}^{p} U_{jj} = \sum_{i=1}^{p} Z_{ii} = \sum_{i=1}^{p} \lambda_i, \tag{3.13}$$

which is simply the sum of the variances of the $u_j(t)$. In other words, $z_i(t)$ contributes the fraction $\lambda_i/T$ of the total variance of the series. Usually most of the variance in the time series is carried out by only a few $z_i(t)$ with relatively large $\lambda_i$. For convenience, we order the $z_i(t)$ in order of decreasing magnitude of the $\lambda_i$.

In the foregoing discussion, we have demonstrated how the original time series $u_j(t)$ can be expressed in terms of a new time series of uncorrelated variables $z_i(t)$

$$u_j(t) = \sum_{i=1}^{p} e_{ij} z_i(t). \tag{3.14}$$

This is accomplished by means of linear transformation of the original series making use of the eigenvectors of its covariance matrix. The eigenvector component $e_{ij}$ determines the sign and relative weight of the contribution which the $j$th input variables makes to the $i$th transformed variable (or the base function). Thus, each eigenvector $\mathbf{e}_i$ determines a structural relationship between the input variables in a manner completely analogous to the sine and cosine functions of a Fourier series expansion in the parameter domain.

The important properties of the empirical orthogonal function representation can be summarized as follows (Wallace and Dickinson, 1972):

1. The eigenvectors are orthogonal in the parameter domain because the covariance matrix is symmetric. They can be normalized to unity so that

$$\sum_{j} e_{ij} e_{kj} = \delta_{ik}. \tag{3.15}$$

2. The elements of the transformed time series $z_i(t)$ are uncorrelated at zero lag (*cf*, Eq.3.12).
3. The variance explained by the $i$th empirical orthogonal function is given by

$$< z_i^2 >= \lambda_i, \tag{3.16}$$

where $\lambda_i$ is the $i$th eigenvalue of the covariance matrix $U_{jl}$. Summing over all the eigenvalues, we get the trace of $Z_{ik}$ which is the total variance of all the variables, and also the trace of the covariance matrix $U_{jl}$.

4. The fraction of the variance of the $j$th parameter explained by the $i$th empirical orthogonal function is given by the square of the coefficient of the correlation between the $u_j(t)$ and $z_i(t)$ series, which can be expressed in the form

$$\gamma_{ij} = \frac{< u_j z_i >^2}{< u_j >^2 < z_i >^2} = \frac{e_{ij}{}^2 \lambda_i}{< u_j{}^2 >}. \tag{3.17}$$

From this relation one can compute the amplitude of the fluctuations of each parameter $u_j$ in each of the empirical orthogonal functions.

One can readily extend the theory just summarized to the frequency domain by using the eigenvectors of the cross-spectrum matrix in place of the covariance matrix to represent the parameter space structure of a multiple time series. The eigenvectors of the cross-spectrum matrix are not directly applied to the original time series as in the time domain case demonstrated in Eq.3.11. Here, they are applied to an *augmented* time series involving the original time series and its time derivative. The real part of the new time series generated in this manner has properties analogous to those of $z_i$ defined by Eq.3.11.

The time series $u_j(t)$ has the spectral representation

$$u_j(t) = \mathrm{Re} \int_0^\infty \exp(i\omega t) dA_j(\omega), \tag{3.18}$$

where $dA_j(\omega)$ is a random increment function for an interval $d\omega$, which is uncorrelated with $dA_j(\omega')$ if $\omega' \neq \omega$ (*e.g.*, Yaglom, 1962, pp. 37, 81). Formation of the $u_j(t)$ correlation matrix with lag $\tau$ gives

$$U_{jl}(\tau) =< u_j(t)u_l(t+\tau) >= \frac{1}{2}\mathrm{Re}\int_0^\infty \exp(-i\omega\tau) < dA_j(\omega)d\bar{A}_l(\omega) >, \qquad (3.19)$$

where $\bar{A}_l$ denotes the complex conjugate of $A_l$. For $\tau = 0$, $U_{jl}(\tau)$ reduces to the covariance matrix defined by Eq.3.10. The covariance matrix formed by the $dA_j(\omega)$ gives the contribution to $U_{jl}(\tau)$ by the cross-spectrum $\Phi_{jl}(\omega)$ in an infinitesimal frequency interval $d\omega$,

$$\Phi_{jl}(\omega)d\omega = \frac{1}{2} < dA_j(\omega)d\bar{A}_l(\omega) > . \qquad (3.20)$$

We define a filtered time series $u_j^f(t)$ by removing all spectral components outside the frequency interval $\omega$ to $\omega + d\omega$, *i.e.*,

$$u_j^f(t) = \mathrm{Re}[\exp(i\omega t)dA_j(\omega)]. \qquad (3.21)$$

The filtered correlation matrix $U_{jl}^f(\tau)$ is then

$$U_{jl}^f(\tau) = \mathrm{Re}[\exp(-i\omega t)\Phi_{jl}(\omega)]. \qquad (3.22)$$

Since $\Phi_{jl}$ is a Hermitian matrix*, we know that it also has a complete set of orthogonal eigenvectors $\mathbf{e}_i$ and real eigenvalues $\lambda_i$ corresponding to each $\mathbf{e}_i$, but now the eigenvectors are complex-valued. In considering how the components of two complex orthogonal modes multiply together to give zero, one must keep in mind not only the mode shapes but also their phase relationships. Let $D_{ik}(\omega)$ be the diagonal matrix obtained by diagonalizing $\Phi_{jl}(\omega)$:

$$D_{ik}(\omega) = \sum_j \sum_l e_{ij}\bar{e}_{kl} \qquad (3.23)$$

*A Hermitian matrix has the following properties: the diagonal elements are all real-valued, the symmetric off-diagonal elements are complex conjugate pair.

If we can find some transformation of our time series that has the diagonal cross spectra given by Eq.3.23, we have established the desired empirical orthogonal functions. The most obvious choice is the direct analogue of Eq.3.11, which now results in a complex transformed time series $z_i(t)$ since $u_j^f(t)$ is multiplied by eigenvectors which are complex. Since our main purpose in computing $z_i(t)$ is to subject it to further cross-sectrum analysis, it would be more convenient to have a real time series whose power spectrum satisfies Eq.3.23.

In order to obtain such a series, we first define an augmented (complex) time series from $u_j(t)$. Let

$$w_j(t) = u_j^f(t) - \frac{i}{\omega}\frac{du_j^f(t)}{dt}, \tag{3.24}$$

then the desired transformation is

$$z_i(t) = \mathrm{Re}\sum_j e_{ij} w_j(t). \tag{3.25}$$

Upon substituting the right hand side of Eq.3.21 for $u_j^f(t)$ in Eq.3.24, we obtain

$$w_j(t) = \exp(i\omega t) dA_j(\omega) \tag{3.26}$$

and

$$z_i(t) = \mathrm{Re}[\exp(i\omega t)\sum_j e_{ij} dA_j(\omega)]. \tag{3.27}$$

The unitary transformation determined by the $e_{ij}$ does not change the "length" but merely "rotate" $dA_j(\omega)$ in the parameter space. The correlation function for $z_i(t)$ using Eqs.3.20 and 3.23 is then

$$< z_i(t) z_k(t) >= \delta_{ik} D_{ii}(\omega)\cos(\omega\tau) d\omega \tag{3.28}$$

as required.

The empirical orthogonal functions obtained by Eqs.3.24 and 3.25 have properties equivalent to those listed above for the time domain case. The eigenvectors are

orthogonal. The elements of the series in Eq.3.25 have no mutual coherence (*i.e.*, the coherence is nearly zero) in the specified frequency band. The $i$th eigenfunction has the variance

$$< z_i^2 >= D_{ii} = \lambda_i \tag{3.29}$$

and the fraction of the variance of the $j$th filtered parameter explained by the $i$th empirical orthogonal function in given by the coherence square between $u_j$ and $z_i$ in the specified frequency band, which can be expressed in terms of the filtered analogue of Eq.3.17.

The theory we just summarized was described in terms of a transformation of a time series where all frequencies had been filtered outside the *infinitesimal* band $\omega$ to $\omega + d\omega$. The transformation was determined in terms of the eigenvectors of the cross-spectrum matrix at $\omega$. In practice, though, a statistically significant cross-spectrum matrix determined from a data sample of finite length is necessarily averaged over frequency bands of *finite* width. With such averaging, the theory we just outlined is no longer strictly applicable. If, as may be expected, the eigenvectors change little with frequency over the frequency range, the transformation of an averaged cross spectrum should yield time series which are nearly uncorrelated over the specified frequency range.

The $u_j$ series under consideration need not be identified with a single parameter such as temperature. In many cases (such as in present study), the index $j$ may refer to a number of different parameters, each measured in terms of its own characteristic units. In order to ensure that the resulting empirical orthogonal function is not dominated by one particular variable which happens to be measured in units which give rise to large numerical fluctuations in its time series, some form of normalization is necessary. There are a number of possible approaches. Earlier studies (Wallace and Dickinson, 1972; Hogg, 1981) have indicated that

the results would not depend strongly upon the particular normalization scheme one chose to perform. By far the most frequently used and perhaps the least arbitrary normalization scheme is the *coherence normalization*, which is to divide each $u_j$ by the square root of its variance in the specified frequency band. Upon performing this scheme, all the diagonal elements in the cross-spectrum matrix $\Phi_{jl}$ become unity, and the absolute magnitude of the off-diagonal elements becomes equal to the coherence between $u_j$ and $u_l$ in the frequency band. This scheme has the advantage of giving an equal weight to all variables. We used the coherence normalization scheme for the present study.

The linear combination of the $u_j^f$'s prescribed by a particular mode in an empirical orthogonal function expansion with complex eigenvectors may be thought of as representing a specific wave structure in which the amplitude and phases of the various $u_j^f$ are defined by their corresponding eigenvector components $e_{ij}$. The question of whether this structure represents a genuine physical entity, a fabrication of the statistics, or a manifestation of random noise must be decided.

### 3.3.2 Mode-Selection Rules

To recast the problem in hand, suppose a time series can be expressed in the EOF expansion as*

$$u_j(t) = \sum_{i=1}^{p} \sqrt{\lambda_i} e_{ij} z_i(t) \tag{3.30}$$

The next step is to examine the sequence of eigenvalues $\lambda_1 \geq \lambda_2 \geq \cdots \geq \lambda_p \geq 0$. Occasionally the magnitudes of the $\lambda_i$, after a certain index $p'$, drop relatively abruptly and become relatively small. Hence, on this basis, only the first $p'$ eigenvalues may be considered important in the representation of the total variance of

*For simplicity, we take the time-domain EOF modal expansion as example, the same idea can be readily expanded to the frequency-domain approach.

the data set $u_j(t)$. The resultant representation of Eq.3.30 takes the form

$$u_j(t) = \sum_{i=1}^{p'} \sqrt{\lambda_i} e_{ij} z_i(t) + \sum_{i=p'+1}^{p} \sqrt{\lambda_i} e_{ij} z_i(t) \tag{3.31}$$

The second sum is therefore considered to contain a non-significant amount of variance while the first sum is thought of as the "signal" of interest. Concurrently, when one plots the first $p'$ eigenvector components $e_{ij}$ $(j = 1, 2, \cdots, p)$, they invariably look simpler and less "noisy" than those of $e_{ij}$ $(j = 1, 2, \cdots, p)$ for $i > p'$. As a result of visual analysis of the sequence of eigenvalues $\lambda_i$ and the patterns of $\mathbf{e}_i$, one decides on $p'$, drops the second sum in Eq.3.31, and represent the time series by

$$u_j(t) \approx \sum_{i=1}^{p'} \sqrt{\lambda_i} e_{ij} z_i(t). \tag{3.32}$$

Unfortunately, assurance of statistical significance does not necessarily guarantee physical significance. Since our ultimate goal is to express our geophysical data set as a combination of a set of physically meaningful "signals", there is a need to establish objective, physically and statistically reasonable rules for selection of the truncation parameter $p'$.

There are three broad classes of procedures (Preisendorfer, 1988), each resulting in a set of "selection rules" whereby the parameter $p'$ in Eq.3.31 may be determined or, more generally, whereby the subset of summands in Eq.3.31 which differ significantly from noise, may be selected. The three classes of procedures are:

1. *The dominant-variance rules*: they are based on the premise that the larger variance terms (as represented by $\lambda_i$) are associated with the physically meaningful "signals".
2. *The time-history rules*: they examine the time series $z_i(t)$, $t = 1, 2, \cdots, N$, for significant, non-noisy temporal behavior.
3. *The space-map rules*: these rules intercompare the $i$th eigenvector compo-

nents $e_{ij}$, $j = 1, 2, \cdots, p$, with a specified $k$th mode of geophysical signal $h_{kj}$, $j = 1, 2, \cdots, p$, over the same spatial domain. For example, the latter may be one of the normal modes of a dynamical system which is hypothesized to have generated the data set in hand.

The significance test of eigenmodes in this study was based on the class 1. The important parameter to be examined is the frequency-domain analogue to $\gamma_{ij}$ defined in Eq.3.17. Since this parameter can be viewed as the coherence square between $u_j$ and $z_i$ in the frequency band under investigation, we can obtain some indication of the significance of the $i$th mode in the variable $u_j$ by applying some standard tests for coherence. In this way we can single out those $\gamma_{ij}$'s which are large enough so that the corresponding phase relationships have some meaning. The remaining information may be regarded as noise.

As we have demonstrated so far in this section, the EOF analysis has the following appealing features: 1) it provides a way to reduce the dimensionality of the representation of the geophysical field; 2) it extracts the maximum amount of information out of a given data set; and 3) it partitions the measurements in such a way that possibly lead to a recognition of the physical mechanism(s) governing the field.

To justify the use of the EOF analysis, though, one must always keep in mind the assumption underlying this method, *i.e.*, the wave structures generated by different physical processes in the real geophysical setting are mutually orthogonal and that they are not coupled with one another. The question then arises: is this assumption a reasonable one? The answer to this question is given by Wallace and Dickinson (1972):

> "It seems difficult to conceive of physically distinct waves that do not have some orthogonal degrees of freedom, but the orthogonal variable may not necessarily be present in a given set of observations. ...

it is apparent that when more than one wave type is present in a particular frequency band, the success of complex eigenvectors analysis depends crucially upon the selection of a combination of parameters, $u_j$, in which the waves have a substantial degree of orthogonality. If such a combination cannot be found, then the waves will not be distinguishable from one another by this method or, for that matter, by any other method."

Table 3.1: Information about the current meter moorings.

| Mooring ID | Latitude | Longitude | Bottom Depth (m) | Instrument Depth (m) | Beginning Date | Ending Date | Rotating Angle (°) | Number of Data |
|---|---|---|---|---|---|---|---|---|
| F011 | 27°0.0′N | 79°59.10′W | 75 | 10 | 10/05/84 | 03/12/85 | 0 | 635 |
| F013 | 27°0.0′N | 79°59.10′W | 75 | 50 | 10/05/84 | 03/13/85 | 0 | 637 |
| F014 | 27°0.0′N | 79°59.10′W | 75 | 72 | 10/05/84 | 03/13/85 | 0 | 637 |
| F032 | 28°0.02′N | 79°59.57′W | 75 | 30 | 10/05/84 | 03/15/85 | -5 | 647 |
| F033 | 28°0.02′N | 79°59.57′W | 75 | 50 | 10/05/84 | 01/30/85 | -5 | 469 |
| F034 | 28°0.02′N | 79°59.57′W | 75 | 72 | 10/05/84 | 03/15/85 | -5 | 647 |
| F061 | 29°0.19′N | 80°8.18′W | 75 | 10 | 10/05/84 | 03/16/85 | -10 | 651 |
| F063 | 29°0.19′N | 80°8.18′W | 75 | 50 | 10/05/84 | 03/16/85 | -10 | 651 |
| F064 | 29°0.19′N | 80°8.18′W | 75 | 72 | 10/05/84 | 03/16/85 | -10 | 651 |
| F111 | 29°59.86′N | 80°15.88′W | 75 | 10 | 10/05/84 | 03/19/85 | 0 | 663 |
| F112 | 29°59.86′N | 80°15.88′W | 75 | 30 | 10/05/84 | 03/19/85 | 0 | 663 |
| F113 | 29°59.86′N | 80°15.88′W | 75 | 50 | 10/05/84 | 03/19/85 | 0 | 663 |
| F114 | 29°59.86′N | 80°15.88′W | 75 | 72 | 10/05/84 | 03/19/85 | 0 | 663 |
| BTOP | 30°50.80′N | 80°2′W | 75 | 17 | 12/14/76 | 04/06/77 | 30 | 452 |
| ETOP | 31°35.80′N | 79°40.20′W | 75 | 17 | 12/14/76 | 01/30/77 | 30 | 188 |
| EBOT | 31°35.80′N | 79°40.20′W | 75 | 72 | 12/14/76 | 03/18/77 | 30 | 378 |
| SAI9601 | 32°34.48′N | 78°38.65′W | 47 | 12 | 11/16/78 | 03/20/79 | 50 | 499 |
| SAI9602 | 32°34.48′N | 78°38.65′W | 47 | 24 | 11/16/78 | 03/20/79 | 50 | 499 |
| SAI9603 | 32°34.48′N | 78°38.65′W | 47 | 45 | 11/16/78 | 03/20/79 | 50 | 499 |
| B170007D4 | 32°55.02′N | 78°9.72′W | 75 | 7 | 08/13/84 | 03/18/85 | 39 | 868 |
| B170040D4 | 32°55.02′N | 78°9.72′W | 75 | 40 | 08/13/84 | 03/23/85 | 39 | 889 |
| B170070D4 | 32°55.02′N | 78°9.72′W | 75 | 70 | 08/13/84 | 03/23/85 | 39 | 889 |
| C110020D4 | 33°40.80′N | 76°45.48′W | 75 | 20 | 08/14/84 | 03/06/85 | 38 | 817 |
| C110071D4 | 33°40.80′N | 76°45.48′W | 75 | 71 | 08/14/84 | 03/18/85 | 38 | 863 |

# 4. Statistical Analyses

In this chapter, we first describe the prominent features observed in the forty-hour low-pass filtered current and temperature time series. We then present the basic statistics for both current components and temperature. This is followed by a detailed discussion on their implication to the energetics along the shelf break. Attention is then devoted to the results of power spectrum calculations. A subsequent discussion on the energy distribution in the frequency domain lead to this finding: the energy associated with the low-frequency fluctuations in the currents are primarily concentrated in three different period bands: 1) 3–7 days—presumably induced by the synoptic scale weather system; 2) 7–14 days—governed by the Gulf Stream meandering activities; and 3) a somewhat loosely defined period band centered around 28 days whose generating mechanism is yet to be determined. In an effort to capture the characteristics of the 28-day fluctuations and eventually unveil its nature, we present the statistic results of our frequency-domain empirical orthogonal function analyses of the time series.

## 4.1 Basic Statistics

Figures 4.1 to 4.18 show the forty-hour low-pass filtered time series of the alongshore and cross-shelf currents, as well as temperature with the seasonal trend at selected meter sites. The time series reveal some familiar features, for example, the outburst of the onshore flow is almost always accompanied by the diminishing of the northward alongshore flow, occasionally the alongshore flow even reverses its direction, and by the decrease in temperature. This scenario results from the

meandering activity of the Gulf Stream or strong northerly wind event, the latter mainly takes place during winter season. Other noticeable features depicted by the time series include: 1) upstream of the Charleston Bump, the fluctuations of temperature were substantially larger near the bottom (7–8°C) compared to those near the surface (1–2°C), contradicting to what one would expect; 2) at the southernmost meter location (inside the Florida Straits), the temperature records in the lower layer (at F013 and F014) clearly reveal episodes of impulse-like temperature drops of 7–8°C. These events, which typically last for 2–3 days, are apparently distinguished from the more gradual and smaller temperature fluctuations usually associated with the diminishing of the northward alongshore flow. The signature of this impulse-like event remains recognizable, though much weaker, as far away as some 300 km to the north and appears to be advected northward by the mean alongshore current.

The basic statistics for all moorings are listed in Table 4.1. The cross-shelf current component, as expected, is generally weak and variable. The alongshore current, from the southernmost mooring site northward to around 32°35′, is consistently northward throughout the water column. Further north at 32°55′, prolonged southward flow is evident from surface to bottom (at B170007D4, B170040D4 and B170070D4), and curiously, the strongest alongshore flow occurs near the bottom (at B170070D4). Pietrafesa and Janowitz (1980) postulated that the shelf break region off Charleston is part of a large counterclockwisely rotating gyre (called "Charleston Gyre") that has the inshore side of the Gulf Stream as its southern, eastern and northern boundaries and is closed on its shoreward side by a southerly flowing current (see Figure 2 of Pietrafesa, Janowitz, and Wittman, 1985). Apparently the particular location we just cited is at the shoreward side of the Gyre and the persistent southward bottom flow is a manifestation of it. At its northern

neighboring mooring site, the alongshore current again turns northward, implying the longshore dimension of the Gyre is no larger than the distance between the two mooring sites (about 214 km) which bracket the location where southward flow prevails.

The kinetic energy of mean flow is calculated by taking the square of the mean velocity. The eddy momentum transfer $\overline{u'v'}$, cross-shelf heat transfer $\overline{u'T'}$ and eddy kinetic energy $\overline{u'^2}$ and $\overline{v'^2}$ are calculated by taking the ensemble average of each pair*. The results of energetic calculations along with momentum and heat fluxes calculations are listed in Table 4.2. The magnitude of the kinetic energy of the fluctuations (or eddy kinetic energy) are generally comparable to that of the mean flow. Similarly to that the Reynolds number being a measure of the turbulency in a flow, the eddy kinetic energy to the mean flow kinetic energy ratio (EKE/MKE) provides another measure to the turbulency in a flow. This ratio, as can be seen in Table 4.2, increases going down the water column at all mooring sites and almost always achieves its maximum near the bottom, suggesting the flow becomes increasingly turbulent towards the bottom, probably due to the gradual loss of the Gulf Stream integrity as going down the water column. Near surface, the maximum EKE/MKE occurs immediately downstream of the Charleston Bump (at SAI9601), indicating a turbulent readjustment process takes place as the Stream veers shoreward after being deflected seaward by the Bump.

As discussed in detail by Webster (1961b), at the cyclonic shear zone (shoreward side) of the Gulf Stream, *i.e.*, where $\partial\overline{v}/\partial x > 0$ holds, a positive value of eddy momentum flux $\overline{u'v'}$ indicates the kinetic energy is from the fluctuations to the mean flow, and *vice versa*. The results of our eddy momentum flux calculations indicate that along shelf break the kinetic energy transfer proceeds both ways.

*For these calculations, the temperature data without de-trending were used.

Near surface, the transfers are generally from the fluctuations to the mean flow, in agreement with earlier findings (*e.g.*, Webster, 1961b; Schmitz and Niiler, 1969), except at two mooring sites, one (at meter F011) located inside the Florida Straits (but near its northern exit), the other (at meter BTOP) is situated immediately upstream of the Charleston Bump. Both observations (Lee and Atkinson, 1983; Lee *et.al.*, 1991) and numerical studies (*e.g.*, Oey, 1988) show that upon leaving the confines of the Straits, the Gulf Stream becomes more turbulent. It seems conceivable that prior to the flow becoming more turbulent, the kinetic energy transfer should be directed from mean flow to the fluctuations in order to supply an additional amount of energy for the turbulence to grow. By the same argument, the area situated just upstream of the Charleston Bump is another place where growing turbulence is expected. It is tempting to suggest that the kinetic energy transfer from the mean flow to the fluctuations at these two particular locations is in fact consistent with previous discoveries. Upstream of the Charleston Bump, kinetic energy transfer in the lower layer is from the mean flow to the fluctuations, which explains the fact that near bottom flow is more turbulent. Downstream of the Charleston Bump, the kinetic energy transfer is from the fluctuations to mean flow at all depths, suggesting that after the initial readjustment, the flow gradually stabilizes as it moves along.

During winter season, the shelf waters are usually cooler than 20°C, while the characteristic temperature of the Gulf Stream remains 26°C. If, under this circumstance, the motion is purely horizontal, one would expect that the heat flux is directed onshore (*i.e.*, $\overline{u'T'} < 0$). An offshore directed heat flux (*i.e.*, $\overline{u'T'} > 0$) during this season is inevitably associated with the Gulf Stream meandering activity. Recall that a typical scenario as a meander trough (frontal eddy) passing by is an outburst of the onshore flow accompanied by a decreasing northward flow,

followed by a temperature drop resulting from an upward motion of the water column. As we have discussed in Chapter 2, this upwelling originates near the bottom. Therefore if an offshore directed heat flux is indeed induced by a frontal eddy, two characteristics should be present: 1) if the heat flux is directed towards offshore at a certain level at a given location, the heat flux should be all directed towards offshore everywhere below that level at that location; 2) the intensity of this event, which may be represented by the value of $\overline{u'T'}$, is at its maximum near the bottom and weakens upward. An examination of our results in Table 4.2 confirms that this is precisely the case.

## 4.2 Power Spectral Analysis

Power spectra calculated for selected time series are shown in Figures 4.19 to 4.24, where energy densities are displayed in the logarithmic scale as a function of the linearly spaced frequencies. The equivalent degrees of freedom ($\mu$) is 20 for all time series except for one. Since the time series have different number of observations ($N$), the effective frequency bandwidth $B_e$ ranges from 0.0045 to 0.0213 cpd (cycle per day). The details are given in Table 4.3.

The power spectra of currents (Figures 4.19–4.24) exhibit the two characteristics which are thought to be typical of the flow field on the continental margins as opposed to that in the open ocean (Düing *et al.*, 1977): 1) there is a decline of energy towards periods longer than a month; 2) they have a greater cut-off frequency at the high frequency end. The significance of these difference is that they imply distinct controlling mechanisms. While the general shape of the subinertial frequency spectrum in the open ocean is probably governed by planetary Rossby waves, it is thought to be governed by topographic Rossby waves on the continental margins (Düing *et at.*, 1977). It is helpful to bear this in mind when we discuss

the controlling mechanims later on.

The energy level of alongshore current ($v$) fluctuations generally decreases rapidly downward. Cross-shelf current ($u$) fluctuations, on the contrary, can have an entirely different character: the fluctuation near the bottom is actually more energetic than that near the surface (see the power spectra for locations at F01 and F03).

The power spectra indicate that energy associated with the cross-shelf current are concentrated typically in 3–5-day and 7–10-day period bands. The former falls in the period band of the synoptic scale weather systems (see, for example, Wunsch, 1980) the latter that of Gulf Stream meanders. This suggests that the cross-shelf current fluctuations along the shelf break are essentially a mixed response to synoptic scale weather systems and Gulf Stream meanders. The energy associated with the alongshore current, like the cross-shelf component, generally peaks at around 5 and 10 days. In addition, many of the power spectra show a predominant peak at around 28 days. To quantify the strength of this 28-day fluctuation, we multiply the energy density by a suitable bandwidth, say, 0.036 cpd. The power spectra of the alongshore currents suggest (see Figures 4.19–4.24) that the energy density (power) at the period of 28 days is typically 8000 $cm^2/s^2$·cpd, thus the total energy concentrated in this frequency band is typically 288 $cm^2/s^2$, corresponding to a current fluctuation of 17 cm/s. While the governing mechanisms of the former two bands having been identified, the nature of the latter is somewhat puzzling and requires more investigation. We will try to address this question later in this chapter.

Not surprisingly, the energy of the temperature fluctuations peaks at around the periods of 5 and 7 days, since both synoptic scale weather and the Gulf Stream meander can greatly alter the thermal structure of the water column along the shelf

break. The most noticeable feature of the temperature spectra, though, is that the temperatures at the mid- to lower water column consistently show prominent peaks at, again, around the period of 28 days in mid- to lower water column. Is this 28-day temperature fluctuation just a coincedence or does it suggest a close connection to the 28-day oscillation of alongshore current? Once again, the question is being raised: what is the nature of this 28-day fluctuation? To answer this question, we need to find out more details, such as, what are the relationships between signals detected at different mooring sites? Are they well-correlated? How big are the phase lags between each other? What is the spatial scale of the fluctuations? With the aid of the frequency-domain empirical orthogonal function analysis, we will be in a position to address those characteristics associated with the fluctuations.

## 4.3 Empirical Orthogonal Function Analysis

To further investigate the nature of the 28-day fluctuations presented in alongshore current and temperature records, the frequency-domain empirical orthogonal function analysis technique was applied to the concurrent current and temperature data as described in Section 3.3. In the process of seeking the leading eigenmodes, we are interested in finding the various aspects concerning each mode, in particular, 1) the eigenvalues, which indicate the relative contributions in the total normalized variance; 2) the complex eigenvectors, which represent the amplitudes and phases corresponding to each mode to the linear representation of an observed time series.

Several different combinations of the data on hand were subjected to the EOF analysis. It is found that the most consistent and significant results are from data obtained from the upstream side of the Charleston Bump. This implies that the current fluctuations at the two sides of this topographic irregularity are likely dominated by different dynamic mechanisms. We shall present the results using

data obtained at the upstream side only.

To place the technique in perspective, we need to select a proper frequency band. For analyzing the current records, the frequency band was chosen to be from 0.018 to 0.054 cpd centering at 0.036 cpd, corresponding to a 19–56 day period band. The technique was performed using the alongshore currents obtained from all meter sites south of the Charleston Bump*: F011, F013, F014, F032, F034, F061, F063, F064, F111, F112, F113 and F114. Since there were 12 concurrent records in this group, the EOF analysis yielded 12 eigenmodes. The percentages of total normalized variance explained by each mode are displayed in Figure 4.25. Clearly the percentage decreases exponentially as the index of the eigenmode increases. As a rule of thumb, one can ignore those modes with indices higher than the one corresponded by the mode at which the slope of the curve changes most abruptly. In our case, this rule implies that the third and higher modes can be considered as statistic noise and can be discarded. The first two modes together account for more than 82% of the total normalized variance. Figures 4.26(a) and (b) show the normalized amplitudes (which can also be viewed as the coherency between the time series and the eigenmode) at each meter site for the first and second modes, respectively, as a function of the longshore distance measured from the southernmost mooring site. The solid line indicates the 95% confidence level. Figures 4.27(a) and (b) show the phases in degrees against the longshore distance for the first and second modes, respectively, where the phase with a coherency exceeding the 90% confidence level is represented by an open circle while that with a coherency less than the 90% confidence level is represented by a solid circle. It is apparent from Figure 4.27(a) that for those time series

*Except the time series from meter F033, which was excluded from the frequency-domain EOF analysis because of its much shorter time span due to an intrumental failure.

highly coherent (coherency exceeding 90% confidence level) with the first eigenmode, their corresponding phases lag progressively southward and lie closely to the sloping line which represents a *southward* propagation with a wavelength of about 5000 km. Assuming the signals have a 28-day period, the phase speed of these propagating signals is about 178 km/day or 2.1 m/s. For the second mode, assuming that the phase differences between two adjacent moorings are within the range of [0°, 360°]†, if we are to "fix" the phases for the currents measured at the southernmost mooring site and allow the phases for currents measured at other locations be represented by angles outside of the range of [−180°, 180°], we then get a revealing picture (Figure 4.27(b)). The phases almost all lie in the vicinity of the straight line, which indicates the signals propagated *northward* with a much shorter wavelength (about 360 km) in comparison to the first mode, corresponding to a phase speed of about 13 km/day, or 0.15 m/s.

We have also performed the EOF analysis using another group of time series which includes the temperature records obtained at the mid- to lower layers (those show prominent spectral peaks at around 28-day period) along with the alongshore current records. The results indicate that the current and temperature do not share common mode, which means that they are statistically incoherent. It is safe to conclude that at this frequency band the current and temperature fluctuations each have their own generating mechanisms.

To study the characteristics of the temperature fluctuations, the EOF analysis was applied to a group of temperature records obtained at the mid- to lower layers over the 0.0–0.072 cpd frequency band, recall this frequency band contains the most energetic fluctuations in the temperature records after the removal of the seasonal

†This is equivalent to assuming that the distance between two ajacent mooringsdoes not exceed one wavelength.

trends. Though the center frequency was still 0.036 cpd, the bandwidth was chosen to be a broader one*. Figure 4.28 shows the percentage of total variance explained by each eigenmode. The first and second modes each account for 65% and 22% of the total variance. Figure 4.29(a) and (b) shows the normalized amplitude for each time series corresponding to the first and second eigenmodes, against the longshore distance, the solid line again indicates the 95% confidence level. Figure 4.30(a) and (b) show the phases corresponding to the first and second modes against the longshore distance. As can be seen in Figure 4.30(a), the phases at different locations are nearly all on the same straight line, which represents a northward propagation with a wavelength of about 1000 km. The phase speed is estimated as 0.41 m/s, approximately equaling the speed of the mean alongshore current south of the Charleston Bump. Apparently this mode represents the thermal signature of the mean alongshore current along the shelf break. The phase relationships for the second mode (Figure 4.30(b)), however, are not that straightforward. We noticed from Figure 4.29(b) that this mode is significant only at the northernmost mooring site (off St. Augustine at 50 m and 72 m depths), and therefore does not seem to propagate along the shelf. It is likely that this mode represents only a local effect.

*Upon removal of the seasonal trends, the magnitude of temperature fluctuations becomes relatively small compare to the resolution of the thermometers, thus the detrended temperature data have a lower signal to noise ratio. It will improve the statistical significance of the results to analyze the detrended temperature records over a wider frequency band.

Table 4.1: Basic statistics of the time series, velocity components in cm/s, temperature in °C.

| | $u$ | | | | $v$ | | | | $T$ | | | |
|---|---|---|---|---|---|---|---|---|---|---|---|---|
| Mooring ID | min. | max. | mean | std. dev. | min. | max. | mean | std. dev. | min. | max. | mean | std. dev. |
| F011 | -25.34 | 39.15 | -5.69 | 7.51 | -82.68 | 217.98 | 84.43 | 54.59 | 21.73 | 27.73 | 25.02 | 1.58 |
| F013 | -32.59 | 27.54 | -3.13 | 7.24 | -87.10 | 148.43 | 41.73 | 39.95 | 15.11 | 27.50 | 23.80 | 2.25 |
| F014 | -17.23 | 46.47 | 1.20 | 11.12 | -58.22 | 70.46 | 11.13 | 22.90 | 10.17 | 27.26 | 22.02 | 3.26 |
| F032 | -22.43 | 14.57 | -0.52 | 6.10 | -61.63 | 120.94 | 57.09 | 35.90 | 18.44 | 27.86 | 24.81 | 2.02 |
| F033 | -19.24 | 17.70 | -1.05 | 5.76 | -56.73 | 142.91 | 48.66 | 38.94 | 20.74 | 27.57 | 25.02 | 1.58 |
| F034 | -28.75 | 42.96 | 0.10 | 10.99 | -22.22 | 47.59 | 16.40 | 14.82 | 13.23 | 27.21 | 22.47 | 2.89 |
| F061 | -33.83 | 29.58 | 2.57 | 9.02 | -74.75 | 190.84 | 63.30 | 46.66 | 21.40 | 27.40 | 24.61 | 1.79 |
| F063 | -31.78 | 39.10 | 0.26 | 9.20 | -60.73 | 100.27 | 34.01 | 27.47 | 17.76 | 27.13 | 23.57 | 2.36 |
| F064 | -25.47 | 31.59 | -2.98 | 8.99 | -52.94 | 56.47 | 15.15 | 19.20 | | | | |
| F111 | -47.78 | 36.36 | -1.40 | 10.86 | -69.65 | 112.47 | 30.70 | 35.85 | 20.90 | 27.51 | 24.58 | 1.76 |
| F112 | -50.09 | 26.38 | -1.33 | 10.38 | -68.91 | 99.79 | 28.04 | 34.19 | 19.77 | 27.48 | 24.30 | 1.95 |
| F113 | -45.59 | 26.02 | -0.91 | 10.32 | -64.40 | 73.36 | 18.67 | 31.36 | 16.06 | 27.07 | 23.51 | 2.39 |
| F114 | -20.68 | 24.57 | 1.80 | 6.20 | -53.43 | 50.13 | 6.23 | 17.89 | 15.19 | 26.71 | 22.37 | 2.81 |
| BTOP | -26.96 | 19.41 | -1.53 | 8.43 | -39.96 | 146.32 | 62.34 | 40.25 | 17.24 | 24.00 | 20.70 | 1.49 |
| ETOP | | | | | | | | | 17.18 | 23.15 | 20.39 | 1.48 |
| EBOT | -17.04 | 23.19 | 0.57 | 6.04 | -19.59 | 34.59 | 2.16 | 10.67 | 9.81 | 20.81 | 15.59 | 2.69 |
| SAI9601 | -27.51 | 42.62 | 5.66 | 15.05 | -55.64 | 118.87 | 12.68 | 33.91 | 13.26 | 27.13 | 20.72 | 3.45 |
| SAI9602 | -23.87 | 36.10 | 5.17 | 13.22 | -51.05 | 104.34 | 7.75 | 30.70 | 13.07 | 27.10 | 20.48 | 3.47 |
| SAI9603 | -9.91 | 20.45 | 4.63 | 5.11 | -42.68 | 61.34 | 1.29 | 19.83 | 12.06 | 26.34 | 19.60 | 3.64 |
| B170007D4 | -34.60 | 45.70 | -6.11 | 10.72 | -63.60 | 43.60 | -10.34 | 17.86 | 16.95 | 27.54 | 22.44 | 2.92 |
| B170040D4 | -40.40 | 38.50 | -5.35 | 12.22 | -84.70 | 67.50 | -4.69 | 25.30 | 17.99 | 28.58 | 24.00 | 2.67 |
| B170070D4 | -48.10 | 101.80 | -1.79 | 18.82 | -124.70 | 53.50 | -28.72 | 28.93 | 16.04 | 27.04 | 21.55 | 2.96 |
| C110020D4 | -64.70 | 61.30 | 1.90 | 18.63 | -86.31 | 125.50 | 16.79 | 40.65 | 19.10 | 29.08 | 24.50 | 2.39 |
| C110071D4 | -25.90 | 94.60 | 3.17 | 12.32 | -64.30 | 44.10 | -3.36 | 21.60 | 14.96 | 26.99 | 22.34 | 2.91 |

Table 4.2: The energetics, momentum and heat fluxes at each meter sites; energy and momentum flux in $cm^2/s^2$, heat flux in cm·°C/s.

| Mooring ID | $\overline{u}^2$ | $\overline{v}^2$ | $\overline{u}^2+\overline{v}^2$ | $\overline{u'^2}$ | $\overline{v'^2}$ | $\overline{u'^2}+\overline{v'^2}$ | EKE/MKE | $\overline{u'v'}$ | $\overline{u'T'}$ |
|---|---|---|---|---|---|---|---|---|---|
| F011 | 32 | 7128 | 7160 | 56 | 2980 | 3036 | 0.42 | -202±687 | 0.35±11.27 |
| F012 | 10 | 1741 | 1751 | 52 | 1596 | 1648 | 0.94 | -167±411 | 3.10±16.53 |
| F014 | 1 | 124 | 125 | 124 | 525 | 649 | 5.19 | -183±351 | 12.21±33.62 |
| F032 | 0 | 3259 | 3259 | 37 | 1289 | 1326 | 0.41 | 30±229 | -0.33±12.78 |
| F033 | 1 | 2368 | 2369 | 33 | 1516 | 1549 | 0.65 | -47±206 | -0.94±10.04 |
| F034 | 0 | 269 | 269 | 121 | 220 | 341 | 1.27 | -51±154 | 8.99±32.48 |
| F061 | 7 | 4007 | 4014 | 81 | 2177 | 2258 | 0.56 | 66±476 | -3.10±16.52 |
| F063 | 0 | 1157 | 1157 | 85 | 755 | 840 | 0.73 | -50±281 | -1.01±23.58 |
| F064 | 9 | 230 | 239 | 81 | 369 | 450 | 1.88 | -98±251 | |
| F111 | 2 | 942 | 944 | 118 | 1285 | 1403 | 1.49 | 51±454 | -1.74±17.74 |
| F112 | 2 | 786 | 788 | 108 | 1169 | 1277 | 1.62 | 100±388 | -0.67±17.88 |
| F113 | 1 | 349 | 350 | 107 | 983 | 1090 | 3.11 | 62±360 | -0.04±21.93 |
| F114 | 3 | 39 | 42 | 38 | 320 | 358 | 8.52 | -28±156 | -0.64±14.75 |
| BTOP | 2 | 3886 | 3888 | 71 | 1620 | 1691 | 0.43 | -85±332 | -4.44±13.20 |
| ETOP | | | | | | | | | |
| EBOT | 0 | 5 | 5 | 36 | 114 | 150 | 30.0 | -19±72 | 0.24±15.89 |
| SAI9601 | 32 | 161 | 193 | 226 | 1150 | 1376 | 7.13 | 349±524 | 0.77±51.14 |
| SAI9602 | 27 | 60 | 87 | 175 | 943 | 1118 | 12.9 | 297±396 | 1.10±43.91 |
| SAI9603 | 21 | 2 | 23 | 26 | 393 | 419 | 18.2 | 1±100 | 1.68±16.86 |
| B170007D4 | 37 | 107 | 144 | 115 | 319 | 434 | 3.01 | 140±260 | -5.63±30.20 |
| B170040D4 | 29 | 22 | 51 | 149 | 640 | 789 | 15.5 | 228±398 | -6.32±33.59 |
| B170070D4 | 3 | 825 | 828 | 354 | 837 | 1191 | 1.44 | 202±645 | -9.76±51.27 |
| C110020D4 | 4 | 282 | 286 | 347 | 1652 | 1999 | 6.99 | 500±835 | -7.75±48.40 |
| C110070D4 | 10 | 11 | 21 | 152 | 466 | 618 | 29.4 | 82±275 | -7.78±52.34 |

Table 4.3: Information about power spectrum calculation for time series obtained at each meter.

| Mooring ID | $N$ | $M$ | $\mu$ | $B_e$ (cpd) |
|---|---|---|---|---|
| F011 | 635 | 115 | 20 | 0.0063 |
| F013 | 637 | 115 | 20 | 0.0063 |
| F014 | 637 | 115 | 20 | 0.0063 |
| F032 | 647 | 115 | 20 | 0.0062 |
| F033 | 469 | 85 | 20 | 0.0085 |
| F034 | 647 | 115 | 20 | 0.0062 |
| F061 | 651 | 115 | 20 | 0.0061 |
| F063 | 651 | 115 | 20 | 0.0061 |
| F064 | 651 | 115 | 20 | 0.0061 |
| F111 | 663 | 120 | 20 | 0.0060 |
| F112 | 663 | 120 | 20 | 0.0060 |
| F113 | 663 | 120 | 20 | 0.0060 |
| F114 | 663 | 120 | 20 | 0.0060 |
| BTOP | 452 | 80 | 20 | 0.0088 |
| ETOP | 188 | 65 | 10 | 0.0213 |
| EBOT | 378 | 70 | 20 | 0.0106 |
| B170007D4 | 868 | 155 | 20 | 0.0046 |
| B170040D4 | 889 | 160 | 20 | 0.0045 |
| B170070D4 | 889 | 160 | 20 | 0.0045 |
| C110020D4 | 817 | 145 | 20 | 0.0049 |
| C110071D4 | 863 | 155 | 20 | 0.0046 |

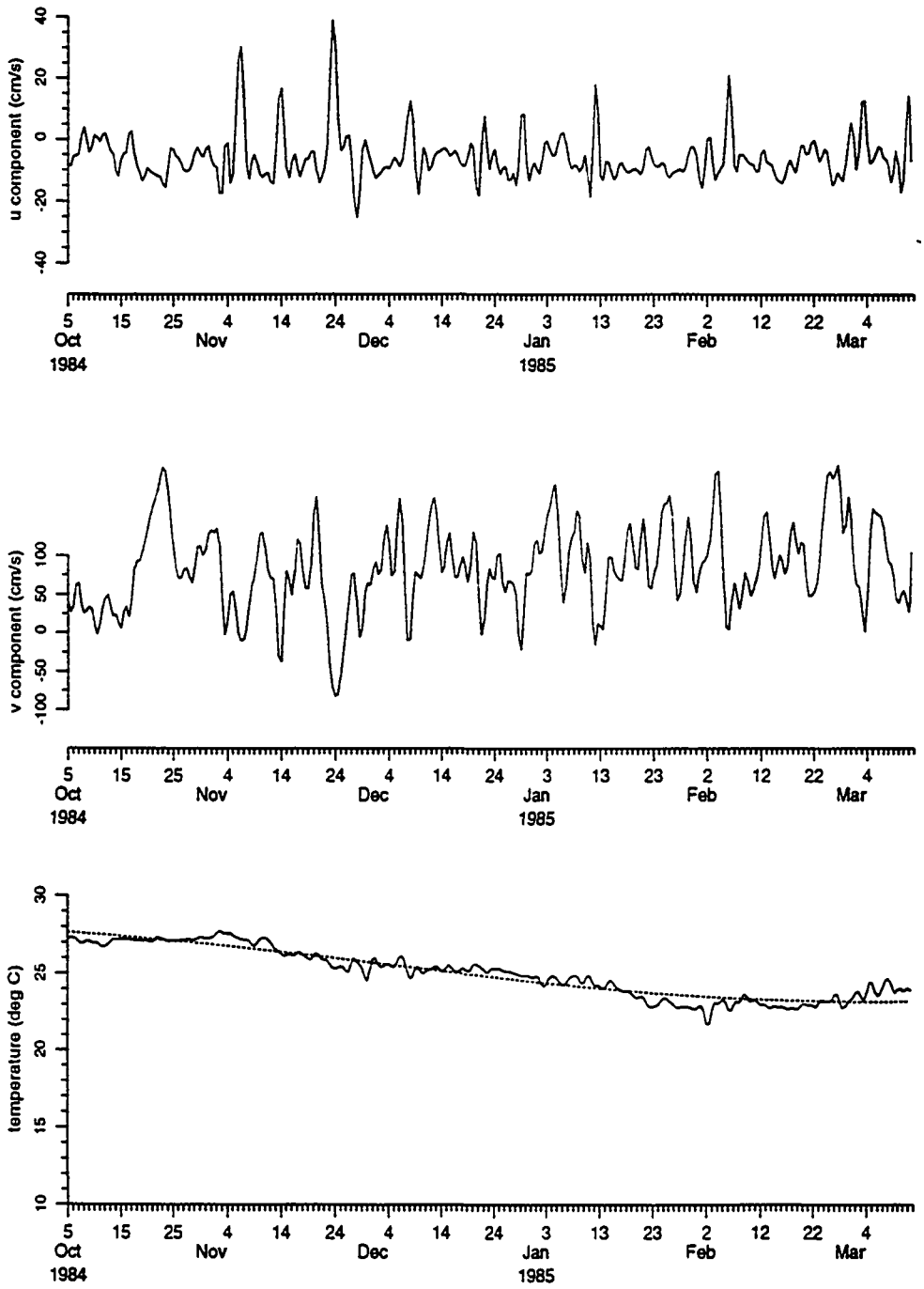


Figure 4.1. Forty-hour low-pass filtered time series of cross-shelf and alongshore currents in cm/sec, as well as temperature in °C with the seasonal trend (shown in dotted line) at meter F011, 10-m depth.

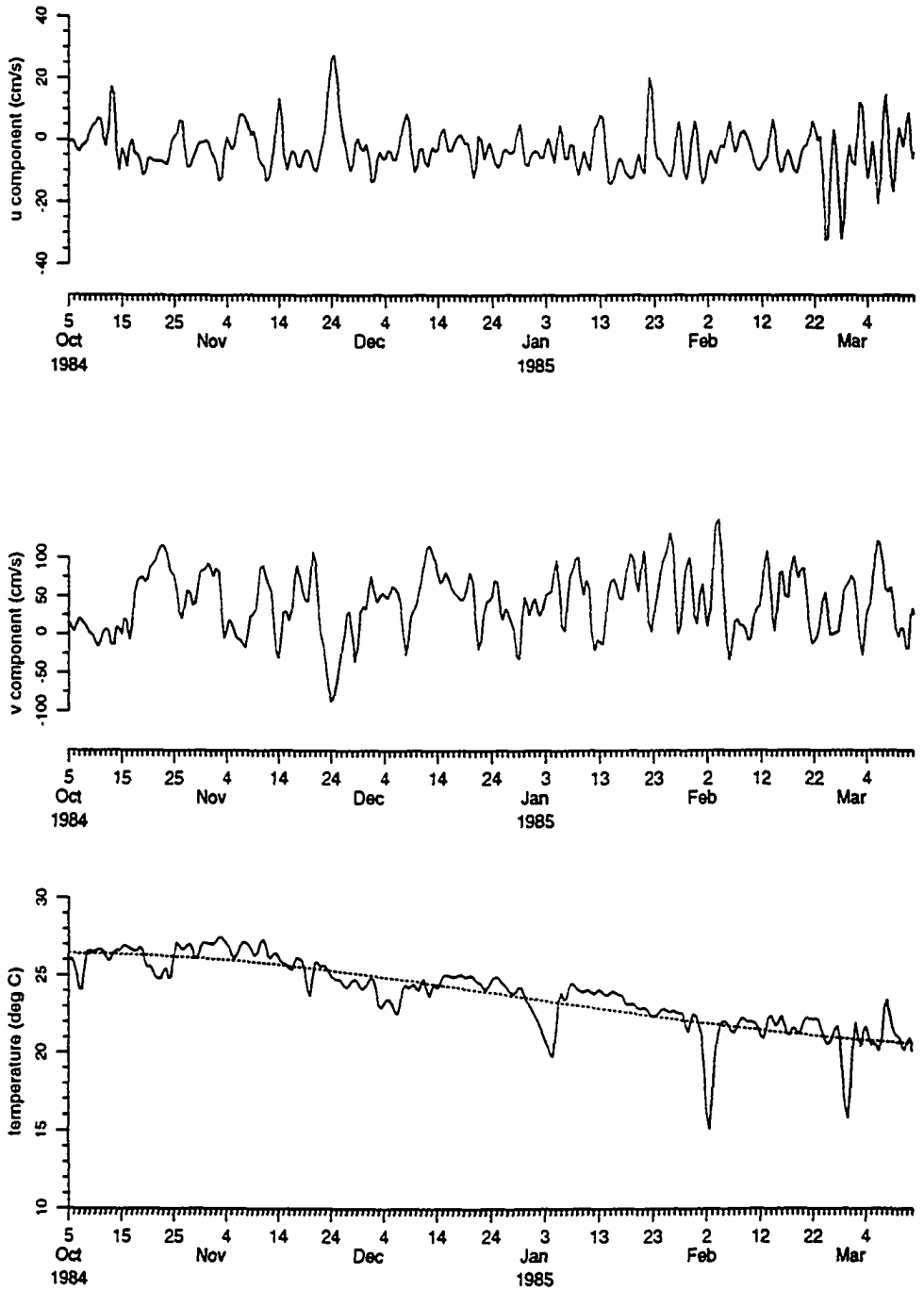


Figure 4.2. Same as in Figure 4.1, except at meter F013, 50-m depth.

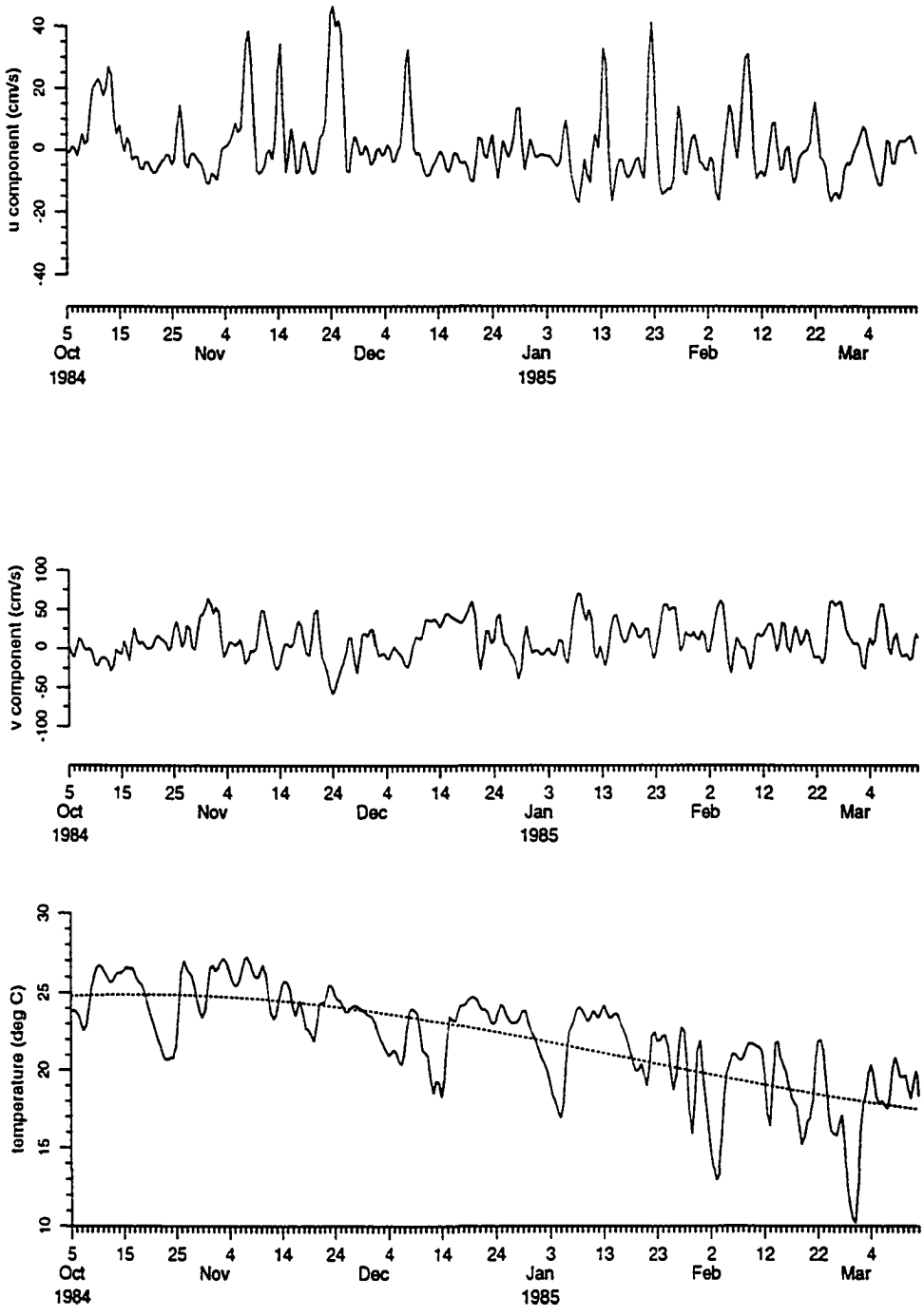


Figure 4.3. Same as in Figure 4.1, except at meter F014. 72-m depth.

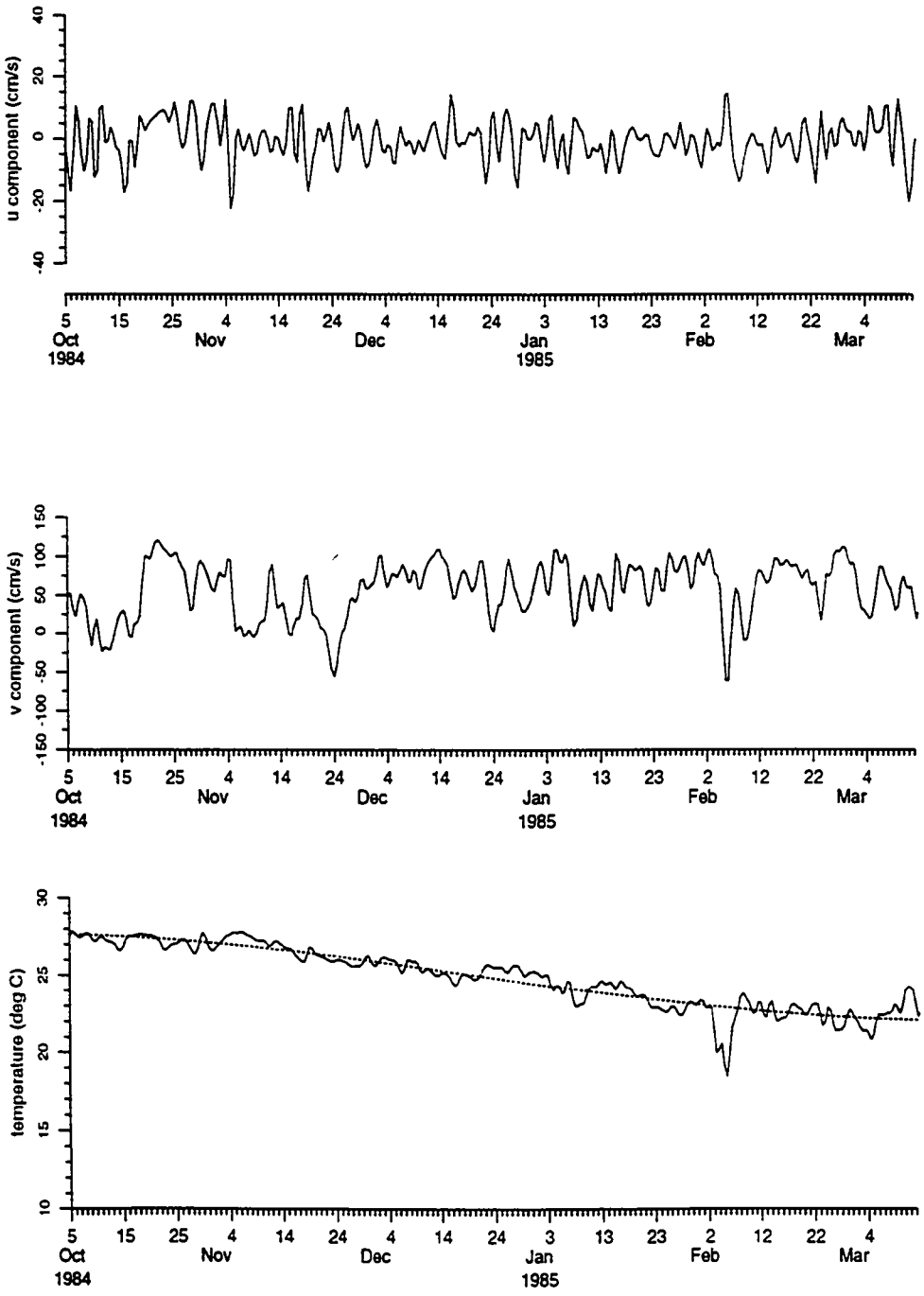


Figure 4.4. Same as in Figure 4.1, except at meter F032, 30-m depth.

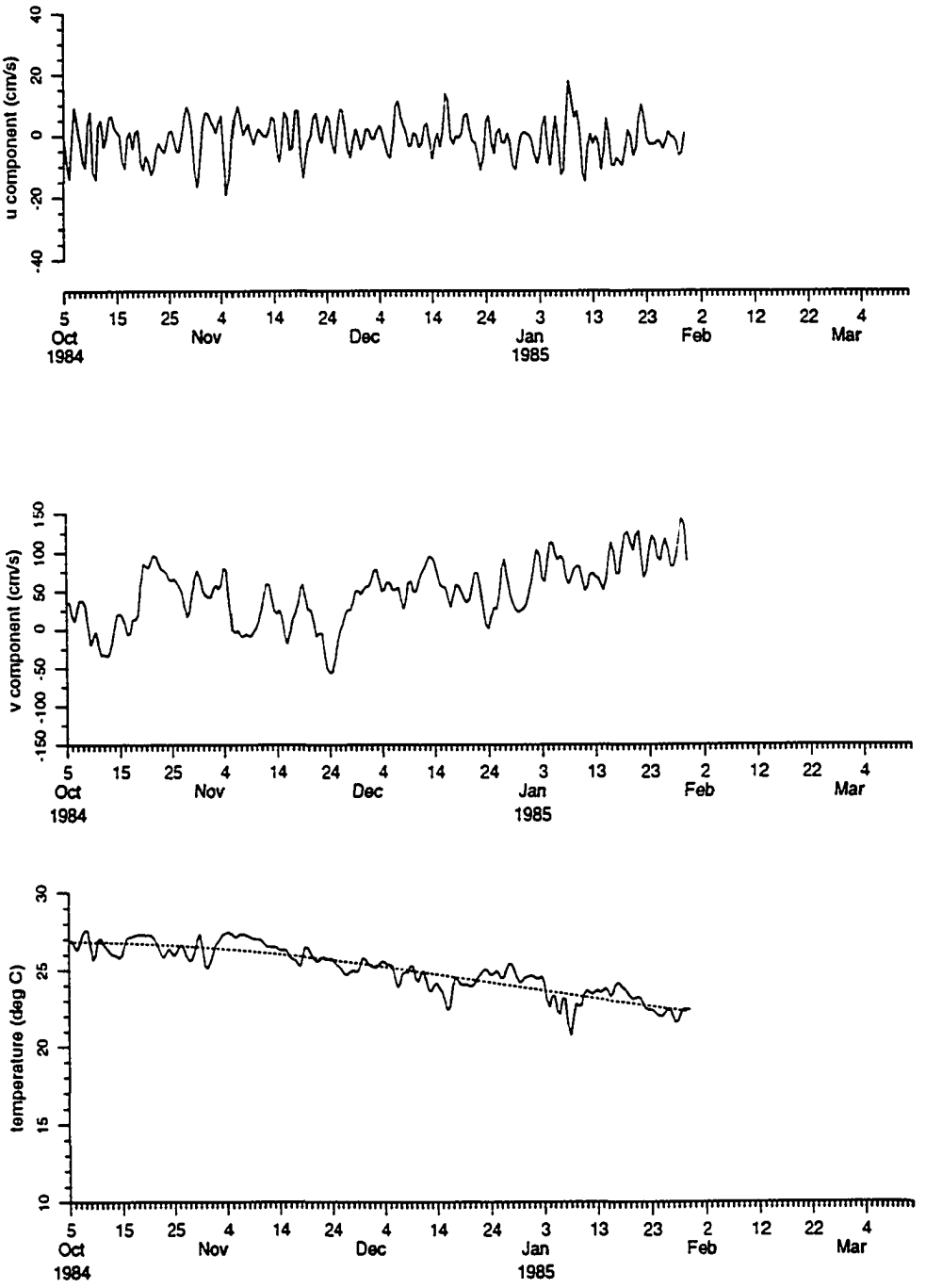


Figure 4.5. Same as in Figure 4.1, except at meter F033, 50-m depth.

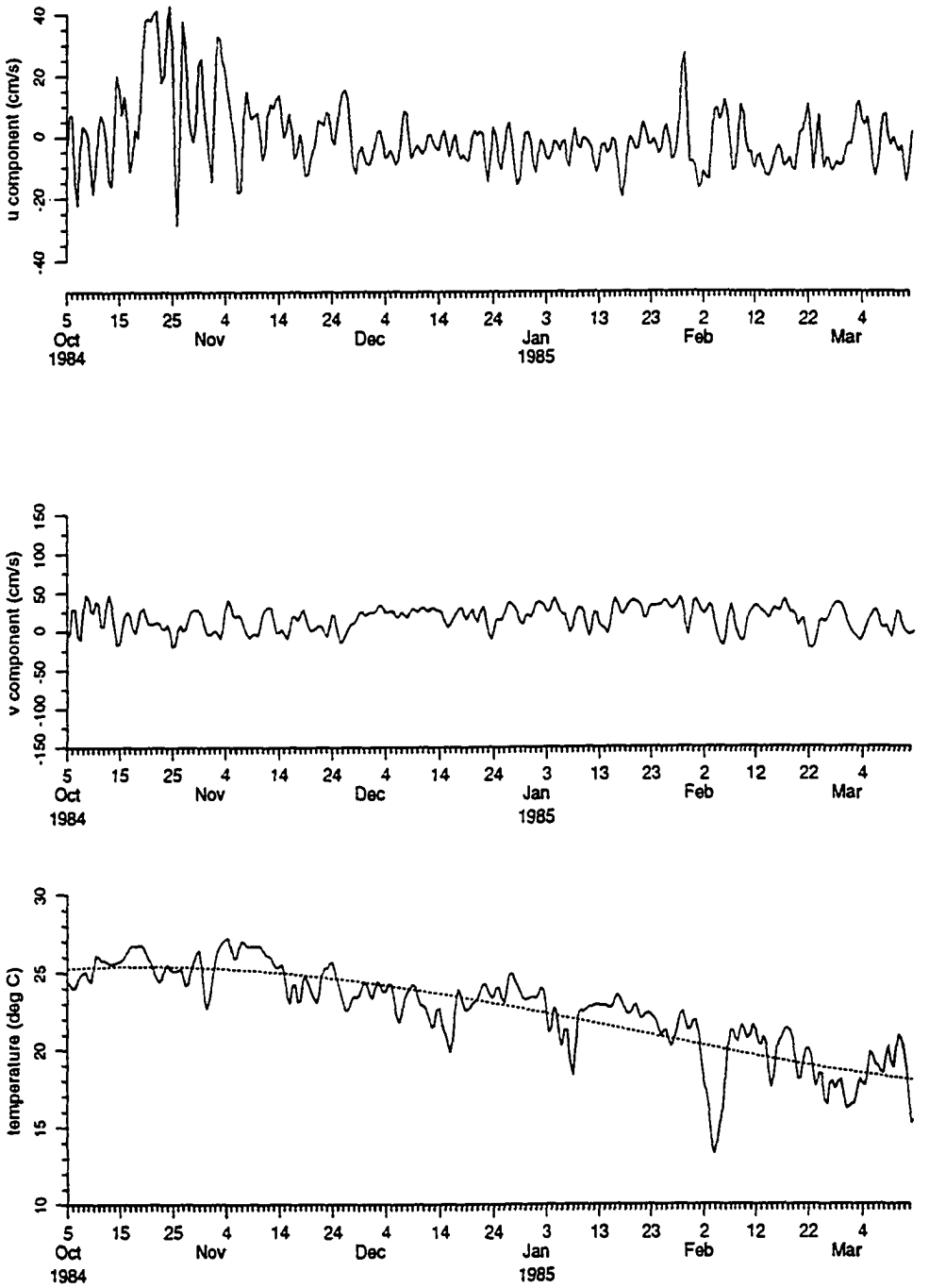


Figure 4.6. Same as in Figure 4.1, except at meter F034, 72-m depth.

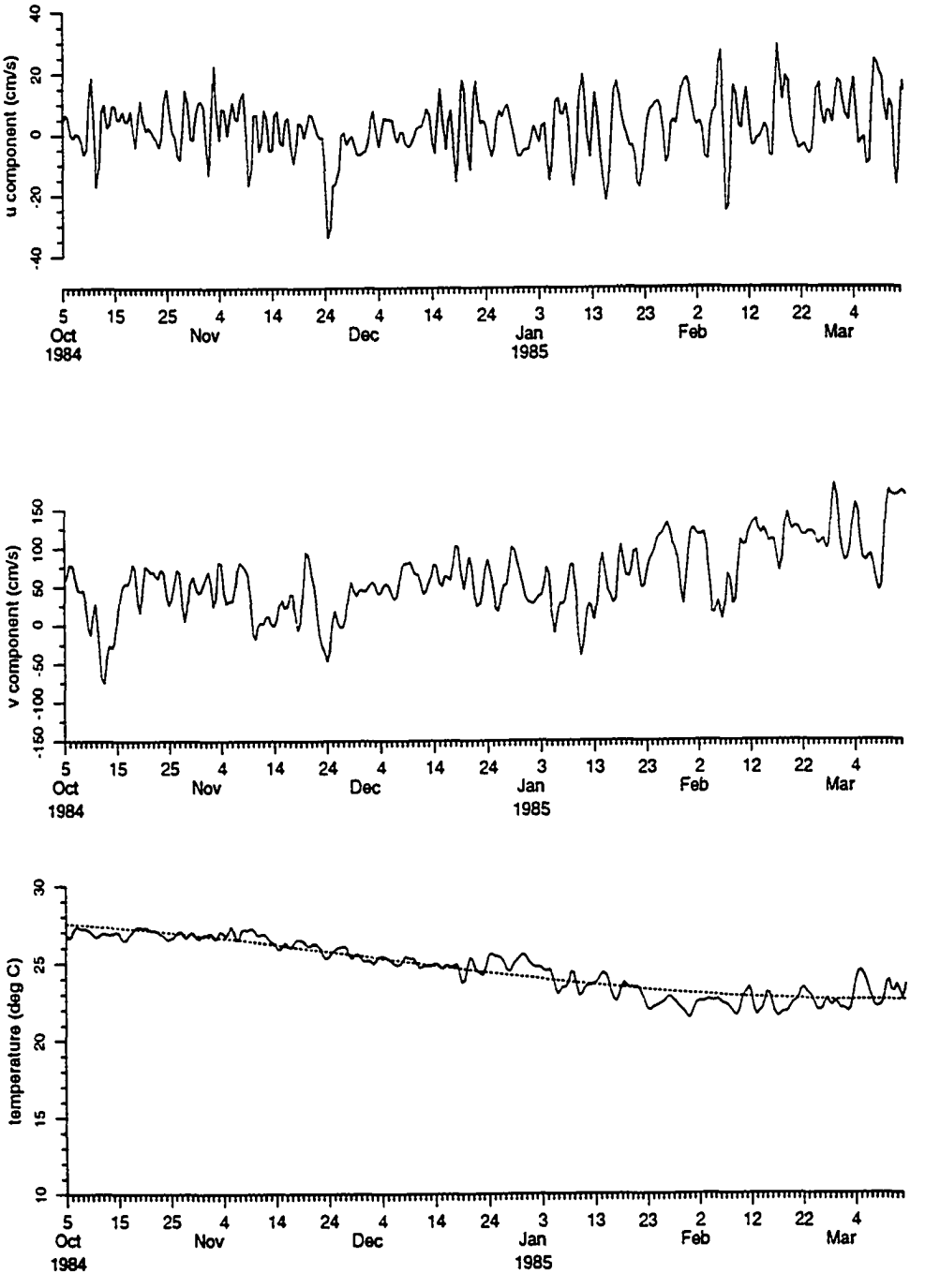


Figure 4.7. Same as in Figure 4.1, except at meter F061, 10-m depth.

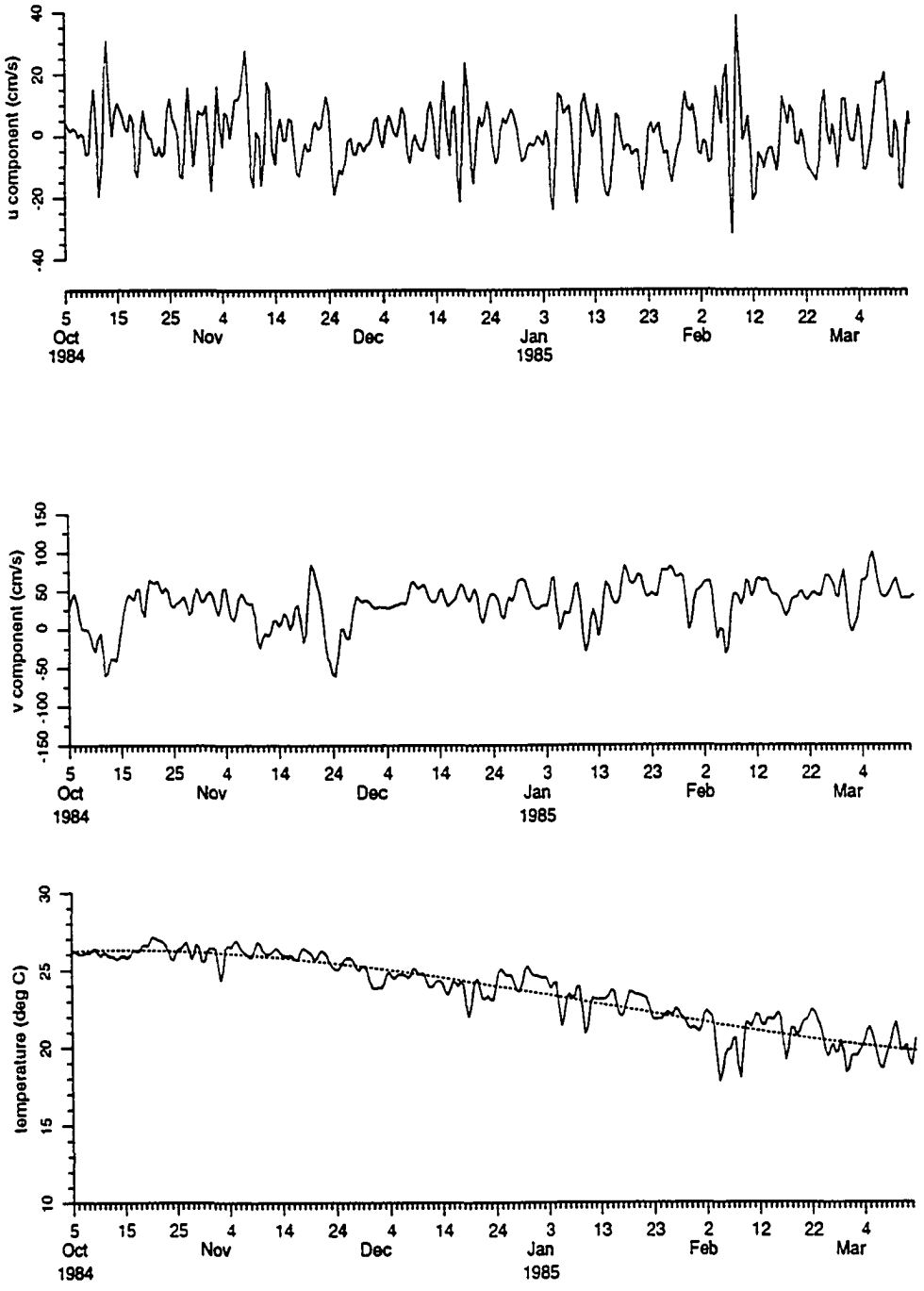


Figure 4.8. Same as in Figure 4.1, except at meter F063. 50-m depth.

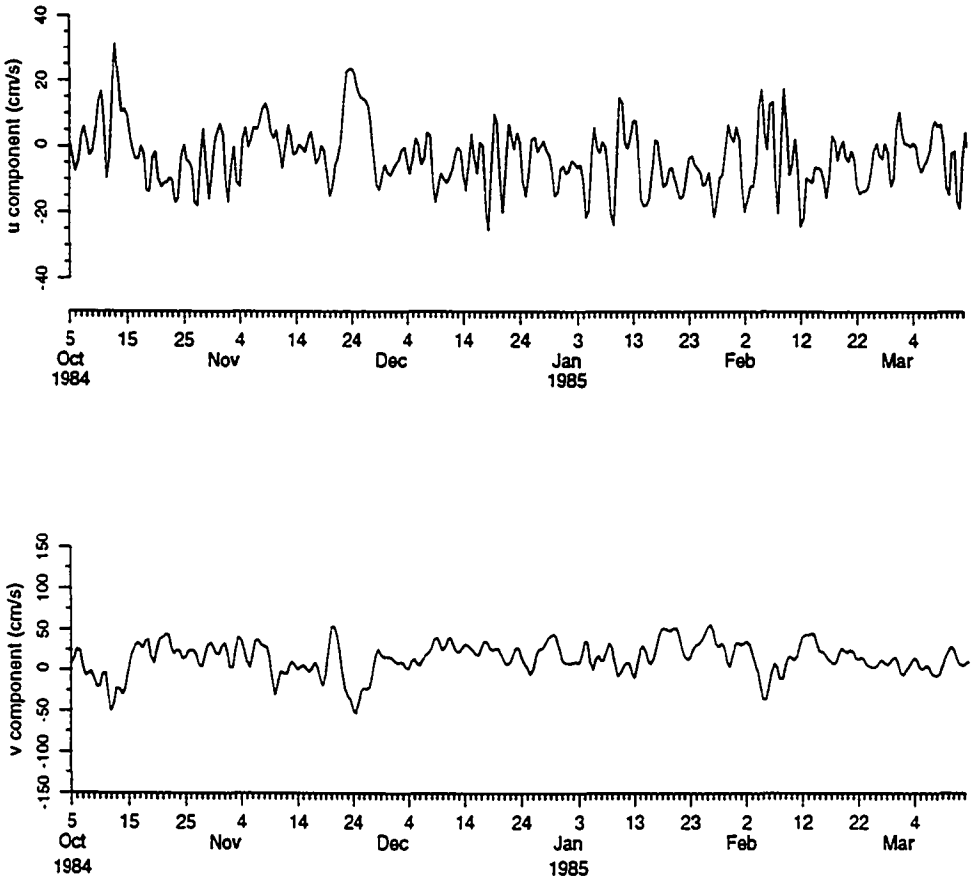


Figure 4.9. Forty-hour low-pass filtered time series of cross-shelf and alongshore currents in cm/sec at meter F064, 72-m depth. The temperature data at this location are not available due to an instrumental failure.

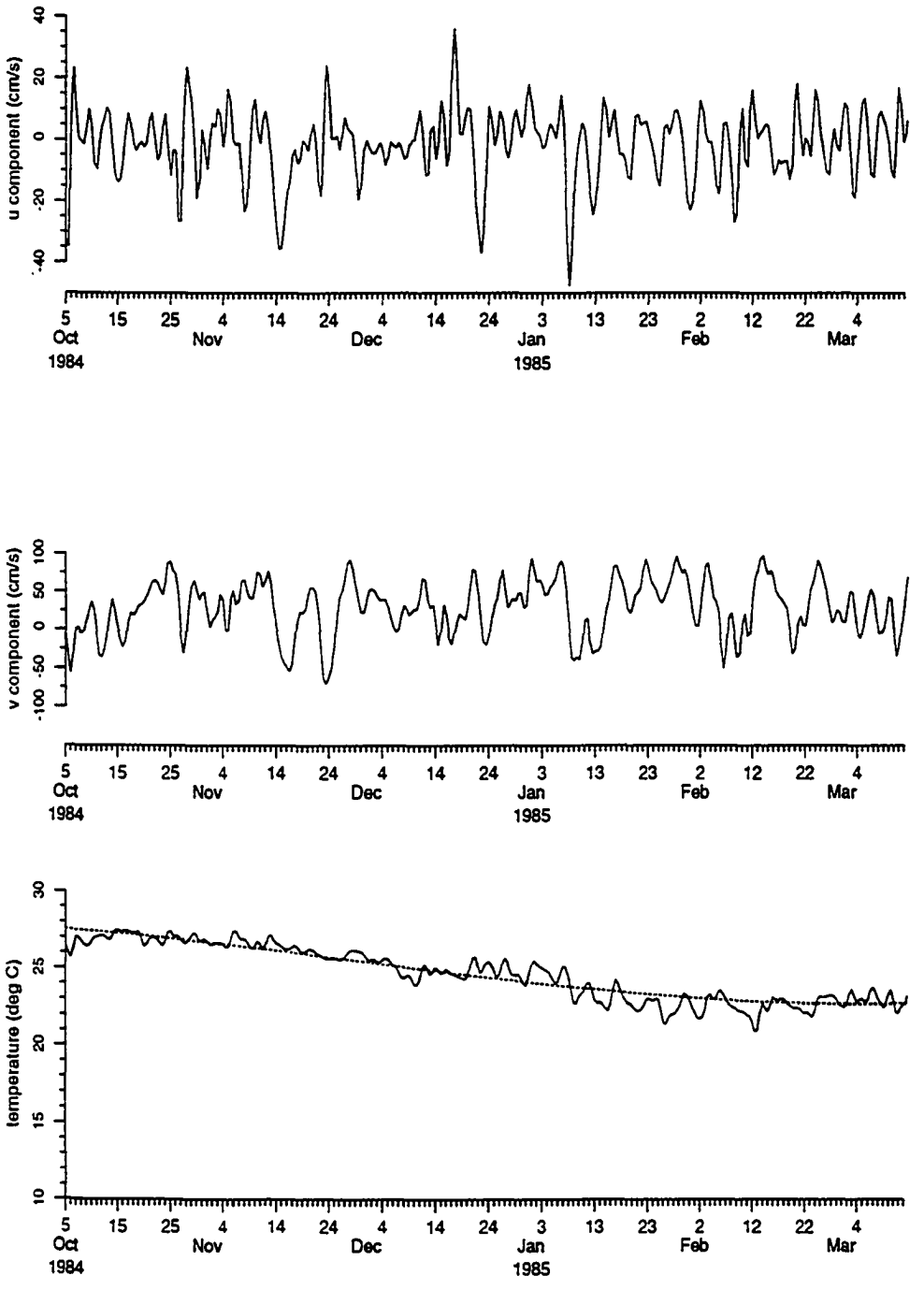


Figure 4.10. Same as in Figure 4.1, except at meter F111, 10-m depth.

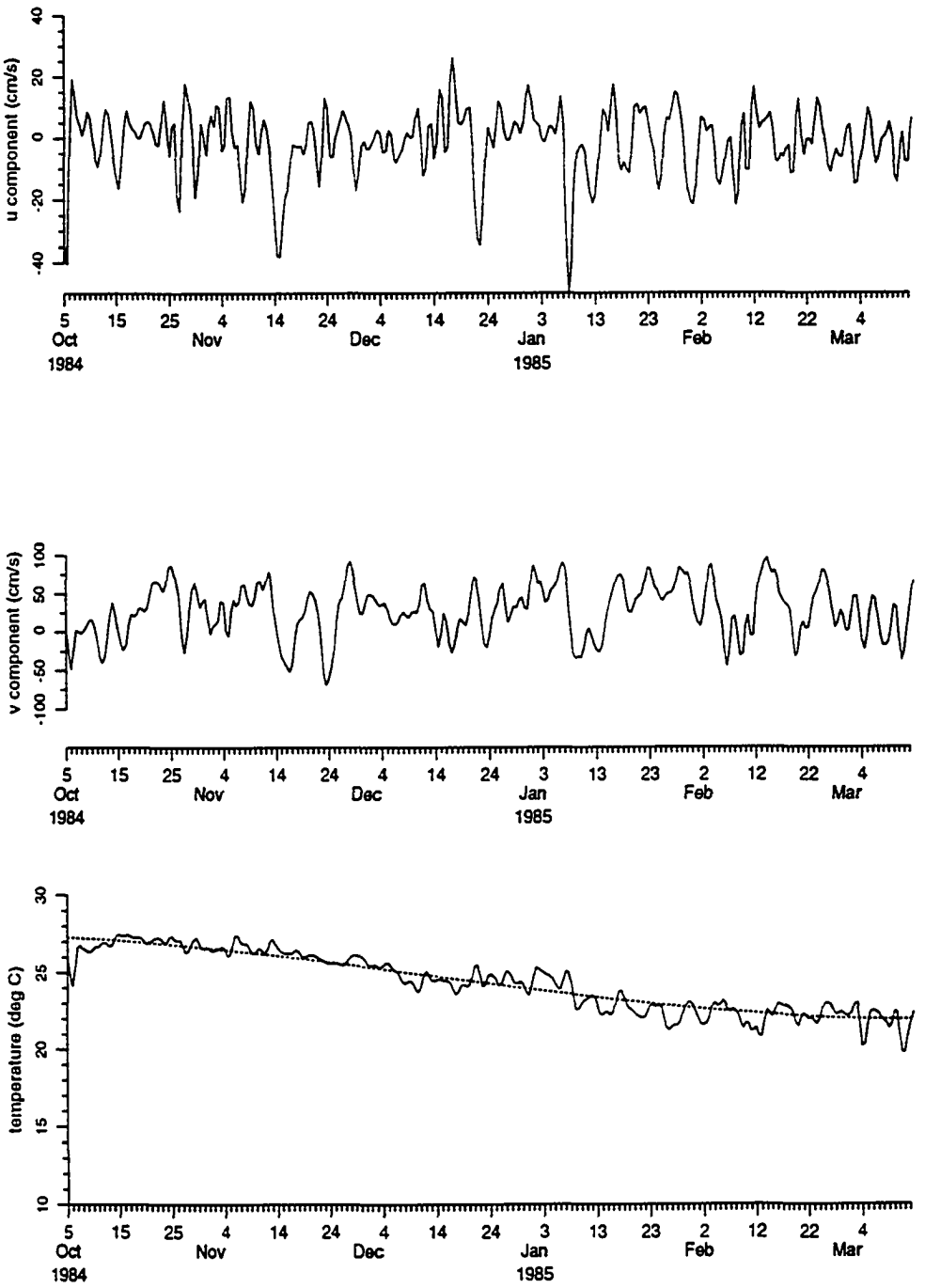


Figure 4.11. Same as in Figure 4.1. except at meter F112. 30-m depth.

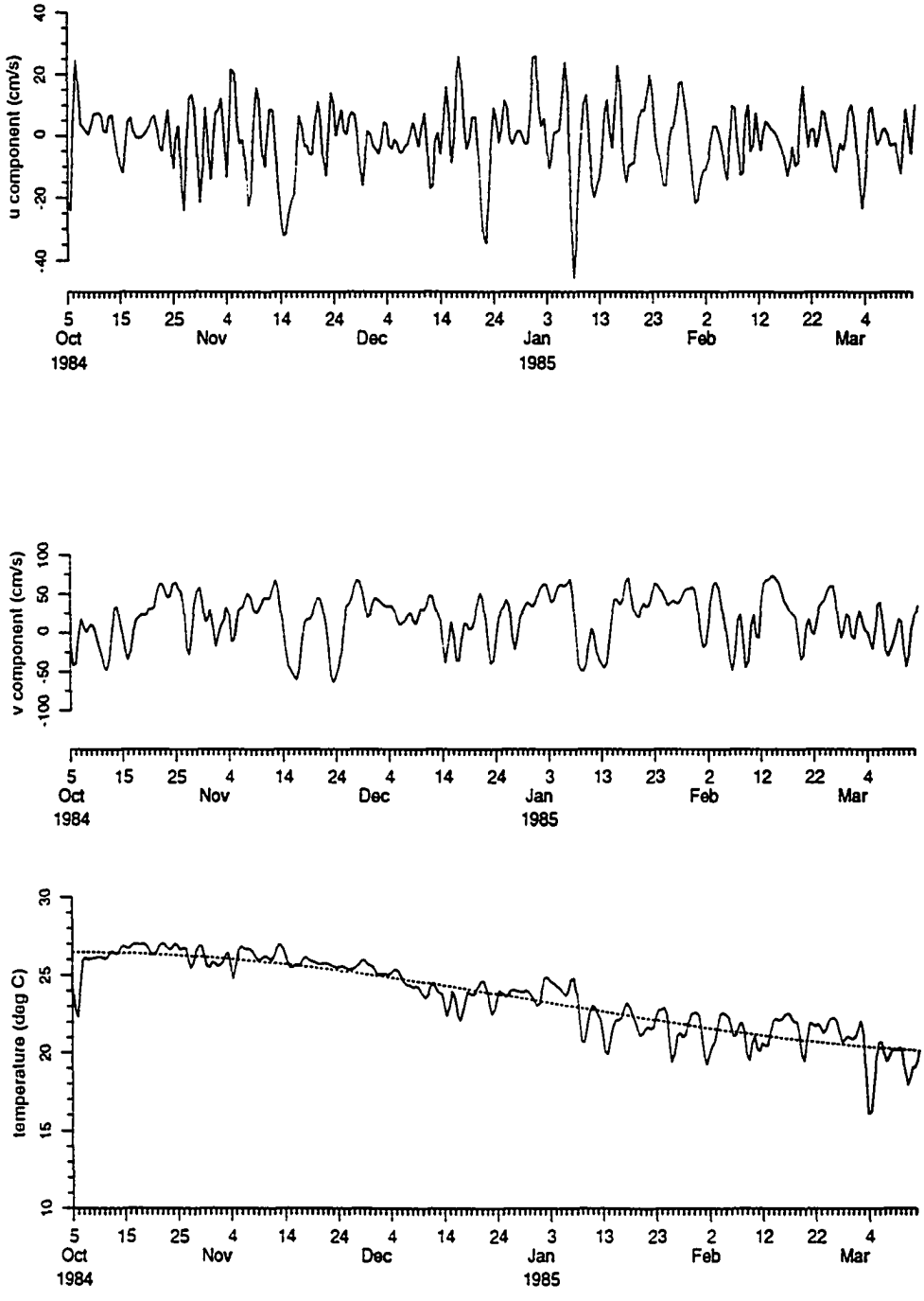


Figure 4.12. Same as in Figure 4.1, except at meter F113, 50-m depth.

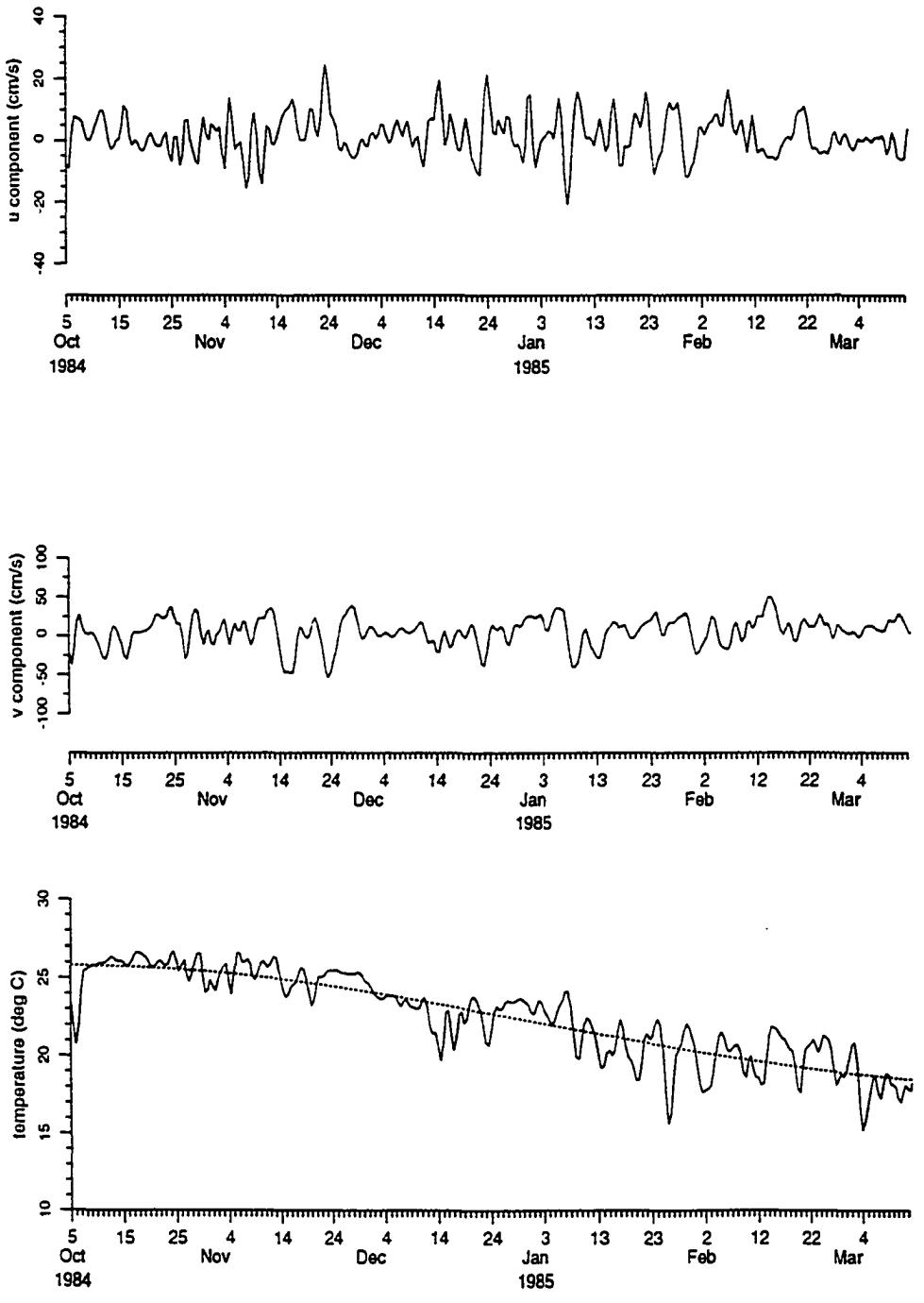


Figure 4.13. Same as in Figure 4.1, except at meter F114, 72-m depth.

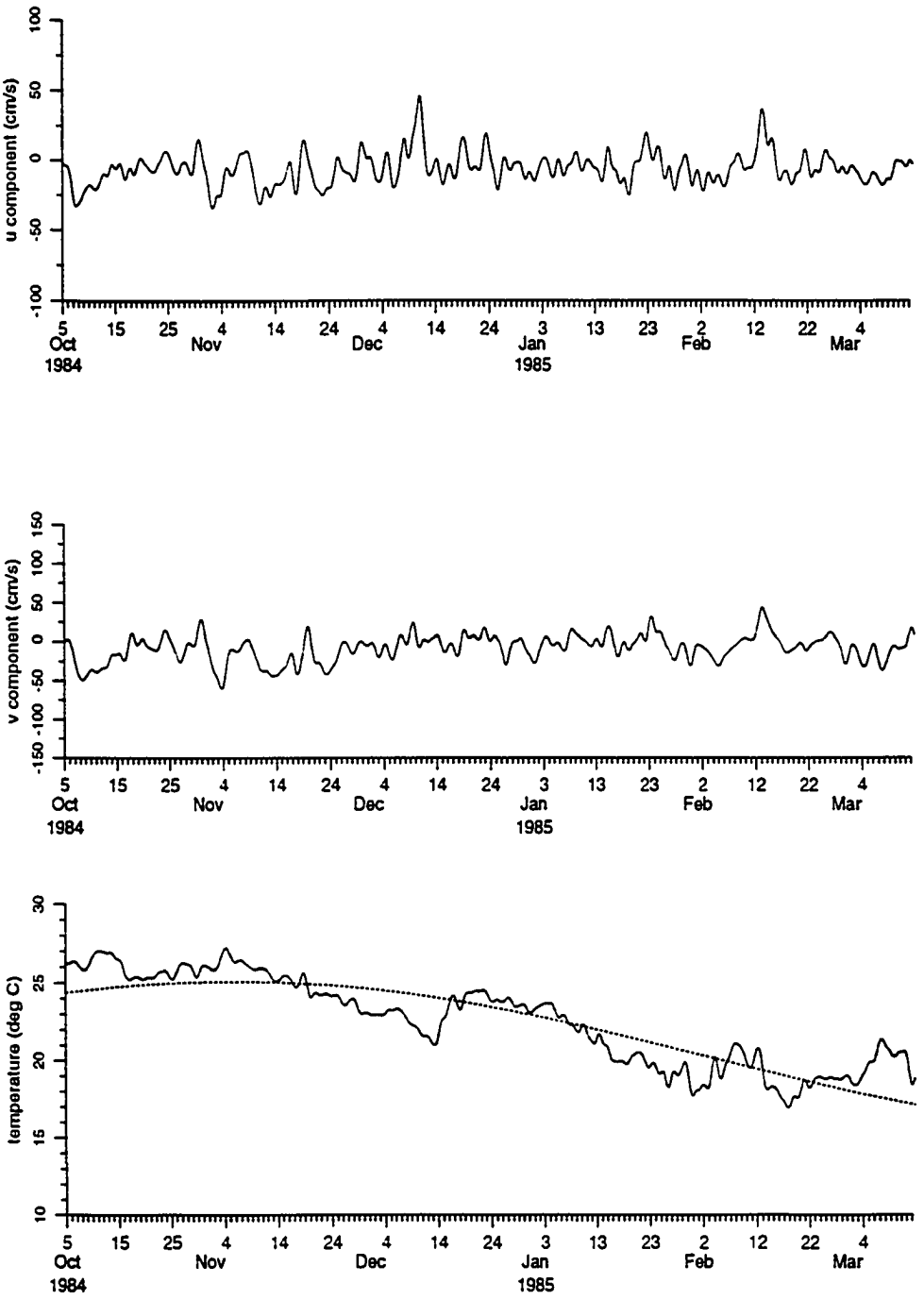


Figure 4.14. Same as in Figure 4.1, except at meter B170007, 7-m depth.

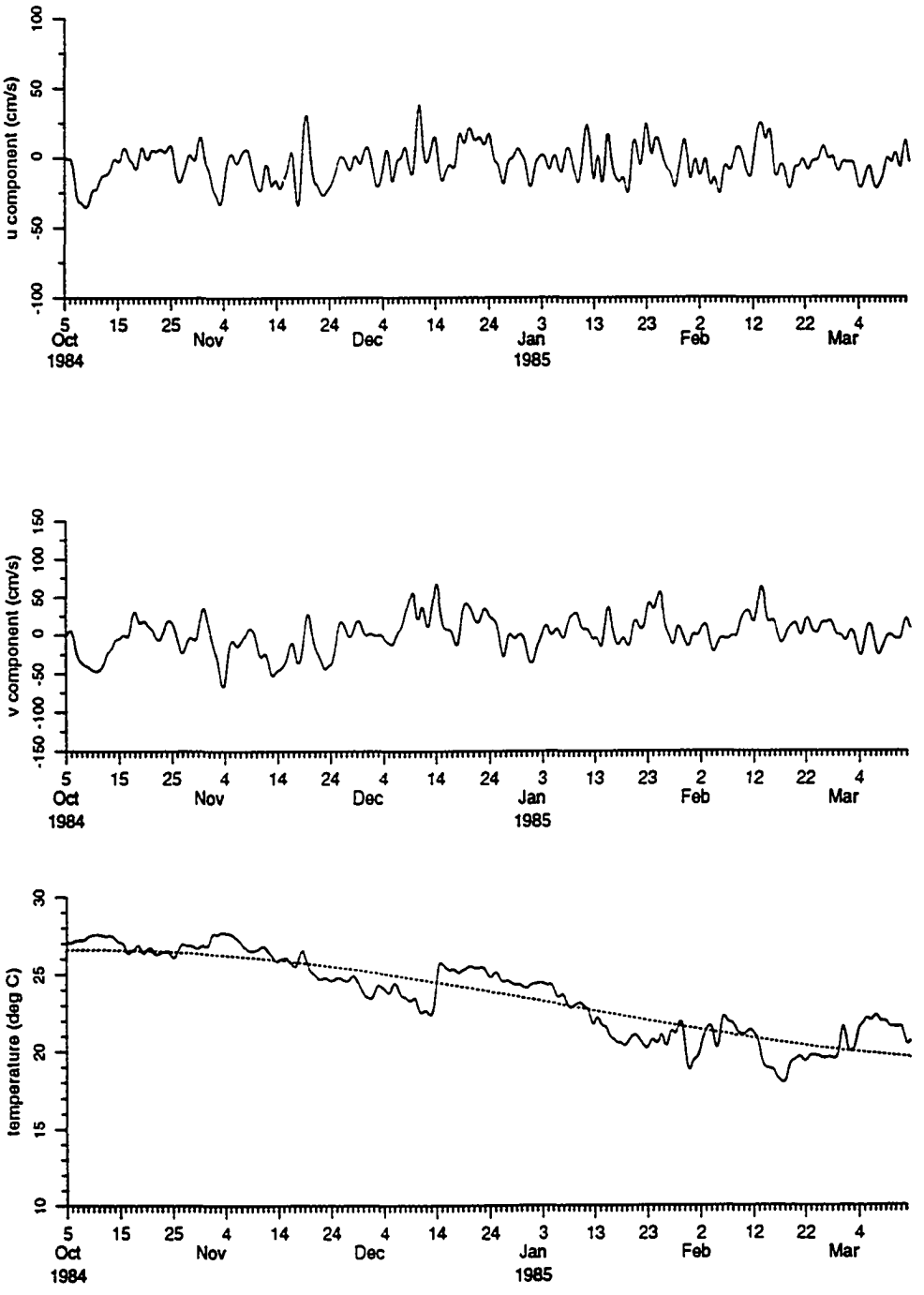


Figure 4.15. Same as in Figure 4.1, except at meter B170040, 40-m depth.

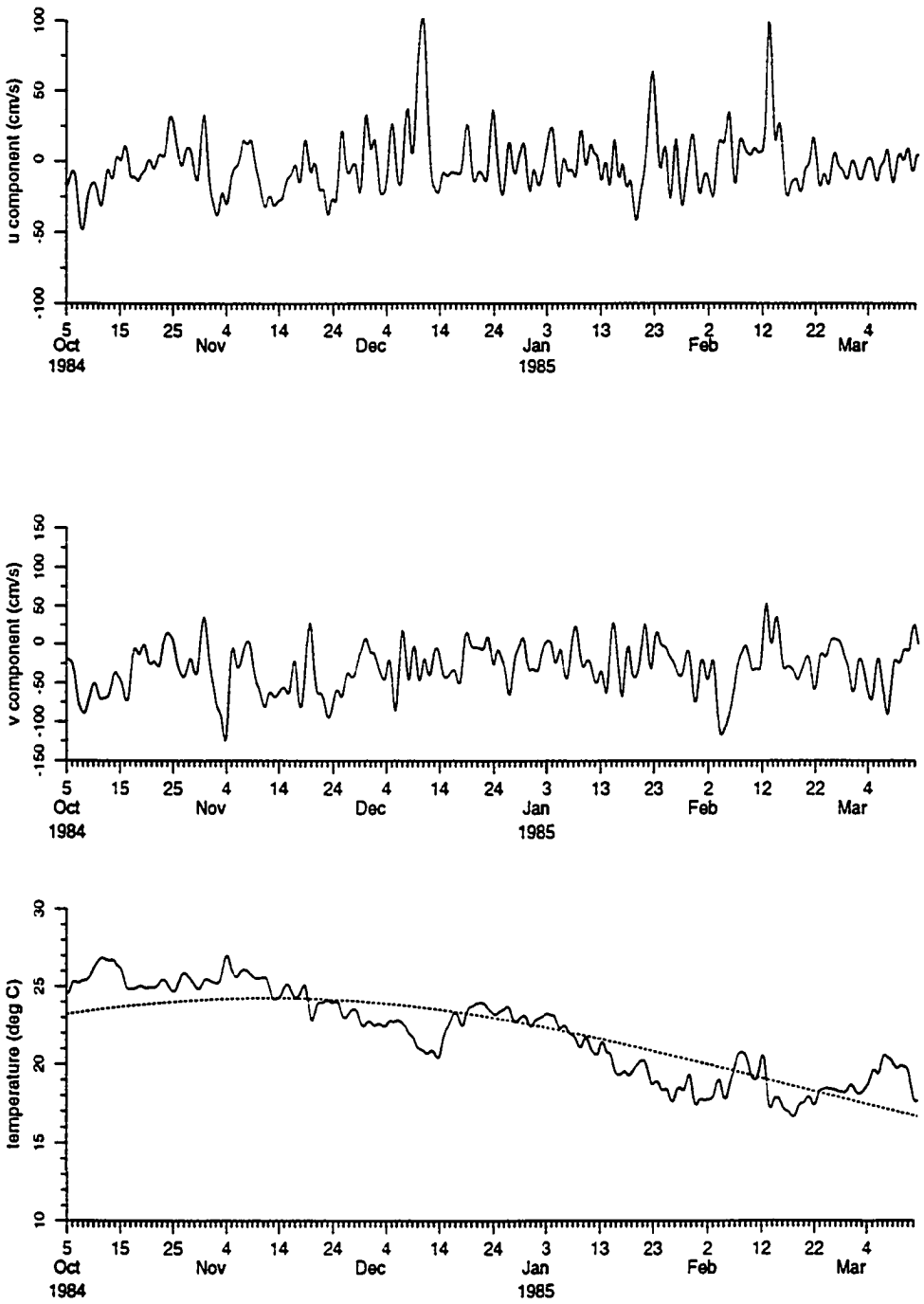


Figure 4.16. Same as in Figure 4.1, except at meter B170070. 70-m depth.

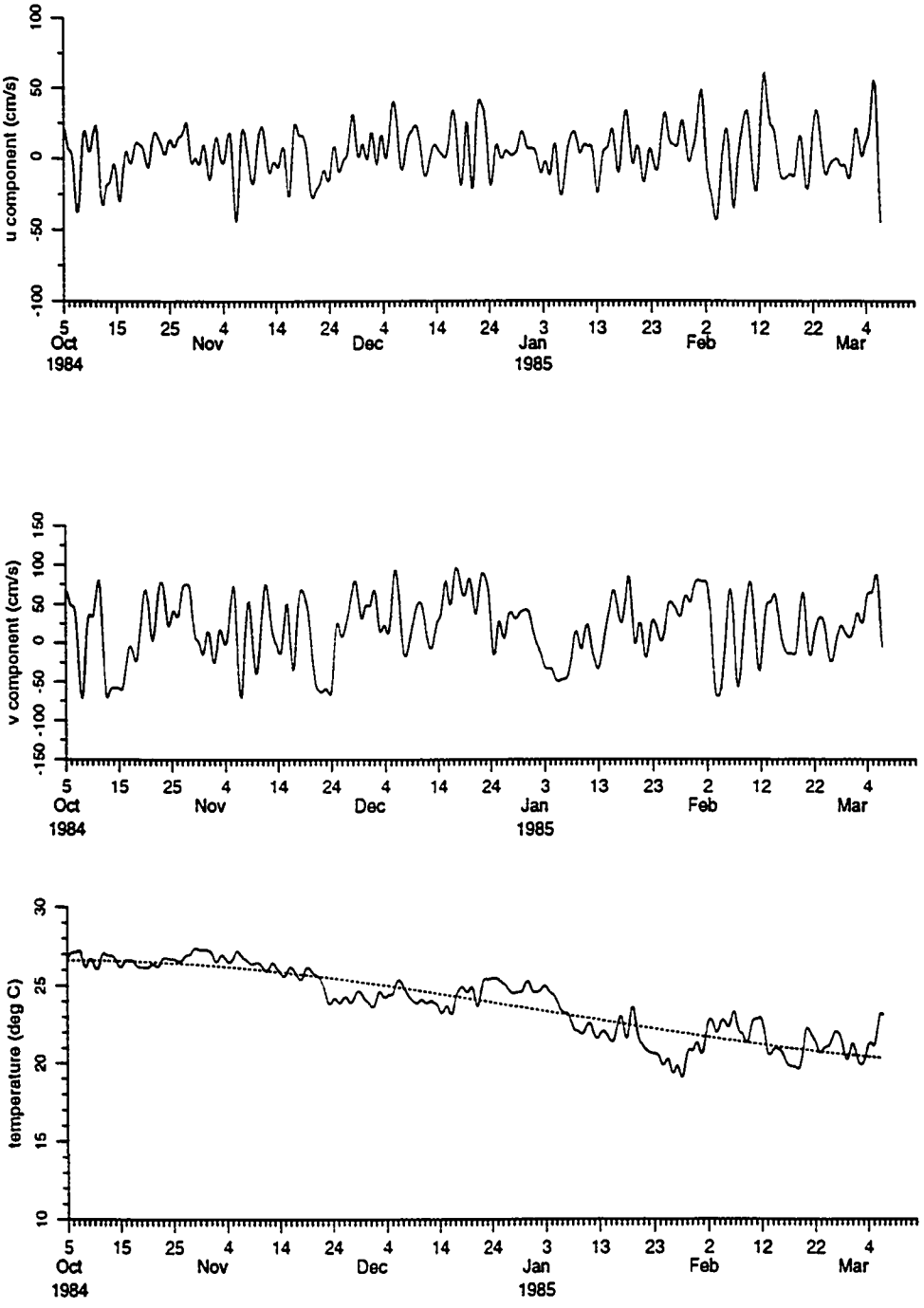


Figure 4.17. Same as in Figure 4.1, except at meter C110020, 20-m depth.

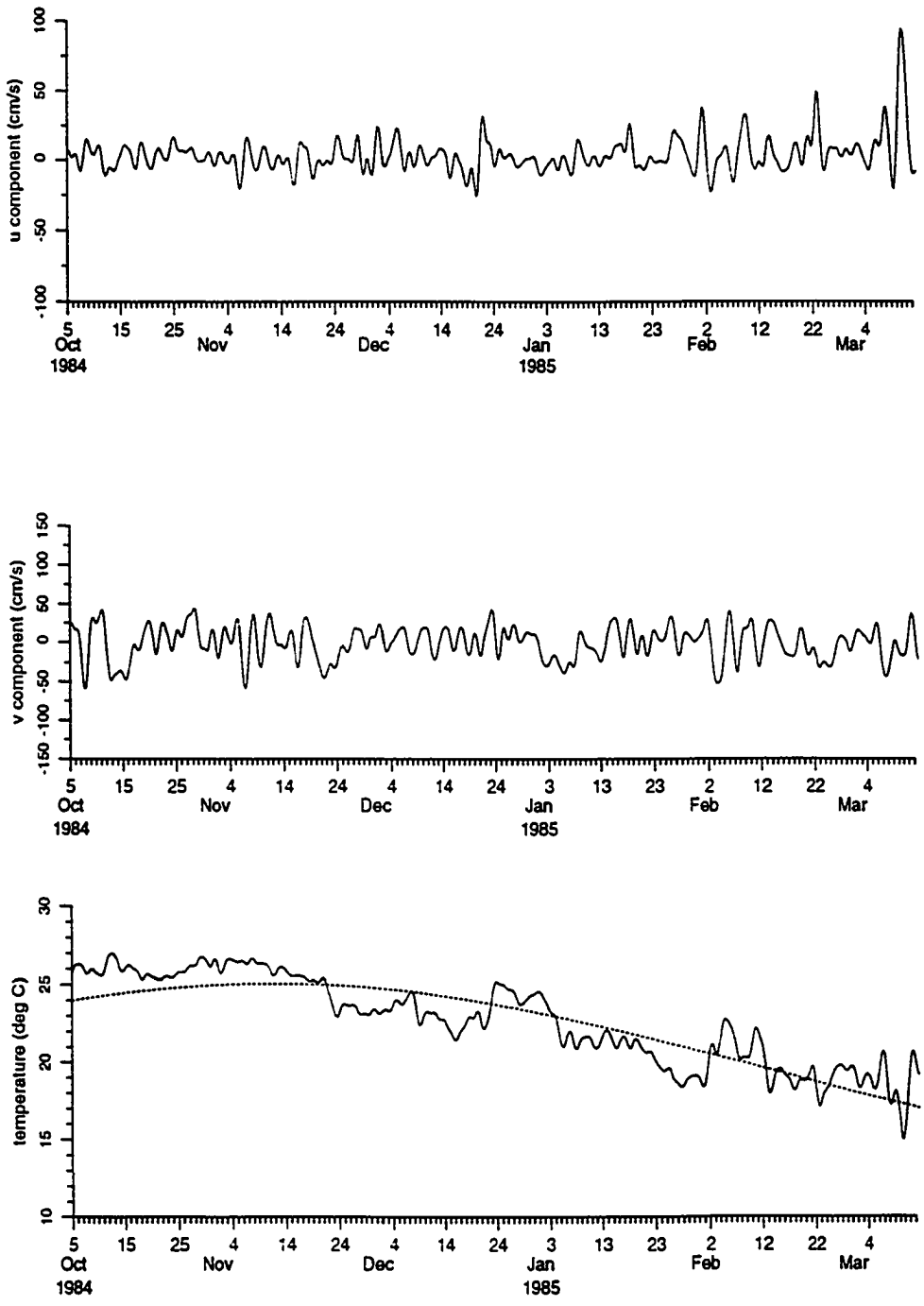


Figure 4.18. Same as in Figure 4.1, except at meter C110071. 71-m depth.

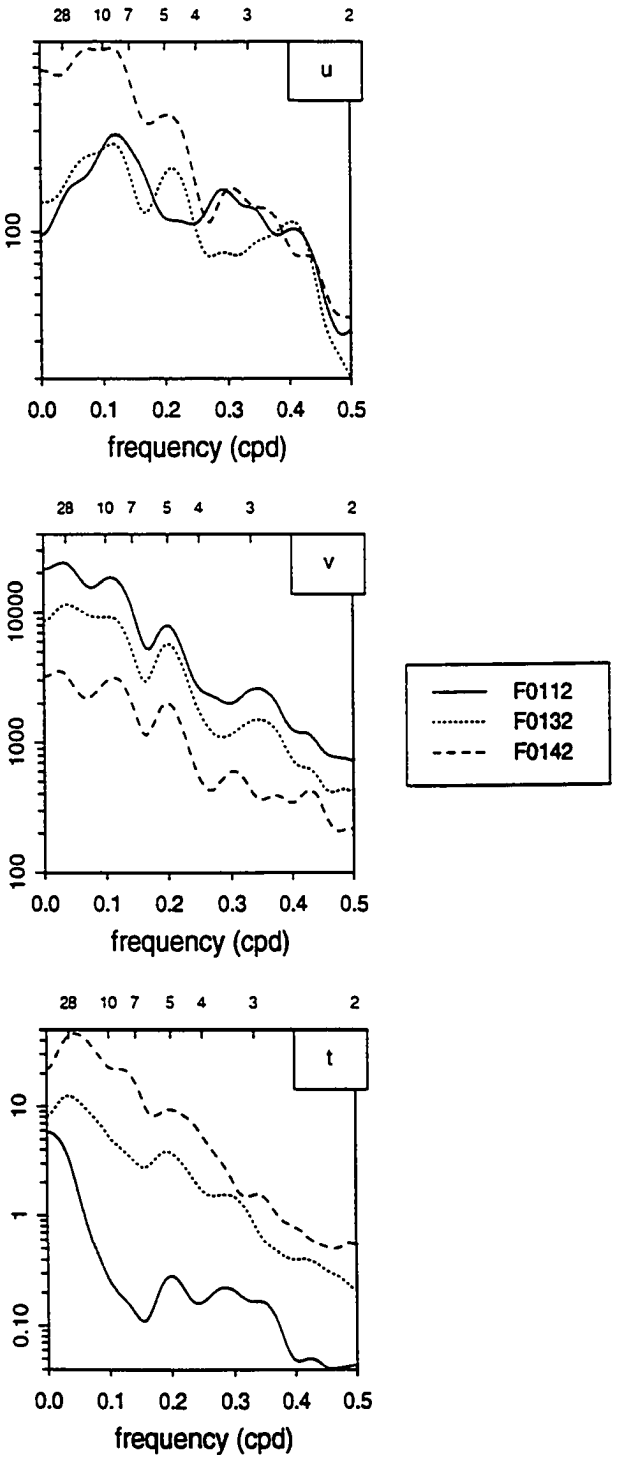


Figure 4.19. Power spectra for cross-shelf ($u$) and alongshore ($v$) currents (both in $cm^2/sec^2/cpd$), as well as temperature (in $(°C)^2/cpd$), for data obtained from mooring F01.

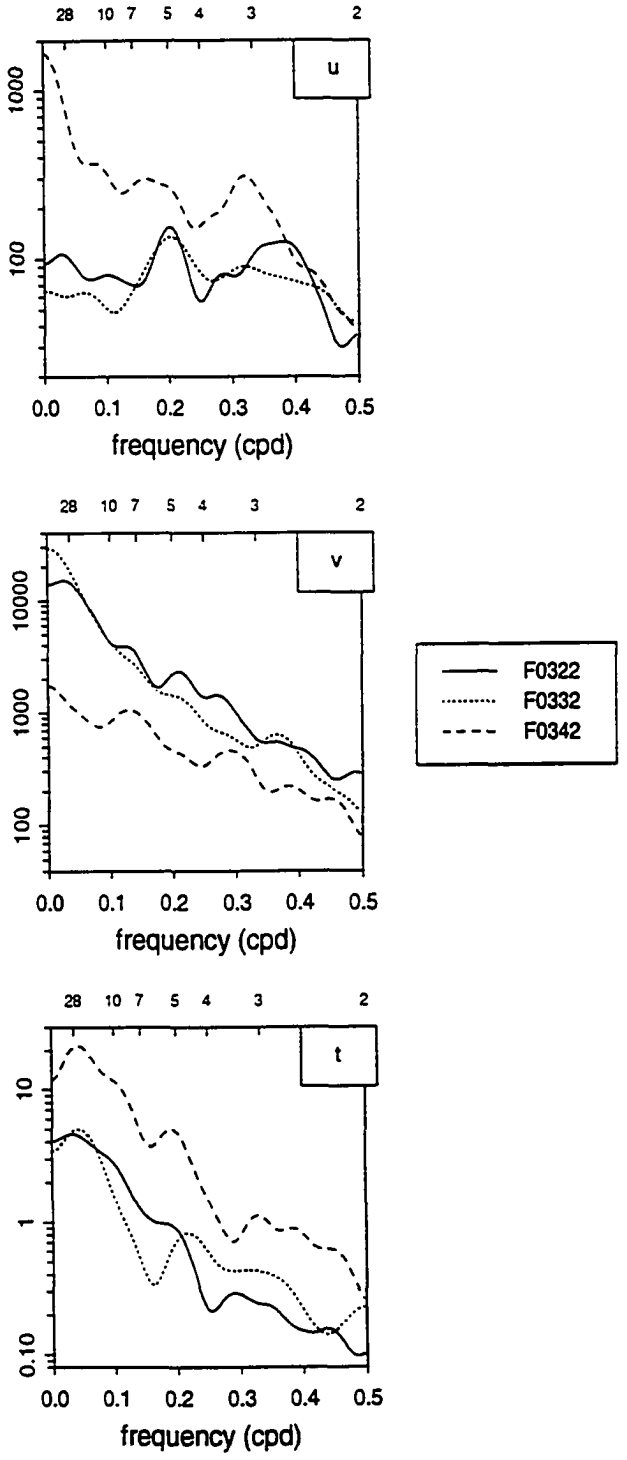


Figure 4.20. Same as in Figure 4.19, except data obtained from mooring F03.

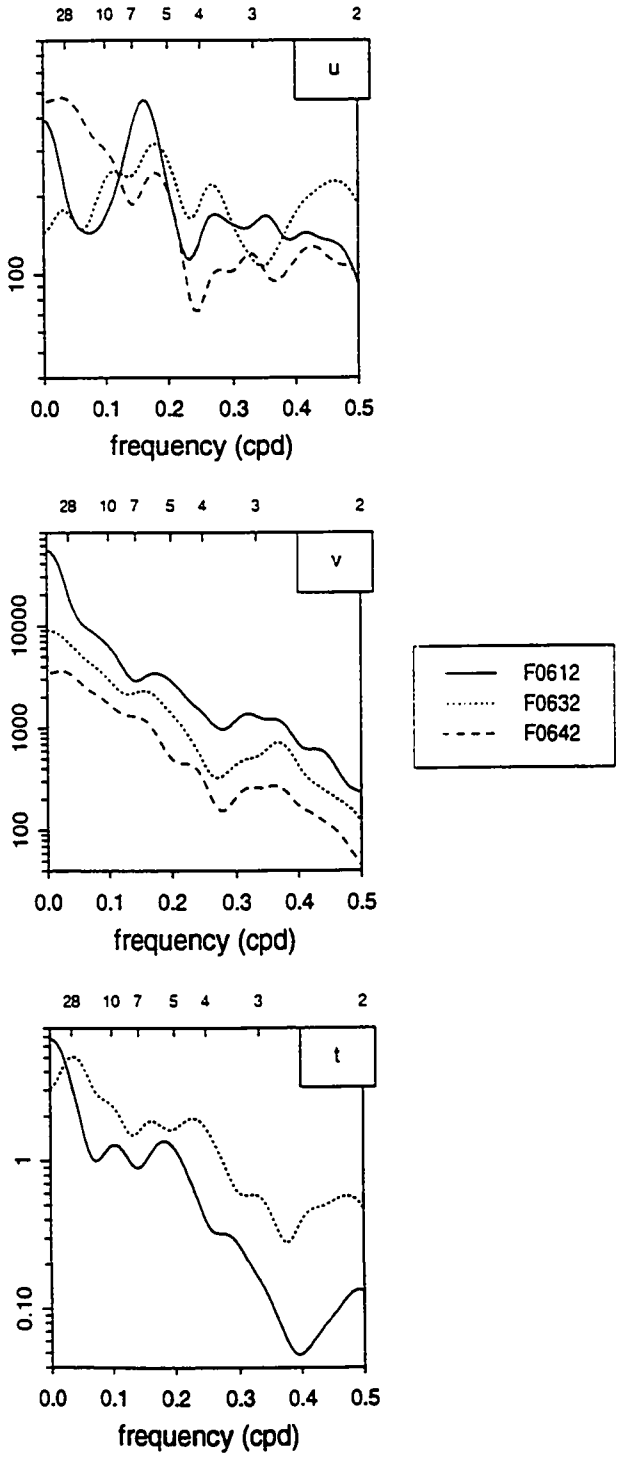


Figure 4.21. Same as in Figure 4.19, except data obtained from mooring F06.

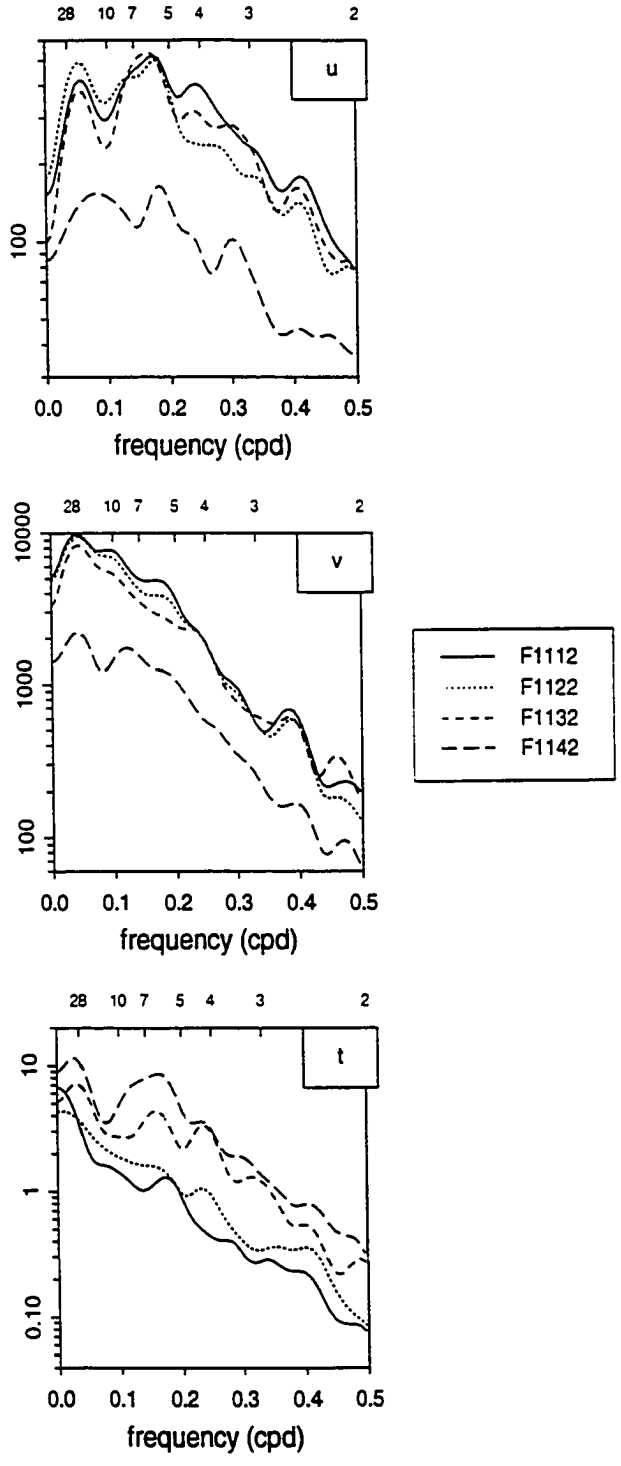


Figure 4.22. Same as in Figure 4.19, except data obtained from mooring F11.

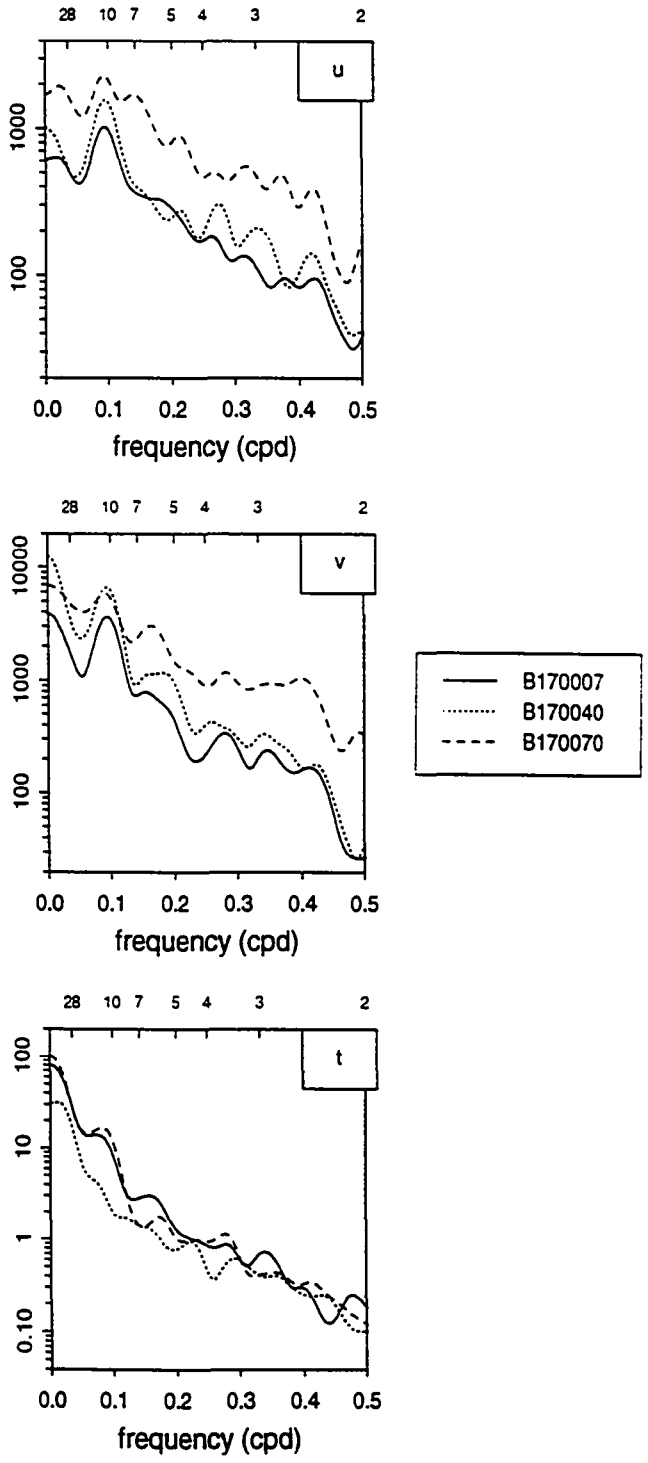


Figure 4.23. Same as in Figure 4.19, except data obtained from mooring B17.

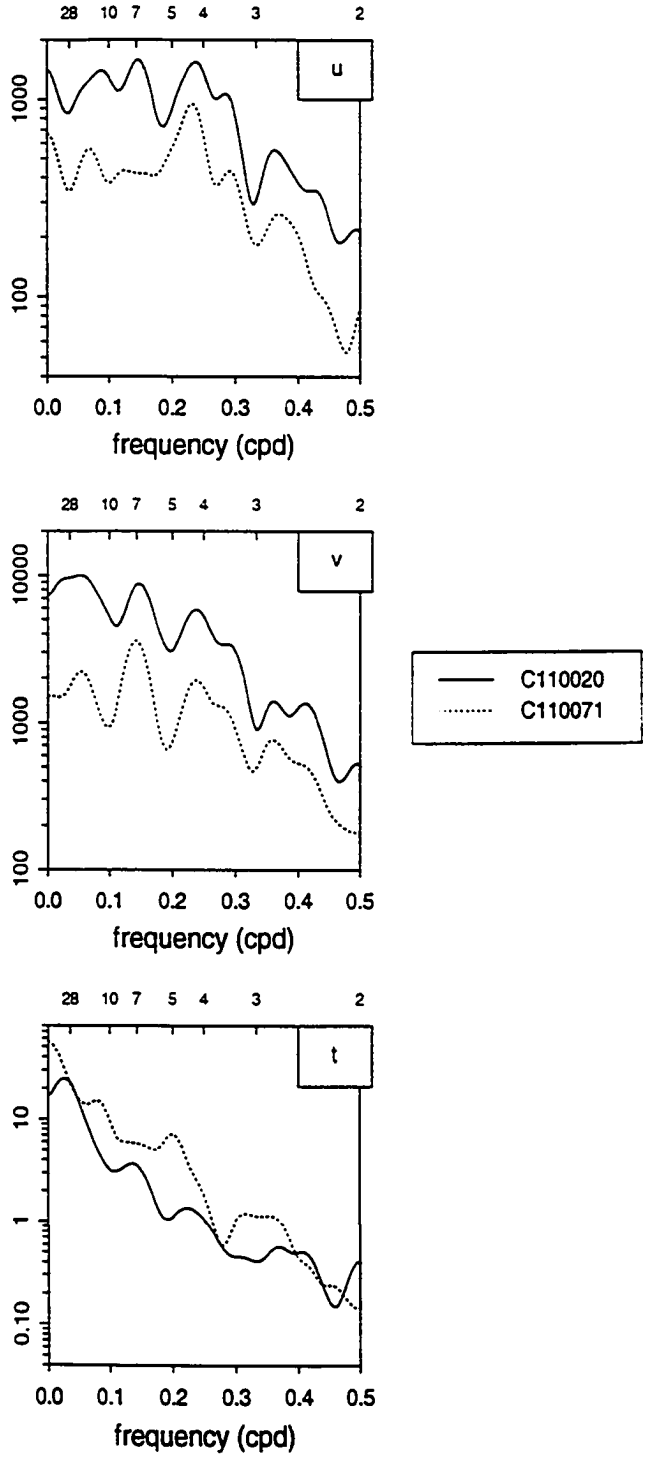


Figure 4.24. Same as in Figure 4.19, except data obtained from mooring C11.

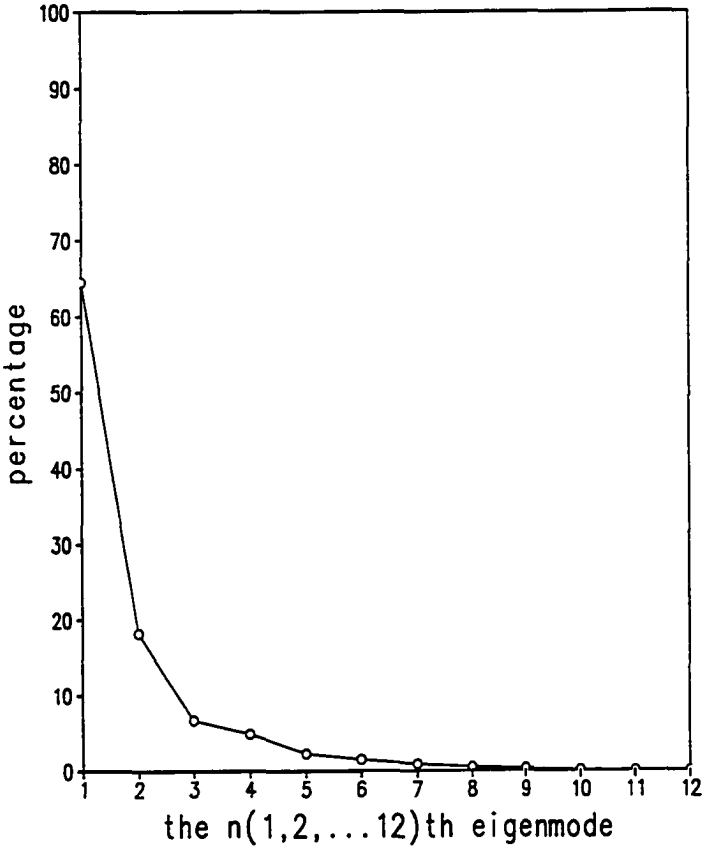


Figure 4.25. Percentage of total normalized variance explained by the 12 EOF modes for the 12 alongshore current records.

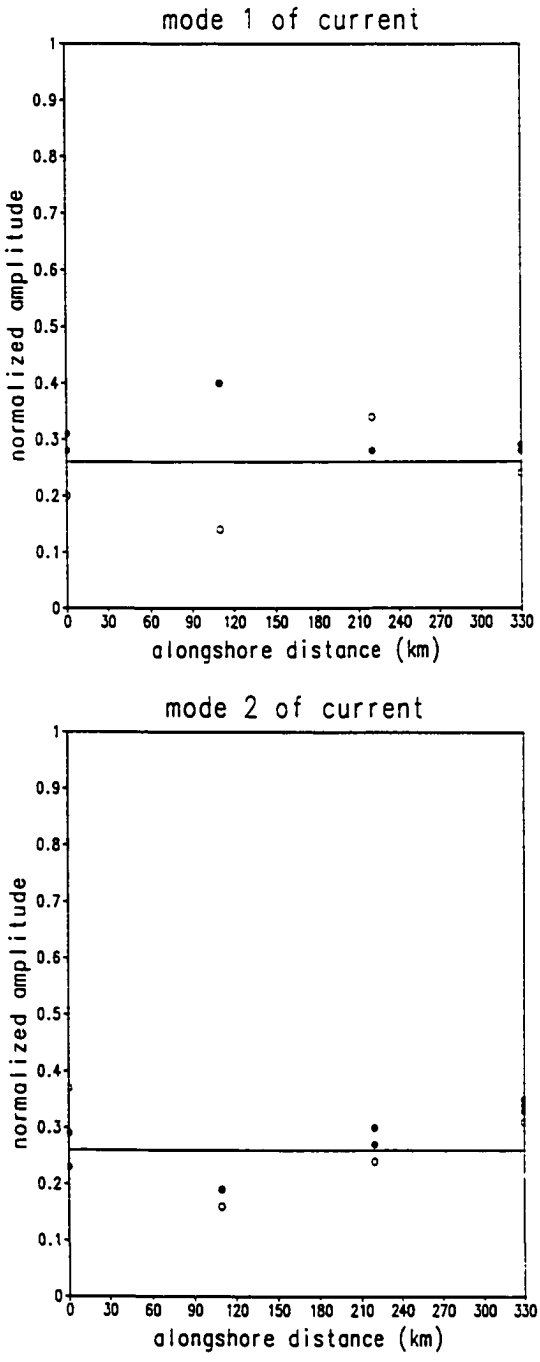


Figure 4.26. Normalized amplitude (coherency) in each alongshore current record corresponding to (a) the first and (b) the second EOF modes for the alongshore currents, open cirles indicate data are from near bottom, straight line denotes the 90% confedence level.

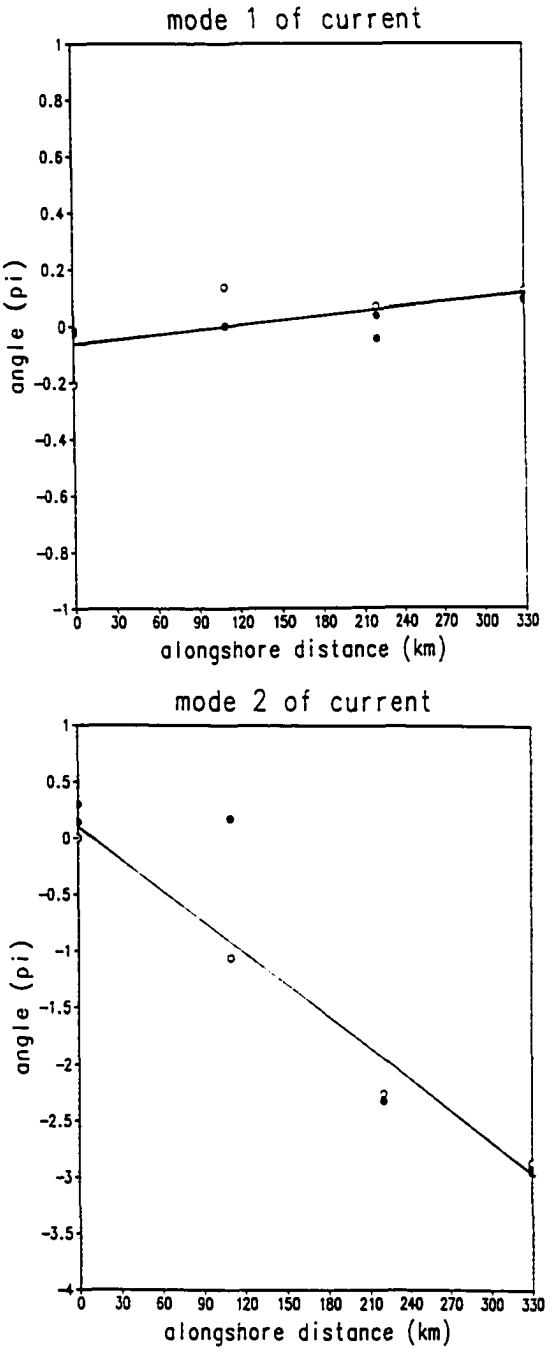


Figure 4.27. Phase lag in each alongshore current record correponding to (a) the first and (b) the second EOF modes for the alongshore currents, open cirles indicate data are from near bottom.

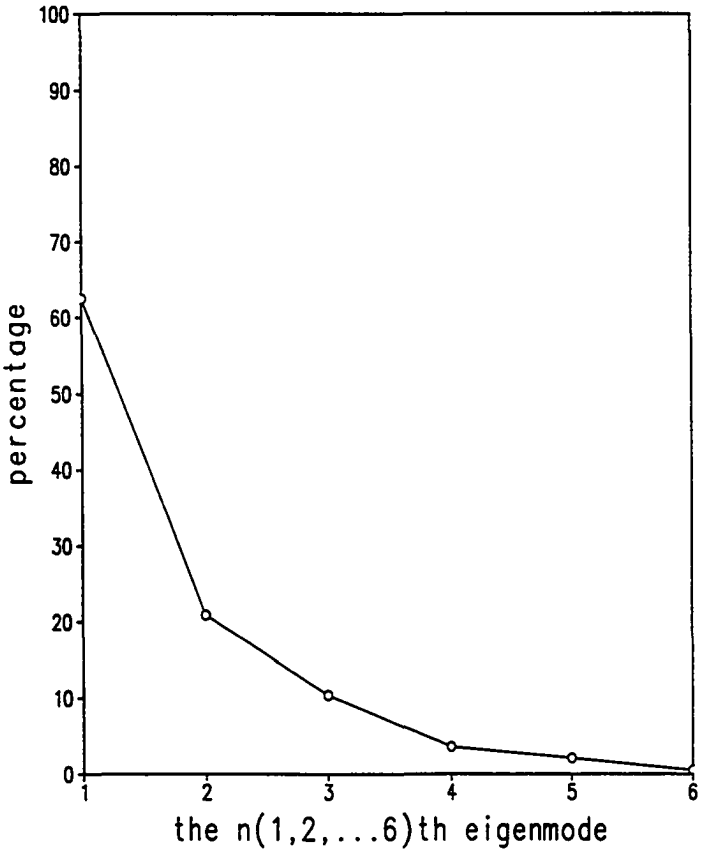


Figure 4.28. Percentage of total normalized variance explained by the 6 EOF modes for the 6 temperature records.

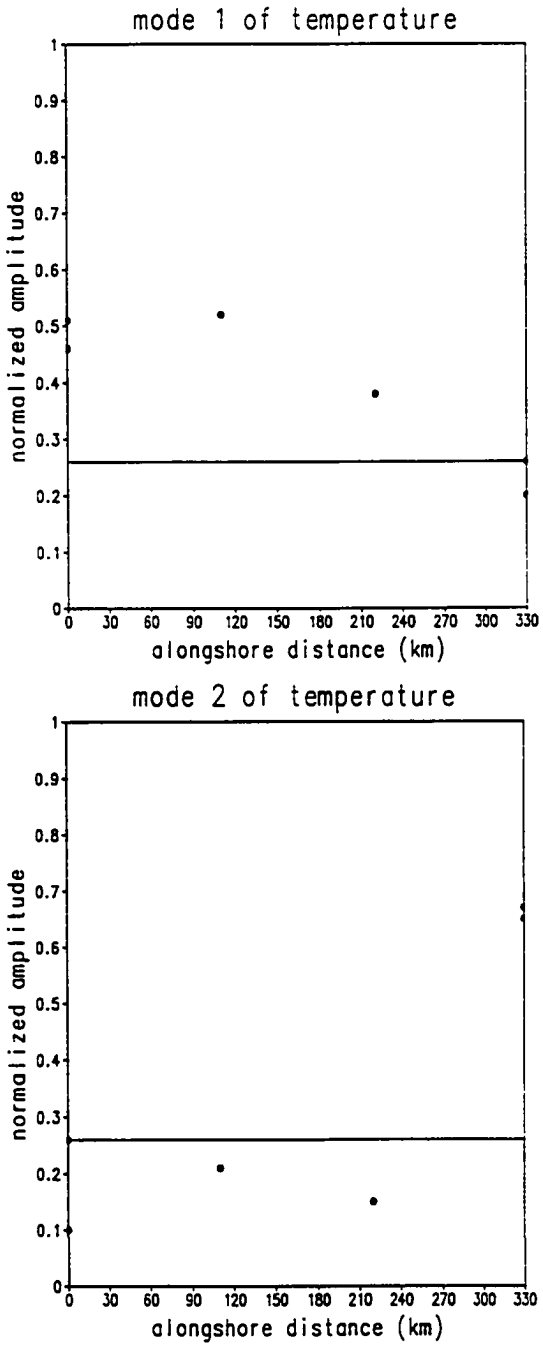


Figure 4.29. Normalized amplitude (coherency) in each alongshore current record corresponding to (a) the first and (b) the second EOF modes for temperatures, the straight line denotes the 90% confidence level.

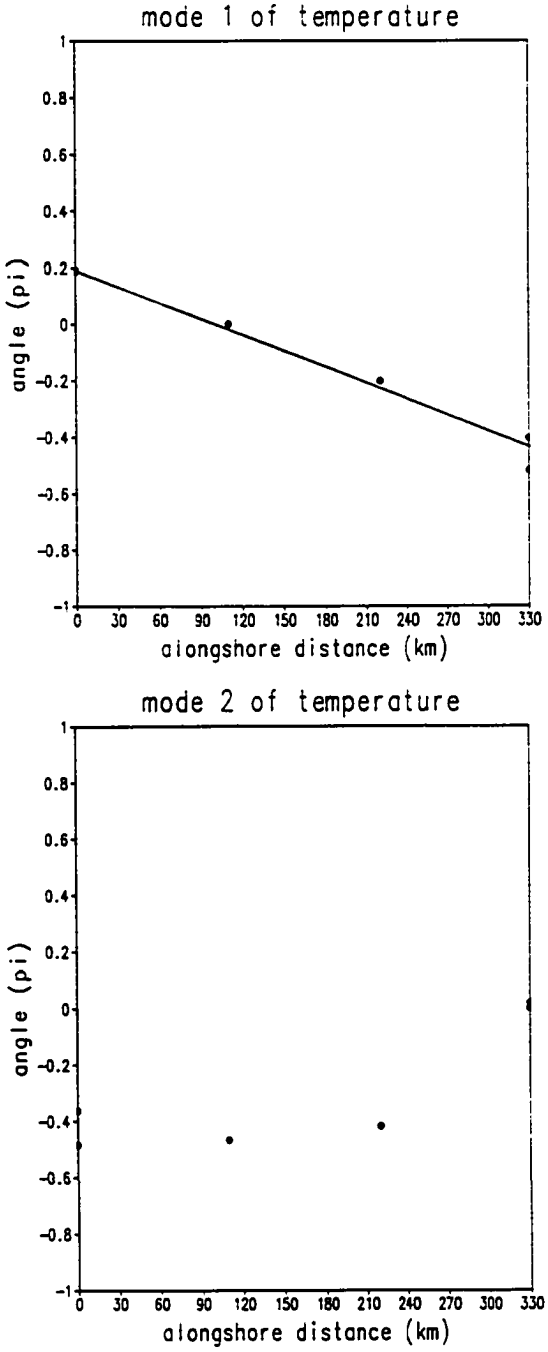


Figure 4.30. Phase lag in each alongshore current records correponding to (a) the first and (b) the second EOF modes for temperatures.

# 5. Theoretical Considerations

As we have noted in last chapter, our power spectra, calculated using the current meter data collected near the shelf break in the South Atlantic Bight from October 1984 to March 1985, strongly suggest that a substantial amount of the energy associated with alongshore current fluctuations was concentrated around the period of 28 days. The frequency-domain EOF analysis based on the current data from south of the Charleston Bump yields two statistically significant eigenmodes, that account for 64.5% and 18.2% of the total normalized variance. The question now is what the possible physical mechanisms that governing theses modes are. In light of the continental shelf dynamics, there appears to be three different classes of mechanism which may be at work, namely: 1) the long-period tides, in particular, the lunar monthly tidal constituent which has a period of 27.6 solar days; 2) the various kinds of continental shelf waves which are coastally trapped in nature; 3) Gulf Stream associated low-frequency fluctuations which are known to exist in data obtained at the immediate proximity of the Stream (*e.g.*, Wunsch, 1980). We shall examine those possible explanations in turn in this chapter.

## 5.1 Long-period Tides

Table 5.1* (from Table 1 in Pietrafesa *et al.*, 1985) lists the principal diurnal and semidiurnal tidal harmonic constituents in the South Atlantic Bight. Although there are total of nine semidiurnal and six diurnal constituents in the table, the

*The energy density values given in both Table 5.1 and Table 5.2 each have been normalized by the values of the principal lunar tide.

principal lunar ($M_2$) tide, with a period of 12.42 solar hours, dominates the SAB tidal dynamics (*e.g.*, Redfield, 1958; Clarke and Battisti, 1981; Pietrafesa, 1983). The tidal regime in the North Atlantic Ocean is in fact chiefly semidiurnal, owing to the fact that the dimensions of the North Atlantic Basin are such that its natural period of resonance is close to the period of the principal lunar ($M_2$) tide (Redfield, 1980).

As a general rule, the energy contributed by the tides decreases rapidly offshore. In the SAB, according to Pietrafesa *et al.*'s (1985) measurements and calculations, energy at semidiurnal frequencies dominates the inner shelf and mid-shelf regions, accounting for almost 80% of the total kinetic energy there; at the outer shelf, semidiurnal energy accounts for less than 30% of the total energy.

In order to gain a perception as to how much energy may be accounted for by the long-period tides, particularly the lunar monthly tide, we wish to estimate the order of magnitude of energy made up by the lunar monthly constituent in terms of the total energy associated with the low-frequency fluctuations. Since there are no suitable long term current measurements available in this area for conducting a long-period tidal harmonic analysis, we are prompted to make our estimates based upon the indirect measurements and calculations.

Let us represent the energy density contributed by the various agents as follows:

$E$ the total fluctuation energy density;

$E_l$ the energy density contributed by the low-frequency fluctuations whose period are longer than forty hours;

$E_h$ the energy density contributed by the high-frequency fluctuation whose period are shorter than forty hours;

$E_s$ the energy density accounted for by the semidiurnal tides;

$E_{M_2}$ the energy density accounted for by the principal lunar ($M_2$) tide;

$E_{M_m}$ the energy density accounted for by the lunar monthly ($M_m$) tide.

Obviously, we have

$$E = E_l + E_h \approx E_l + E_s. \tag{5.1}$$

To be consistent with the earlier estimates we quoted in the last paragraph, we assume that the semidiurnal tides can at most contribute 30% of the total energy, *i.e.*,

$$E_s = 0.30 \times E, \tag{5.2}$$

or, making use of Eq.5.1,

$$E_s = 0.43 \times E_l, \tag{5.3}$$

while

$$E_s = \sum_J E_J, \tag{5.4}$$

where $J$ denotes one of the nine semidiurnal tidal constituents listed in Table 5.1, and the summation goes over all nine of them. We are then able to obtain an estimate for

$$\frac{E_{M_2}}{E_s} = \frac{E_{M_2}}{\sum_J E_J} = 0.78,$$

or in terms of $E_l$,

$$E_{M_2} = 0.78 \times 0.43 \times E_l = 0.335 \times E_l. \tag{5.5}$$

We further assume that the energy density ratios provided by Table 5.2 (after Table 13.1 in Pond and Pickard, 1983) are representative to the SAB region, we can obtain an estimate for $E_{M_m}$ in terms of $E_{M_2}$ as

$$E_{M_m} = 0.008 \times E_{M_2}. \tag{5.6}$$

Finally, making use of Eq.5.5, we have

$$E_{M_m} = 0.008 \times 0.335 \times E_l = 0.003 \times E_l. \tag{5.7}$$

That is, the energy contributed by the lunar monthly tidal constituent can at most account for 0.3% of the total low-frequency current fluctuations. Thus we are fully convinced that the long-period tides can be safely neglected as far as the energy of subinertial current fluctuations is concerned.

## 5.2 Continental Shelf Waves

It has been well recognized that the continental shelf acts as an efficient wave guide for the propagation of subinertial sea level and current fluctuations over vast distances. These propagating oscillations are generally referred to as continental shelf waves. In the northern (southern) hemisphere, they propagate their phases with the coast to the right (left). At mid-latitudes (as the SAB is), shelf waves typically have long wavelengths ($\lambda \gg L$, $L$ being shelf width), low-frequencies ($\omega \ll f$, $f$ being Coriolis parameter or local inertial frequency), and small amplitudes (with sea level fluctuations at $O$(10 cm)) (Mysak, 1980). In the SAB, the values for $L$ and $f$ are $O$(75 km) and $O(7.5 \times 10^{-5}$ radian/sec) (corresponding to an inertial frequency of 1.03 cpd), respectively. In regions where intense western currents occur (*e.g.*, the east coast of the United States—where the SAB is located) the mean shear of the current $\partial v/\partial x$ can be comparable in magnitude to $f$. In that case, three new effects may arise (Mysak, 1980): (1) shelf waves can be significantly advected by the current and have their propagation characteristics strongly modified; (2) shelf waves can become amplified, extracting kinetic energy from the mean flow through the process of barotropic instability; and (3) a new class of shear waves can exist.

As we have discovered in our current data analysis in the last chapter, the first and second current EOF modes each represents southward and northward propagating signals with wavelengths of 5000 km and 360 km, respectively. Since

the characteristics of the shelf waves seem to fit the two EOF modes, it is natural for us to ask: do these two modes actually belong to the class of continental shelf waves?

The length scale (~5000 km) of the first EOF mode is indeed enormous. It is difficult to imagine how such a long wave can exist in a continental margin that has a north-south dimension only at the order of 2000 km (*e.g.*, the distance between Nova Scotia and the Straits of Florida). The nature of this "very low frequency" fluctuation which has an extraordinarily long wavelength is puzzling. Interestingly, in analyzing a completely different type of data obtained from the SAB between the Straits of Florida and Cape Haterras, Miller (1994) found annual signals also with exceptionally long wavelength (2000–3000 km) propagating southward (northward) in the region south (north) of the Charleston Bump. In that study, the Navy ocean frontal analysis charts for the 12-year period, 1976–1988, which cover the SAB were digitized. Time series of distance from the shelf break to Gulf Stream's western edge at ten equally spaced cross-isobath transects were extracted. The 30-day low-pass filtered data were then subjected to the time domain and frequency domain EOF analyses. The signals suggest an annual generation of a perturbation in the vicinity of the bump which radiates away as a long annual wave which may be related to, or part of the mechanism which produces the annual modulation of Gulf Stream transport (Miller, 1994).

There are several similarities between our leading EOF mode and Miller's: 1) both data sets directly or indirectly represent current velocity near the shelf break; 2) they all have exceptionally long wavelength; 3) in the region south of the Charleston Bump, they all propagate southward. In addition, Miller's results show that at regions south and north of the bump, the leading modes have different wavelength (3000 km *vs.* 2000 km) and propagate to different directions

(southward *vs.* northward), which substantiates our finding that the southern and northern regions do not share a commom mode (or, have different wave characters). The major difference between the two being that the signals in Miller's study have even longer periods (monthly to annually) than ours (monthly). In spite of the difference, the similarities seems to imply a dynamical connection between the two. Without detailed theoretical analysis, the interpretation of the signals can only be speculative. It is probably safe to conclude that our first EOF mode does not belong to the shelf waves. The nature of this mode is likely to be more complex, probably related to the interaction between topographically induced (by the Charleston Bump) wave signals and the Gulf Stream current.

In analyzing sea level oscillations along the coast of North Carolina, Brooks (1978) constructed a barotropic continental shelf wave model based on the bottom topography and mean flow conditions off North Carolina coast, and worked out the dispersion curves for the first three barotropic shelf wave modes (Figure 5.1). We feel that the results of this model may shed some light to the interpretation of our current EOF modes, noting the similarity in both cases as in bottom topography (both can be charaterized by an exponential function) and mean flow conditions (the Rossby number in his case in 0.11, while in our case is 0.13). Figure 5.1 shows that modes higher than the first have a high-wavenumber cutoff for upstream (southward) propagation in the mean current (upstream propagation is indicated by $\sigma > 0$). The first mode does not have an upstream cutoff for large wave number because it is effectively trapped against the boundary, out of the high mean current region offshore (Brooks, 1978). Additionally, at the long wavelength end, the first mode always has a much longer wavelength compared to the higher modes at the same frequency, and thus has a higher phase speed to offset the downstream advection. On the contrary, the second and higher modes are partially trapped

over the shelf-slope juncture in the high mean current region, where they are subject to strong downstream advection. As a result, waves traveling downstream in the range of the mean current experience critical points at which their phase speed vanishes relative to the mean current, and they may become unstable (Niiler and Mysak, 1971). Stable downstream waves can also exist, but their frequency spectrum is not discrete (Brooks, 1975; Mckee, 1977). Rather, the downstream half of the dispersion diagram for stable waves is a *continuum*, and the curves in Figure 5.1 do not cross the wavenumber axis (Brooks, 1978). The results imply that for a given frequency of a downstream propagation (in our case, 0.036 cpd), we can find a neighborhood within the accuracy of the calculation, where many wavenumbers (or wavelengths) containing any giving wavenumber (in our case, the wavelength of 360 km) exist. This provides us a theoretical basis to believe that it is possible that our second current EOF mode belongs to a shelf wave mode higher than the first mode, which is advected downstream by the swift current along the shelf edge.

## 5.3 Gulf Stream Associated Low-frequency Fluctuations

In literature, oceanographers often classify the different time scales for the low-frequency fluctuations presented in the geophysical data sets, from the short end towards the long end, as *synoptic*, *mesoscale* (or *eddy-containing* band), *annual*, *interannual* and so on (Wunsch, 1980). Though clear distinctions between the neighboring time scales are not available, they are generally referred to the period band of 1-day to a half month, a half month to several months (but less than a year), a year or so, and those much longer than a year, respectively. A period range around 28-day would fall into the mesoscale band, over which geophysical data generally show a significant amount of, if not the most of, energy (*e.g.*, Wunsch,

1980).

Figures 5.2a and b (from Schmitz, 1978) display the spectra of data records obtained in the near proximity of the Gulf Stream, in *log-log* form and *covariance-preserving* form, respectively. As noted by Schmitz, the motion is much more barotropic in character than in the records obtained elsewhere. This result is consistent with the observation by Richman, Wunsch and Hogg (1977) in that the fluctuation kinetic-energy density increases much faster toward the Gulf Stream than does the potential energy. The near-Gulf Stream records exhibit a strong peak in the 25–30-day range for meridional velocity, but in the zonal velocity, the peak is shifted toward lower frequency. Given the geographic similarity between this location and the current mooring sites where our data are from, (all in the vicinity of the Gulf Stream), it appears that the repeated occurance of the spectral peak around 28-day is more than a mere coincidence, but a well-founded phenomenon, one likely to have a close connection to the Gulf Stream.

Important questions to be answered are from where the fluctuations draw their energy and what processes are involved? Wunsch (1980) lists the four most likely sources as: open-sea generation by meteorology, open-sea baroclinic instability, topographic generation and generation and radiation from strong boundary current, *i.e.*, the Gulf Stream. Meteorologic forcings, mainly the wind stress, since atmospheric-pressure forcing is a very insignificant process compared to the winds and the thermal forcing is known to be comparably weak except on the largest time scales that determine the *mean* (as opposed to the *fluctuating*) thermohaline general circulation, seems to be coherent with currents only at the short-period end of the spectrum, namely, periods shorter than about 10 days (*e.g.*, Düing, Mooers and Lee, 1977; Wunsch and Wimbush, 1977). Further, since the SAB is constrained by the coast to the west and the Gulf Stream to the east, the open-sea

baroclinic instability seems to be simply out of reach to the current variability in the SAB.

If we rule out open-sea generation by meteorology and open-sea baroclinic instability as mesoscale eddy sources, we are left only with topographic generation and the generation and radiation from the Gulf Stream as possible significant eddy sources. As Wunsch (1980) asserts, both are difficult to evaluate quantitatively. In the SAB, the most noticeable topographic irregularity is the Charleston Bump. Lee waves are found to be generated by a topographic irregularity which mimic the Charleston Bump in numerical models (*e.g.*, Chao and Janowitz, 1979), but this topographic impact appears to be confined to the downstream side of the Bump. At the present time, the most likely major source of eddy energy seems to be the Gulf Stream.

As for the processes that are responsible for redistributing the energy, both barotropic and baroclinic instabilities can play an important role. In addition, the radiation process may also be a contributing factor. It is difficult to quantify all these processes, partly because of the inadequate sampling, and partly because of the fact that details of these process are still not fully understood. Our data permits us only to have a somewhat obscure picture of the baroclinic instability process (as we have discussed in Section 4.1): this process appears to be a two-way channel in that the energy conversion from potential energy to kinetic energy can proceed either way between the mean flow and the eddy fields, and for the most part the values of $\overline{u'T'}$ are much smaller than the error bar (see Table 4.3), making it very difficult to decide which way the energy is heading to. However, there is some evidence (Lee *et al.*, 1991) suggesting there are preferred areas where the energy flow has a definite direction. More current and temperature records designed to give a finer spatial resolution (in both longshore and cross-shore directions) and

a longer time span (preferably over a year) are needed before final words can be spoken on the subjects of both low-frequency fluctuations and the energy transfer.

Table 5.1: Principal tidal harmonic constituents in the South Atlantic Bight (after Pietrafesa *et al.*, 1985).

| Species and name | Symbol | Period (solar hours) | Measured Energy Density |
|---|---|---|---|
| **Semi-diurnal:** | | | |
| Luni-solar semidiurnal | $K_2$ | 11.97 | 0.038 |
| Principal solar | $S_2$ | 12.00 | 0.037 |
| Larger solar elliptic | $T_2$ | 12.01 | 0.038 |
| Smaller lunar elliptic | $L_2$ | 12.19 | 0.010 |
| Principal lunar | $M_2$ | 12.42 | 1.000 |
| Larger lunar evectional | $\omega_2$ | 12.63 | 0.080 |
| Larger lunar elliptic | $N_2$ | 12.66 | 0.071 |
| Variational | $\mu_2$ | 12.87 | 0.006 |
| Lunar elliptic second order | $2N_2$ | 12.91 | 0.005 |
| **Diurnal:** | | | |
| Smaller lunar elliptic | $J_1$ | 23.10 | 0.010 |
| Luni-solar diurnal | $K_1$ | 23.93 | 0.051 |
| Principal solar diurnal | $P_1$ | 24.07 | 0.048 |
| Smaller lunar elliptic | $M_1$ | 24.84 | 0.009 |
| Principal lunar diurnal | $O_1$ | 25.82 | 0.007 |
| Larger lunar elliptic | $Q_1$ | 26.87 | 0.004 |

Table 5.2: Characteristics of some of the principal tidal constituents in global oceans (after Pond and Pickard, 1983).

| Species and name | Symbol | Period (solar hours) | Characteristic Energy Density |
|---|---|---|---|
| **Semi-diurnal:** | | | |
| Principal lunar | $M_2$ | 12.42 | 1.000 |
| Principal solar | $S_2$ | 12.00 | 0.221 |
| Larger lunar elliptic | $N_2$ | 12.66 | 0.036 |
| Luni-solar semi-diurnal | $K_2$ | 11.97 | 0.017 |
| **Diurnal:** | | | |
| Luni-solar diurnal | $K_1$ | 23.93 | 0.336 |
| Principal lunar diurnal | $O_1$ | 25.82 | 0.176 |
| Larger lunar elliptic | $Q_1$ | 26.87 | 0.006 |
| **Long period:** | | | |
| Lunar fortnightly | $M_f$ | 327.9 | 0.029 |
| Lunar monthly | $M_m$ | 661.3 | 0.008 |
| Solar semi-annual | $S_{sa}$ | 4383 | 0.006 |

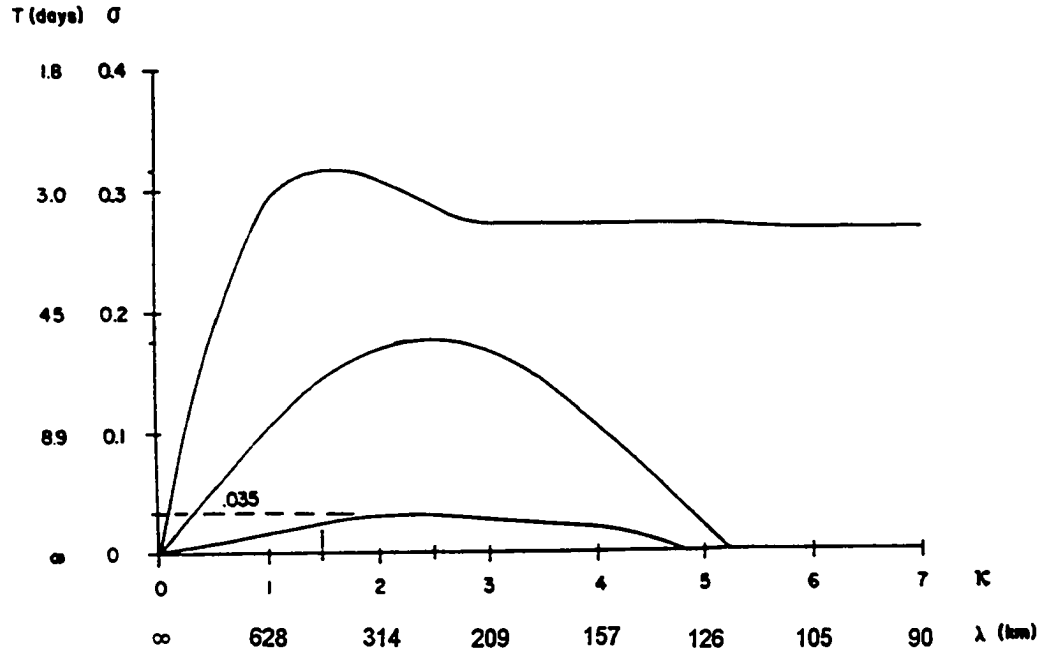


Figure 5.1. Dispersion diagram for the first three continental shelf wave modes constructed by Brooks (1978) for the bottom profile off Wilmington, North Carolina, and barotropic mean flow (Rossby number is 0.11). The normalized (by the inertial frequency) frequency is 0.035 at the dash line (which corresponds to a frequency of 0.036 cpd).

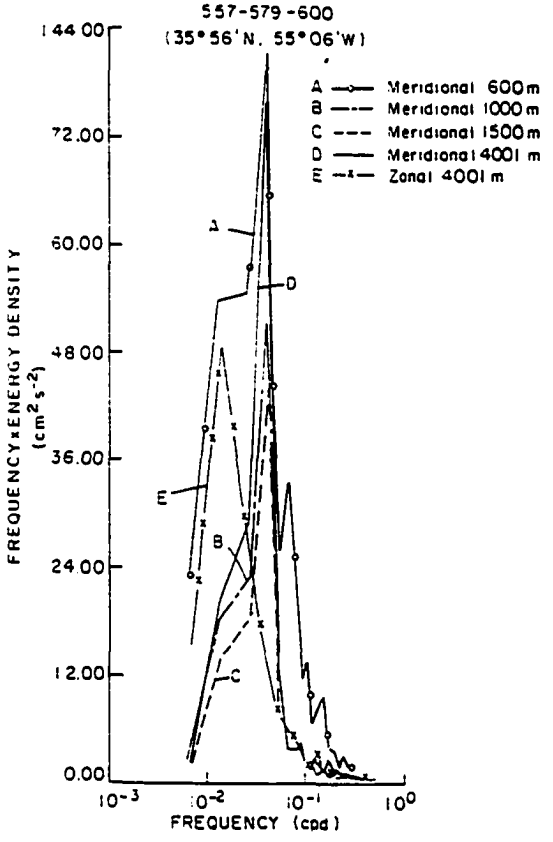


Figure 5.2. Power spectra of the meridional and zonal current components for data obtained at 35°56'N, 55°06'W (in the proximity of the Gulf Stream), from Schmitz, 1978.

# 6. Summary and Conclusions

In this study, we have used the spectral analysis technique to analyze the current meter and temperature data obtained from a series of locations along the shelf break in the South Atlantic Bight. The power spectra for the alongshore current and temperature data calculated based on these data strongly suggest a significant spectral peak at the 28-day period. Low-frequency current fluctuations with periods longer than 2 weeks have seldom been analyzed before due to inadequate sampling. As a result very little is known about them and many questions, such as, the governing mechanisms, the energy sources, and the process(es) in which the energy is transferred, remains open. The greatest difficulty has been, as Wunsch (1980) put it, that not only are there few long records, but the number of long *simultaneous* records, which are crucial for understanding spatial correlations and possible propagation, are even rarer. Since the current meter array from which our data were obtained covers a good portion of the South Atlantic Bight, and the simultaneous data records from those meters have a maximal length of about 150 days, we feel that we may be in a position to explore this subject, at least to lay some groundwork to advance the theory.

In an attempt to capture the spatial characteristics of the 28-day fluctuations, we have adopted a statistical technique called the frequency-domain empirical orthogonal function analysis. A number of combinations of records have been tested. The most consistent and convincing results are from the combination of alongshore current only and that of temperature only, all from the upstream side of the

Charleston Bump. The fact that both alongshore current and temperature fluctuations peak around the 28-day period may be merely coincidental, since they do not share any common mode (this is reflected by the fact that for the mode which is highly coherent with the alongshore currents, the temperature records show very little coherency, and *vice versa*) and exhibit distinct spatial characteristics. This is also consistent with previous findings that correlations between currents and temperatures are generally very weak (*e.g.*, Hamilton, 1987; Lee, Yoder and Atkinson, 1991). The temperature fluctuation in the mid- to lower water column at the 28-day period appears to be purely advective, being carried by the mean alongshore current and gradually losing its intensity along the way.

The first and second EOF modes of the alongshore current at the 28-day period band are found to be statistically significant and each accounts for 64.5% and 18.2% of the total normalized variance, respectively. The first mode represents an upstream (southward) propagation with a wavelength of *circa* 5000 km, the second represents a downstream (northward) propagation with a wavelength of *circa* 360 km. Long-wave signals similar to our first EOF mode are also found in a recent paper (Miller, 1994) from a completely different type of data obtained near the shelf break in the SAB. Although inconclusive, this mode appears to be related to the interaction between topographically induced wave signals and the Gulf Stream current. The characteristics of the second EOF mode is found to be consistent with the dispersion relationship of the barotropic continental shelf waves modeled by Brooks (1978) with characteristically similar bottom profile and flow condition. Hence it is possible that the nature of the second alongshore current EOF mode is the barotropic continental shelf wave. Without the meteorologic, mainly the wind data, we do not know the relationship between the alongshore currents and the atmospheric forcing at this long-period band. However, earlier

results (*e.g.*, Düing, Mooers and Lee, 1977; Wunsch and Wimbush, 1977) seem to suggest that the correlation between the winds and currents are significant only at period shorter than the synoptic time scale, *i.e.*, about 10 days. If this is the case, the first and second EOF modes of the alongshore currents may well represent the free (as opposed to the forced) shelf waves. It is interesting to note that the low-frequency current fluctuations at 28-day period is dominated by the lowest wave mode.

From the results of current data analysis available in the literature, we have noticed that the low-frequency fluctuation of currents at mesoscale or eddy-containing band (as Richman, Wunsch and Hogg (1977) called it) is a well-founded phenomenon (*e.g.*, Schmitz, 1978; Wunsch, 1980). In the immediate vicinity of the Gulf Stream, the current spectra often suggest a time scale *circa* 28-day period. As Gulf Stream is known to be an eddy-spawning ground, as satellite and other remote-sensing imagery have consistently shown, the 28-day period band may be relevant to or even characteristic of the eddy field. If the nature of the mesoscale current fluctuations is that of eddy activity, it is certain that their energy source is the Gulf Stream. The transfer of energy, though, is a two-way process in that eddies not only draw energy from the Stream but occasionally also feed back the mean flow (Webster, 1961b; Schmitz and Niiler, 1968; also the discussion in Section 4.1 in this dissertation). However, there seems to be preferable areas along the Stream where the process is predominated by oneway energy transfer, as a result the eddies tend to grow or decay in those areas (Lee, Yoder and Atkinson, 1991).

A more thorough investigation on the current and temperature fluctuations at periods longer than the synoptic temporal scale would require a current meter array designed to provide a finer and better spatial coverage, in both cross-shore (to study the structure of wave amplitudes) and longshore (to study the propagation

of the waves) directions, and longer temporal span (ideally longer than a year). In addition, wind and hydrographic data are needed to determine the nature of the "very" low-frequency fluctuations. Data and theoretical analyses will likely remain suggestive until more comprehensive surveys are undertaken.

# BIBLIOGRAPHY

Adams, J.K., and V.T. Buchwald, 1969: The generation of continental shelf waves. *J. Fluid Mech.*, **35**, 815–826.

Atkinson, L.P., 1977: Modes of Gulf Stream intrusion into South Atlantic Bight shelf waters. *Geophys. Res. Lett.*, **4**, 583–586.

Atkinson, L.P., T.N. Lee, J.O. Blanton, and W.S. Chandler, 1983: Climatology of the southeastern United States continental shelf waters. *J. Geophys. Res.*, **88**, 4705–4718.

Atkinson, L.P., T.N. Lee, J.O. Blanton, and G.-A. Paffenhöfer, 1987: Summer upwelling on the southeastern continental shelf of the U.S.A. during 1981: Hydrographic observations. *Prog. Oceanogr.*, **19**, 231–266.

Atkinson, L.P., E. Oka, S.Y. Wu, T.J. Berger, J.O. Blantion, and T.N. Lee, 1989: Hydrographic variability of Southeastern United States shelf and slope waters during the Genesis of Atlantic Lows Experiment, Winter 1986. *J. Geophys. Res.*, **94**, 10,699–10,713.

Bane, J.M.,Jr., and D.A. Brooks, 1979: Gulf Stream meanders along the continental margin from the Florida Straits to Cape Hatteras. *Geophys. Res. Lett.*, **6**, 280–282.

Bane, J.M.,Jr., D.A. Brooks, and K.R. Lorenson, 1981: Synoptic observations of the three-dimensional structure, propagation and evolution of Gulf Stream meanders along the Carolina continental margin. *J. Geophys. Res.*, **86**, 6411–6425.

Bane, J.M.,Jr., and W.K. Dewar, 1988: Gulf Stream bimodality and variability downstream of the Charleston Bump. *J. Geophys. Res.*, **93**, 6695–6710.

Brooks, D.A., 1975: Wind-forced continental shelf waves in the Florida Current, *University of Miami (RSMAS) Tech. Rep. 75026*, 268pp., Miami.

Brooks, D.A., and C.N.K. Mooers, 1977: Wind forced continental shelf waves in the Florida current. *J. Geophys. Res.*, **82**, 2569–2576.

Brooks, D.A., 1978: Subtidal sea level fluctuations and their relation to atmospheric forcing along the Carolina coast. *J. Phys. Oceanogr.*, **8**, 481–493.

Brooks, D.A., and J.M. Bane, Jr., 1981: Gulf Stream fluctuations and meanders over the Onslow Bay upper continental slope, *J. Phys. Oceanogr.*, **11**, 247-256.

Chandler, W.S., C.S. Kim, E. Oka, S.Y. Wu, K.A. Bush, P.S. Maher, and L.P. Atkinson, 1987: GALE Hydrographic Data Report January, 1986. *Old Dominion University, ODURF Technical Report No. 87-5*, 355pp., Norfolk.

Chao, S.-Y., and G.S. Janowitz, 1979: The effect of a localized topographic irregularity on the flow of a boundary current along the continental margin. *J. Phys. Oceanogr.*, **9**, 900–910.

Clarke, A.J., and D.S.Battisti, 1981: The effect of continental shelves on tides. *Deep-Sea Res.*, **28**, 665–682.

Csanady, G.T., 1989: Energy dissipation and upwelling in a western boundary current. *J. Phys. Oceanogr.*, **19**, 462–473.

Csanady, G.T., 1990: Physical basis of coastal productivity, the SEEP and MASAR experiments. *Eos Trans. AGU*, **71(36)**, 1060–1065.

Düing, W., C.N.K. Mooers, and T.N. Lee, 1977: Low-frequency variability in the Florida Current and relations to atmospheric forcing from 1972–1974. *J. Mar. Res.*, **35**, 129–161.

Gill, A.E., and E.H. Schumann, 1974: The generation of long shelf waves by the wind. *J. Phys. Oceanogr.*, **4**, 83–90.

Gill, A.E., 1982: *Atmosphere-Ocean Dynamics.* Academic Press. 662pp.

Green, C.K., 1944: Summer upwelling, northeast coast of Florida. *Science*, **110**, 546–547.

Griffiths, R.W., and P.F. Linden, 1982: Laboratory experiments on fronts, Part I: Density-driven boundary currents. *Geophys. Astrophys. Fluid Dyn.*, **19**, 159–187.

Hamilton, P., 1987: The structure of shelf and Gulf Stream motions in the Georgia Bight. *Prog. Oceanogr.*, **19**, 329–351.

Hamon, B.V., 1962: The spectrums of mean sea level at Sydney, Coff's Harbour and Lord Howe Island. *J. Geophys. Res.*, **67**, 5147–5155.

Hamon, B.V., 1976: Generation of shelf waves on the east Australian coast by wind stress. *Mem. Soc. Roy. Sci. Liege, Ser. 6, X*, 359–367.

Hogg, N.G., 1981: Topographic waves along 70°W on the continental rise. *J. Mar. Res.*, **39**, 627–649.

Huthnance, J.M., 1981: Waves and currents near the continental shelf edge. *Prog. Oceanog.*, **10**, 193–226.

Ishizaka, J., 1990: Coupling of coastal zone color scanner data to a physical-biological model of the southeastern U.S. continental shelf ecosystem, 1, CZCS data description and Lagrangian particle tracing experiments. *J. Geophys. Res.*, **95**, 20,167–20,181.

Kielmann, J., and W. Düing, 1974: Tidal and sub-inertial fluctuations in the Florida Current. *J. Phys. Oceanogr.*, **4**, 227–236.

Killworth, P.D., N. Paldor, and M.E. Stern, 1984: Wave propagation and growth on a surface front in a two-layer geostrophic current. *J. Mar. Res.*, **42**, 761–785.

Kundu, P.K., and J.S. Allen, 1976: Some three-dimensional characteristics of low-frequency current fluctuations near the Oregon coast. *J. Phys. Oceanogr.*, **6**, 181–199.

Lee, T.N., and D.A. Brooks, 1979: Initial observations of current, temperature and coastal sea level response to atmospheric and Gulf Stream forcing on the Georgia shelf. *Geophys. Res. Lett.*, **6**, 321–324.

Lee, T.N., and L.P. Atkinson, 1983: Low-frequency current and temperature variability from Gulf Stream frontal eddies and atmospheric forcing along the southeast U.S. outer continental shelf. *J. Geophys. Res.*, **88**, 4541–4568.

Lee, T.N., V. Kourafalou, J.D. Wang, W.J. Ho, J.O. Blanton, L.P. Atkinson, and L.J. Pietrafesa, 1985: Shelf circulation from Cape Canaveral to Cape Fear during winter, in *Oceanography of the Southeastern U.S. Continental Shelf*, edited by L.A.Atkinson, D.W.Menzel, and K.A.Bush, 33–62, American Geophysical Union, Washington, D.C.

Lee, T.N., R. Zantopp, and F. Schott, 1986: Current meter measurements in the Florida Current, in Florida Atlantic Coast Transport Study (FACTS), final report, *MMS86-0079*, vol.2, Chap.3, pp.5–133, Miner. Manage. Serv., Washington, D.C.

Lee, T.N., E. Williams, J. Wang, R. Evans, and L.P. Atkinson, 1989: Response of South Carolina continental shelf waters to wind and Gulf Stream forcing during winter of 1986. *J. Geophys. Res.*, **94**, 10,715–10,754.

Lee, T.N., J.A. Yoder, and L.P. Atkinson, 1991: Gulf Stream frontal eddy influence on productivity of the southeast U.S. continental shelf. *J. Geophys. Res.*, **96**, 22,191–22,205.

Legeckis, R., 1979: Satellite observations of the influence of bottom topography on the seaward deflection of the Gulf Stream off Charleston, South Carolina. *J. Phys. Oceanogr.*, **9**, 483–497.

Luther, M.E., and J.M. Bane,Jr., 1985: Mixed instabilities in the Gulf Stream over the continental slope. *J. Phys. Oceanogr.*, **15**, 3–23.

McKee, W.D., 1977: Continental shelf waves in the presence of a sheared geostrophic current, *Proc. IUTAM Symp. Waves in Water of Varying Depth*, Canberra, *Lecture Notes in Physics*, Vol.64, edited by D.G.Probis and R.Redok, Australian Academy of Science, Canberra, Springer-Verlag, 212–219.

Miller, J.L., 1994: Fluctuations of Gulf Stream frontal position between Cape Haterras and the Straits of Florida. *J. Geophys. Res.*, **99**, 5,057–5,064.

Mooers, C.N.K., and R.L. Smith, 1968: Continental shelf waves off Oregon. *J. Geophys. Res.*, **73**, 549–557.

Mysak, L.A., 1967a: On the theory of continental shelf waves. *J. Mar. Res.*, **25**, 205–227.

Mysak, L.A., 1967b: On the very low frequency spectrum of the sea level on a continental shelf. *J. Geophys. Res.*, **72**, 3043–3047.

Mysak, L.A., and B.V. Hamon, 1969: Low-frequency sea level behavior and continental shelf waves off North Carolina. *J. Geophys. Res.*, **74**, 1397–1405.

Mysak, L.A., 1980: Recent advances in shelf wave dynamics. *Rev. Geophys. and Space Phys.*, **18**, No.1, 211–241.

Niiler, P.P., and L.A. Mysak, 1971: Barotropic waves along an eastern continental shelf. *Geophys. Fluid Dyn.*, **2**, 273–288.

Oey, L.-Y., 1986: The formation and maintenance of density fronts on U.S. southeastern shelf during winter. *J. Phys. Oceanogr.*, **16**, 1119–1133.

Oey, L.-Y., 1988: A model of Gulf Stream frontal instabilities, meanders and eddies along the continental slope. *J. Phys. Oceanogr.*, **18**, 211–229.

O'Malley, P.G., L.P. Atkinson, J.J. Singer, W.S. Chandler, and T.N. Lee, 1978: Hydrographic observations in the Georgia Bight (April 1978), *Tech. Rep. 78-5*, 208pp., Ga. Mar. Sci. Cent., Atlanta.

Orlanski, I., and M.D. Cox, 1973: Baroclinic instability in ocean currents. *Geophys. Fluid Dyn.*, **4**, 297–332.

Paffenhöfer, G.-A., B.K. Sherman, and T.N. Lee, 1987: Summer upwelling on the southeastern continental shelf of the U.S.A. during 1981: Changes in distribution and abundance of particulate matter. *Prog. Oceanogr.*, **19**, 373-401.

Pelegri, J.L., and G.T. Csanady, 1991: Nutrient transport and mixing in the Gulf Stream. *J. Geophys. Res.*, **96**, 2577–2583.

Pietrafesa, L.J., and G.S. Janowitz, 1980: On the dynamics of the Gulf Stream front on the Carolina Capes, in *Proceedings of the Second Onternational Symposium on Stratified Flows*, 184–197, Tapir Publications, Trondheim, Norway.

Pietrafesa, L.J., 1983: Shelfbreak circulation, fronts and physical oceanography: East and west coast perspectives, in *The Shelfbreak: Critical Interface on Continental Margins, Spec. Publ.*33, edited by D.J.Stanley and G.J.Moore, 233–250, Society of Economic Paleontologists and mineralogists, Tulsa, Okla.

Pietrafesa, L.J., G.S. Janowitz, and P.A. Wittman, 1985: Physical oceanographic processes in the Carolina Capes, in *Oceanography of the Southeastern U.S. Continental Shelf*, edited by L.A.Atkinson, D.W.Menzel, and K.A.Bush, 23–32, American Geophysical Union, Washington, D.C.

Pietrafesa, L.J., J.O.Blanton, J.D.Wang, V.Kourafalou, T.N.Lee, and K.A.Bush, 1985: The tidal regime in the South Atlantic Bight, in *Oceanography of the Southeastern U.S. Continental Shelf*, edited by L.A.Atkinson, D.W.Menzel, and K.A.Bush, 63–76, American Geophysical Union, Washington, D.C.

Pond, S., and G.L. Pickard, 1983: *Introductory Dynamical Oceanography*, 2nd Ed., 329pp., Pergamon Press, New York.

Preisendorfer, R.W., 1988: *Principal Component Analysis in Meteorology and Oceanography*, compiled and edited by C.D. Mobley, 425pp., Elsevier, New York.

Priestley, M.B., 1981: *Spectral Analysis and Time Series Analysis*, 890pp., Academic Press, New York.

Redfield, A.C., 1958: The influence of the continental shelf on the tides of the Atlantic coast of the United States. *J. Mar. Res.*, **17**, 432–448.

Redfield, A.C., 1980: *Introduction to Tides: The Tides of the Waters of New England and New York*, 108pp., Marine Science International, Woods Hole, Mass.

Richman, J.G., C. Wunsch, and N.G. Hogg, 1977: Space and time scales and mesoscale motion in the sea. *Rev. Geophys. and Space Phys.*, **15**, 385–420.

Robinson, A.R., 1964: Continental shelf waves and the response of sea level to weather systems. *J. Geophys. Res.*, **69**, 367–368.

Rossby, D.-G., 1936: Dynamics of steady ocean currents in the light of experimental fluid mechanics. *Papers in Phys. Oceangr. and Meteor.*, *5:1*, 43pp.

Schmitz, W.J.,Jr., and P.P. Niiler, 1969: A note on the kinetic energy exchange between fluctuations and mean flow in the surface layer of the Florida Current. *Tellus*, **21**, 814–819.

Schmitz, W.J.,Jr., 1978: Observations of the vertical distribution of low frequency kinetic energy in the Western Atlantic. *J. Mar. Res.*, **36**, 295–310.

Schott, F., and W. Düing, 1976: Continental shelf waves in the Florida Straits. *J. Phys. Oceanogr.*, **6**, 451–460.

Starr, V.P., 1954: Studies of the atmospheric general circulation, Part I. *Final Report General Circulation Project, AF19(122)-153.* Massachusetts Institute of Technology, Dept. of Meteorology, 535pp.

Stefánsson, U., L.P. Atkinson, and D.F. Bumpus, 1971: Hydrographic properties and circulation of the North Carolina shelf and slope waters. *Deep-Sea Res.*, **18**, 383–420.

Stern, M.E., 1985: Lateral wave breaking and "shingle" formation in large-scale shear flow. *J. Phys. Oceanogr.*, **15**, 1274–1283.

Stommel, H.M., 1958: *The Gulf Stream*, 202pp., University of California Press, Berkeley.

Stone, R.B, and T.R. Azarovitz, 1968: An occurance of unusually cold water off the Florida coast. *Underwater Naturalist*, **5**, 14–17.

Taylor, C.B., and H.B. Steward, Jr., 1959: Summer upwelling along the east coast of Florida. *J. Geophys. Res.*, **64**, 33–40.

von Arx, W.S., 1954: Measurements of the oceanic circulation in temperate and tropical latitudes. *Oceanographic Instrumentation, Nat. Res. Counc.* (U.S.) Publ., No. 309, 13–35.

von Arx, W.S., D.F. Bumpus, and W.S. Richardson, 1955: On the fine structure of the Gulf Stream front. *Deep-Sea Res.*, **3**, 46–65.

Wallace, J.M., and R.F. Dickinson, 1972: Empirical orthogonal representation of time series in the frequency domain, Part I: Theoretical considerations. *J. Appl. Meteo.*, **11**, 887–892.

Wang, D.-P., and C.N.K. Moores, 1977: Long coastal-trapped waves off the west coast of the United States, Summer 1973. *J. Phys. Oceanogr.*, **7**, 856–864.

Webster, F., 1961a: A description of Gulf Stream meanders off Onslow Bay. *Deep-Sea Res.*, **8**, 130–143.

Webster, F., 1961b: The effects of meanders on the kinetic energy balance of the Gulf Stream, *Tellus*, **13**, 392–401.

Wunsch, C., and M. Wimbush, 1977: Simultaneous pressure, velocity and temperature measurements in the Florida Straits. *J. Mar. Res.*, **35**, 75–104.

Wunsch, C., 1980: Low-frequency variability of the sea, in *Evolution of Physical Oceanography*, edited by B.A. Warren and C. Wunsch, The MIT Press, Cambridge, Mass., 342–375.

Yaglom, A.M., 1962: *An Introduction to the Theory of Stationary Random Functions.* Englewood Cliffs, N. J., Prentice Hall, 235pp.

Yoder, J.A., L.P. Atkinson, S.S. Bishop, E.E. Hofmann, and T.N. Lee, 1983: Effect of upwelling on phytoplankton productivity of the outer southeastern United States continental shelf. *Cont. Shelf Res.*, **1**, 385–404.

Yoder, J.A., L.P. Atkinson, S.S. Bishop, J.O. Blanton, T.N. Lee, and L.J. Pietrafesa, 1985: Phytoplankton dynamics within Gulf Stream intrusions on the southeastern United States continental shelf. *Cont. Shelf Res.*, **4**, 611–635.

## Autobiographical Statement

**Born**

February 18, 1963, Quanzhou, Fujian Province, China

**Education**

- B.S. Physical Oceanography, Shandong College of Oceanology, China, July, 1984
- Ph.D Physical Oceanography, Old Dominion University, August, 1994

**Work Experience**

- *Editor*, Science Press, Chinese Academy of Science, Beijing, China, August, 1984–January, 1987
- *Research Assistant*, Department of Oceanography, Old Dominion University, January, 1987–September, 1993
- *Faculty Research Staff*, Horn Point Environmental Laborotary, University of Maryland, September, 1993–August, 1994
- *Assistant Research Scientist*, Horn Point Environmental Laboratory, University of Maryland, August, 1994–

**Professional Membership**

American Geophysical Union

**Publications**

- Atkinson, L.P., E.Oka, S.Y.Wu, T.J.Berger, J.O.Blanton, and T.N.Lee, 1989: Hydrographic variability of Southeastern United States shelf and slope waters during the Genesis of Atlantic Low Experiment, Winter, 1986. *J. Geophys.*

*Res.*, **94**, 10,699–10,713.

- Chandler, W.S., C.Kim, E.Oka, S.Y.Wu, K.A.Bush, P.S.Maher, and L.P.Atkinson, 1987: GALE Hydrographic Data Report January, 1986, *ODURF Technical Report No.87-5*, Old Dominion University Research Foundation, Norfolk, VA.